3.3.3.1. Books / Chapters with ISBN:

R.Thenmozhi , Assistant Professor of Chemistry	International Conference on Systems, Science, Control, Communication, Engineering and Technology	-	Preparation of Spherical Silica Nanoparticles by Sol-Gel Method	-	-	International 978-81-929866-6-1	Februar y 2016

International Conference on Systems, Science, Control, Communication, Engineering and Technology 2016 [ICSSCCET 2016]

ISBN	978-81-929866-6-1	**VOL**	02
Website	icssccet.org	**eMail**	icssccet@asdf.res.in
Received	25 – February – 2016	**Accepted**	10 - March – 2016
Article ID	ICSSCCET077	**eAID**	ICSSCCET.2016.077

Preparation of Spherical Silica Nanoparticles by Sol-Gel Method

R Sumathi[1], R Thenmozhi[2]
[1]Assitant Professor, Karpagam Institute Technology, Coimbatore, Tamilnadu, India.
[2]Assitant Professor, Sakthi College of Arts and Science for Women, Oddanchathram, Dindigul, Tamilnadu, India.

Abstract: *Silica nanoparticles were synthesized by sol gel method from tetraethyl orthosilicate (TEOS), ethanol (C_2H_5OH), water (H_2O) and ammonoium hydroxide (NH_4OH) as catalyst. The morphology and structure of colloidal silica particles formed depend on the molar ratio of reagents. The XRD patterns show the amorphous nature of the particles. SEM image shows that spherical structure of silica nano particles, whose particle is varied by using different molar ratio of TEOS, C_2H_5OH and NH_3. TEM image shows that spherical structure of silica nano particles, whose particle is determined by using same molar ratio of TEOS, C_2H_5OH and NH_3 The EDAX analyses prove the successful synthesis of silica material.*

1. INTRODUCTION

Silica nanoparticles are widely used in industrials such as electronic devices, insulator, catalysis or pharmaceuticals [1, 2] due to their attractive properties in optical properties. The most popular process of obtaining silica nanoparticles is through sol gel technique [3-7]. It involves the simultaneous hydrolysis and condensation reaction of the metal alkoxide. The resultants desired particles size and morphology of silica particles are produced through controlling parameters such as concentration of alkoxide, amount of water and concentration of ammonia or acid and solvent and aging time.

2. Experimental Methods

2.1. Preparation of Silica (SiO_2) Nano powder

Chemicals used in this experiment are Tetraethyl Orthosilicate (TEOS), concentrated Ammonia (NH_3) and Ethanol (C_2H_5OH) solution. Tetraethyl Orthosilicate (TEOS) is used as the silica source. Aqueous ammonia solution was used as the catalyst. All the chemicals are purchased from Aldrich without further purification. Distilled water was used throughout the experiment Silica nanoparticles were synthesized using a standard procedure with experimental conditions provided in Table 1. The product was grained to get the silica nanoparticle.

Cite this article as: R Sumathi, R Thenmozhi. "Preparation of Spherical Silica Nanoparticles by Sol-Gel Method". *International Conference on Systems, Science, Control, Communication, Engineering and Technology 2016*: 401-405. Print.

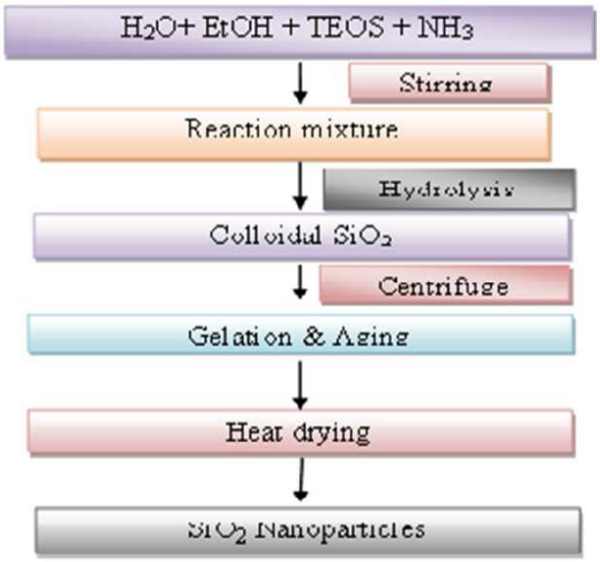

Flow chart for the Synthesis of silica nanoparticles by sol-gel method

Table 1: Molar ratios for the preparation of silica nanoparticles

Sample	Molar Ratio			
	H_2O	TEOS	NH_3	EtOH
a.	1	5	7	14
b.	1	5	9	7
c.	1	7	7	7

2.2. Characterization

The characterization of nanoparticles is done by using different techniques. The crystalline structure, morphology and compositional analysis of the prepared samples are examined by that the X-ray Diffraction (XRD), Scanning Electron Microscope (SEM), and Energy Dispersive Analysis using X-rays (EDAX) respectively. Nature of bonding and the chemical composition were analyzed by Fourier Transfer Infrared spectra (FTIR).

3. Results and Discussion

3.1. X-ray Diffraction Analysis

The crystal structures and phases of all the synthesized nanomaterials were ascertained from the XRD pattern. The figure shows that the XRD patterns of silica nanopowder prepared by sol-gel method for different molar ratios of ammonia, TEOS and ethanol concentration. From the three graphs (Fig 1) shows that the particles are amorphous in nature. The intense peak at $\theta = 23^{\circ}$ indicates, that the silica particles are formed by small nanocrystals. The broadening of peak is high owing to the smaller grain size effect. Other peaks are not present which represents the amorphous in nature due to the smaller particle size effect and incomplete inner structure of the nanoparticles [8]. XRD peaks which represent that silica nanoparticles structure is not changed entirely with small variation in ammonia, TEOS and ethanol concentration. By changing the different concentration, there is no phase change which represents the high purity of the silica nanoparticles. This demonstrates that high percentages of these particles are amorphous [9].

Cite this article as: R Sumathi, R Thenmozhi. "Preparation of Spherical Silica Nanoparticles by Sol-Gel Method". *International Conference on Systems, Science, Control, Communication, Engineering and Technology 2016*: 401-405. Print.

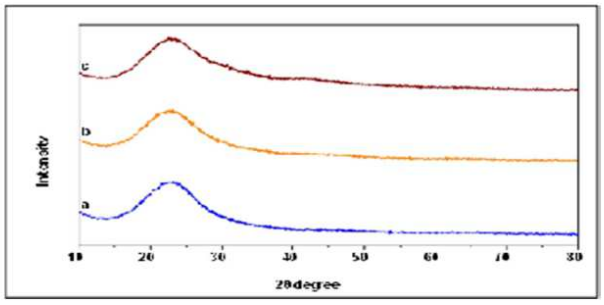

Fig 1: XRD spectrum of silica nanoparticle at different molar ratio of water, TEOS, NH_3, EtOH a) 1:5:7:14 b) 1:5:9:14 c)1:7:7:7

3.2. Morphological Analysis (SEM) & Compositional Analysis (EDAX)

The surface morphology of the silica nanopowder is analyzed using scanning electron microscope at the molar ratios of Water: TEOS: NH_3: EtOH as shown in Figure (2-4). The reaction was performed at lower water molecules in the solution to avoid aggregation of the silica nanoparticles at constant temperature. Therefore, hydrolysis and condensation of the reaction is carried out in alcohol with the presence of basic medium to get uniform distribution of silica nanoparticles. Figures 2-4 shows the spherical and agglomerated silica nanoparticles, which were obtained using different molar ratios of reagents and solvents.

The figure 2 shows that for preparing smaller silica nanoparticles, the reaction mixture should have higher concentration of ethanol and lower concentration of ammonia. Aggregation is always energetically favoured over nanoparticles since it minimizes surface areas and saturates the bonding and co-ordination sites and therefore, in order to prevent the nanoparticles from further growth or aggregation, the particle surfaces should be saturated immediately after nucleation by electrostatic or steric stabilization. Thus, the ammonia and solvent molecule of ethanol plays an important role to produce small size of silica nanoparticles with monodispersed spherical shape.

The figure 3 shows increase in particle size compared to sample 1. The base medium of ammonia is increased where as the amount of ethanol is decreased compared to sample 1. When the concentration of ammonia was changed corresponding decrease in the amount of solvent, many particles agglomerated, although few smaller spheres starts to form bigger silica nanoparticles. With the increase in the amount of ammonia, the sizes of the particle gradually increased and produce irregular spherical nanoparticles with high aggregation effect. The irregular shape of silica particles is obtained due to the fast nucleation process which is difficult to control the reaction by high concentration of basic medium and less solvent effect. And also decrease in the amount of ethanol the particle size increases [10]. Hence the SEM shows an increase in the size and irregular shape of the silica nanoparticles compared to SEM 1.

Figure 4 shows the silica nanoparticles were synthesized with same molar ratio of TEOS, Ammonia and Ethanol giving rise to larger silica nanoparticles with a broad distribution of particle sizes. Uniform orientation of the silica nanoparticles without aggregation is obtained is due to the covalent bond between the neighboring nanoparticles. Synthesis time was necessary because TEOS must be added very slowly to avoid any second nucleation or chemical aggregation. Second or multi nucleation could be avoided by three ways: 1) increase of the ionic force in order to reduce the number of nucleation centers, 2) increase of particle surface in solution, 3) limiting TEOS concentration. Different concentration of TEOS, ammonia and ethanol, spherical silica nanoparticles is formed in different size which is not only alter the particle size and shape, also dramatically affects the optical properties of resultant nanoparticles.Finally we concluded, the particle size decreases with increasing molar ratio of ethanol and the particle size increases with increasing molar ratio of TEOS and ammonia.

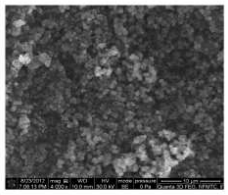

(2)

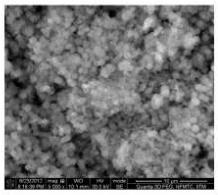

(3)

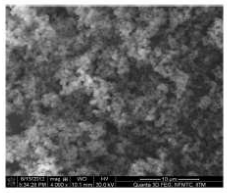

(4)

Fig 2, 3 and 4 shows SEM micrographs of silica nanoparticles obtained from a molarratio of Water: TEOS: NH_3: EtOH a) 1:5:7:14 b) 1:5:9:7 c) 1:7:7:7.

Cite this article as: R Sumathi, R Thenmozhi. "Preparation of Spherical Silica Nanoparticles by Sol-Gel Method". *International Conference on Systems, Science, Control, Communication, Engineering and Technology 2016*: 401-405. Print.

The elements of silica nanoparticles are confirmed by EDAX analysis, this is shown in figures 5,6 and 7. The Composition is given in table 2 [11].

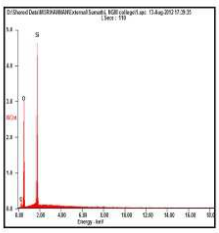
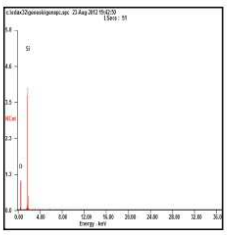
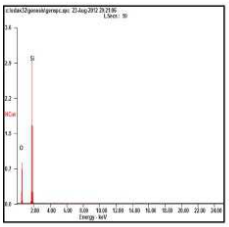

Fig 5,6 and 7 shows EDAX spectrum of Si particles of molar ratio a)1:5:7:14 b)1:5:9:7c)1:7:7:7

Table 2: EDAX result of silica nanoparticleswith different molar ratio

S.No	Molar Ratio				Elements	Atomic %
	H_2O	TEOS	NH_3	EtOH		
a.	1	5	7	14	Si : O	24.43 : 75.70
b.	1	5	9	7	Si : O	36.12 : 63.88
c.	1	7	7	7	Si : O	31.15 : 68.85

3.3 Transmission Electron Microscope

Spherical structure of silica nano particles is prepared by using, same molar ratio of TEOS, C_2H_5OH and NH_3. Whose particle size is determined by using TEM.

From the TEM image, the diameter of the primary particles is about 100 nm.TEM observation, and indicates the rather good monodispersity of the particles.

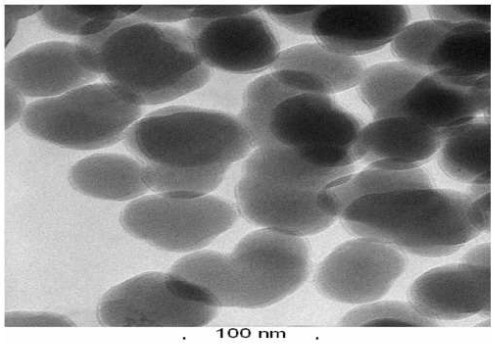

Conclusion

We have successfully synthesized monodisperse silica spheres with the size ranging from >100 nm through sol-gel method. The reaction parameters can be used effectively for the synthesis of spherical silica nanoparticles at different molar ratio of Water, TEOS, NH_3, EtOH. The influence of the matrix obtained from the TEOS precursors and ammonia plays a major role in the evolution of the processes. The morphology and average diameter of colloidal silica particles depend on the proportion of reactants. XRD pattern shows the amorphous nature of silica nanoparticles. The SEM & TEM image shows the spherical structure of nanoparticles, whose particle size decreased with increasing molar ratio of ethanol in sample a. The particle size increased with increasing molar ratio of ammonia and decreasing molar ratio of EtOH in sample b. The particle size is increased for equal molar ratio of TEOS, NH_3, EtOH, in

Cite this article as: R Sumathi, R Thenmozhi. "Preparation of Spherical Silica Nanoparticles by Sol-Gel Method". *International Conference on Systems, Science, Control, Communication, Engineering and Technology 2016*: 401-405. Print.

sample c. The EDAX analyses prove the successful synthesis of the silica material. The resultant spherical silica nanoparticles synthesized can be usedfor various photocatalytic activity, assembly of photonic structures and these microspheres have potential for biomedical applications.

References

1. K.J. Klabunde, Nanoscale Materials in chemistry, Wiley-Interscience, USA 2001.
2. Y.T.Chen. Tamkang J.Sci.Eng. 5(2002) 99.
3. W.Stober, A. Fink, E.Bohn, J. Colloid Interface Sci. 26 (1968) 62-69.
4. N. enomoto. T.Koyano, Z. Nakagawa, Ultrason. Sonochem. 3 (1996) 105-109.
5. G. Buchel, M.Gurnn, K.K. Unger, A. Matasumoto, K.Tsutnami, S-pramol. Sci. 5(1998) 532-559.
6. D. Nagoo, H. Osuzu, A. Yamada, E. Mine, Y. Kobayashi, M. Konno, J. Colloid Interface Sci. 274 (2004) 143-149.
7. S. Tatabaei, A. Shukohfar, R. Aghababazadeh, A.Mirhabibi, j. Phys. Confer. Series 26 (2006) 371-374.
8. E. R. Jisha et al, International Journal of Pharm Tech Research, 4 (2012) 1323-1331.
9. NoorsaiyyidahDarmonSingho, MohdRafie John, Int. J. ElectrochemSci, 7 (2012 5604-5615).
10. AldonaBeganskiene et al,Materials Science, 10 (2004) 287-290.
11. Binary K. Dutta et al, World Academy of Science Engineering and Technology, 73 (2011) 443-447.
12. Y. Shan, L. Guo and S. Zheng, Mater ChemPhys, 88 (2004) 192.
13. W. Posthemus, P. C. M. M. Magusin, J. C. M. Brokken-Zijp, A. H. A. Tinnemans and R. Vander linde, Surface Modification of oxide nanoparticles using 3-methacryloxy propyltrimethoxysilane, Journal of Colloid and Interface Science, 269 (2004) 109-116..
14. J. R. Agger, M. W. Anderson, M. E. Pemble, O. Terasaki and Y. Nozue, J PhysChem B,102 (1998) 3345.
15. J. M. Berquier, L. Teyssedre, C. Jacquiod, Journal of Sol-Gel Science Technology, 13 (1998) 739.

Cite this article as: R Sumathi, R Thenmozhi. "Preparation of Spherical Silica Nanoparticles by Sol-Gel Method". *International Conference on Systems, Science, Control, Communication, Engineering and Technology 2016*: 401-405. Print.

V.Johnsirani Assistant Professor of Chemistry	International Journal of Nano Corrosion Science and Engineering	-	Corrosion Inhibition By Natural Dyes	-	-	International ISSN(Online)-2395-7018	October 2016

Available Online http://www.ijncse.com
ISSN Online: 2395-7018
INTERNATIONAL JOURNAL OF NANO CORROSION SCIENCE AND ENGINEERING

Corrosion Inhibition By Natural Dyes

V.Johnsirani[1], J.Sathiyabama[2] and SusaiRajendran[3]

1. Department of Chemistry, Sakthi college of Arts and Science for Women, Oddanchatram, Dindigul. India. E-mail: johnsirani15 @gmail.com

2. Department of Chemistry, St.Antony's college of Arts and Sciences for Women, Dindigul-624005.

Abstract

The Inhibition efficiency [IE] of an aqueous extract of pipali powder in controlling corrosion of carbon steel in sea water [Thondi, Tamil Nadu, India] has been evaluated by weight loss method. The weight loss study reveals that PD formulation consisting of 10mL of PD (pipali Dye) and 25 ppm of Zn^{2+} has 92% inhibition efficiency in controlling corrosion of carbon steel in sea water. A synergistic effect exists between PD and Zn^{2+}. Polarization study reveals that PD and Zn^{2+} system functions as mixed type inhibitor. The nature of the metal surface has been analysed by FTIR spectra.

Key words : Carbon steel,Corrosion, sea water, Electrochemmical techniques, FTIR, AFM.

Inter Collegiate Meet- National Level Seminar on "New Perspective in Science and Technology", (NPST-2016), 7th October, 2016- St Antony's College of Arts and Sciences for Women, Thamaraipadi, Dindigul, India.

Int J Nano Corr Sci and Engg 3(4)(2016) 115 - 130
Editors: Dr S Rajendran, A Christy Catherine Mary

1. Introduction

Plant extracts are low-cost and biodegradable, and so the study of plant extracts as corrosion inhibitors is an important scientific research field due to both economic and environmental benefits. As early as in 1930, plant extracts (dried stems, leaves and seeds) of Chelidonium majus and other plants were used as corrosion inhibitors for steel in H_2SO_4 pickling baths. In 1972, El Hosary et al. studied the extract of Hibiscus subdariffa (Karkode) as the corrosion inhibitor for Al and Zn in HCl and NaOH solutions. In 1980s, Saleh et al. and reported the inhibition effect of aqueous extracts of some plant leaves (Opuntia, Aleo eru) and fruit peels (orange, mango) on the corrosion of steel, aluminum, zinc and copper in acids and aluminum in NaOH solution. In *1990s, Azadirachta and Vernonia amygdalina (bitter* leaf) leaves extracts were reported as good corrosion inhibitors for steel in HCl and H_2SO_4 solutions.

Most of the inhibitors are synthetic chemicals which may be very expensive and hazardous to living creatures and environment. Natural products are one of the renewable sources, which can be used as inhibitors. Natural products in addition to their environmentally friendly and ecologically acceptable nature are inexpensive, readily available and renewable sources of materials. Among these so-called ''green corrosion inhibitors" are organic compounds that act by adsorption (Ostovari et al., 2009) on the metallic surfaces. Some of these materials are honey (El-Etre et al., 2000), caffeic acid (Souza et al., 2009), caffeine (Trindade et al., 2009), Pennyroyal oil (Bouyanzer et al., 2006), alizarin (Ebenso et al., 2008), Occimumviridis extract (Oguzie, 2006), Rhizome extract (Rajendran et al., 2005), Zenthoxylum alatum extract (Chauhan et al., 2007), Lawsonia (El-Etre et al., 2005; Rajendran et al., 2009), Berberine (Li et al., 2005), garlic extract (Rajendran et al., 2009) and several other extracts of natural substances (Bothi Raja et al, 2008; Sangeetha et al.,2011). The efficiency of these organic corrosion inhibitors is related to the presence of polar functions with S, O or N atoms in their molecular structure, heterocyclic compounds and π electrons (Satapathy et al., 2009).

Phenolic compounds that exist in these plant extracts effectively adsorbed on the metal

surface and then impede the corrosion process (Ostovari et al., 2009; Anuradha et al. 2008). The phenolic content of Chamomile flowers consist of flavonoids, including flavone glycosides (e.g., apigenin 7-glucoside) and flavonols (e.g., quercetin and luteolin glucosides) and phenolic acids including caffeic, chlorogenic, etc (Harbourne et al., 2009). Some authors (Mladěnka et al., 2011) have demonstrated that these phenolic compounds interact with iron. In this research, the corrosion inhibition of carbon steel, in sea water extract of Pipali (Piper longum L.) have been investigated.

2. EXPERIMENTAL

2.1 Preparation of Pipali Dye

10gm of Pippali (Piper longum L.) powder was weighed and boiled with double distilled water. The greydye Pippali was filtered to remove suspended impurities and made up to 100mL. The pippali dye (PD) was used as corrosion inhibitor in the present study.

2.2. Preparation of carbon steel specimens

Carbon steel specimens (0.02 6% S, 0.06% P, 0.4% Mn, 0.1% C and rest iron) of tPE dimensions 1.0 x 4.0 x 0.2 cm were polisPEd to a mirror finish, degreased with trichloroethylene, and used for tPE weight-loss method and surface examination studies.

2.3. Weight- loss method

Carbon steel specimens were immersed in 100 ml of the medium containing various concentrations of the inhibitor in the absence and presence of Zn^{2+} for one day. The weights of the specimens before and after immersion were determined using a Digital Balance (Model AUY 220 SHIMADZU). The corrosion products were cleaned with Clarke's solution . The corrosion IE was then calculated using the equation.

$IE = 100\ [1-(W_2/W_1)]\ \%$

Where W_1 is the weight loss value in the absence of inhibitor

W_2 is the weight loss value in the presence of inhibitor.

Corrosion rate was calculated using the formula

Corrosion rate (mm/year) = 87.6 W/ DAT

Where W = weight loss in milligram

,D = density of specimen g/cm^3

,A = area of specimen in square cm,

T = exposure time in hours.

2.4 Potentiodynamic Polarization Study:

Polarization studies were carried out in a CHI- electrochemical work station with impedance model 660A. It was provided with iR compensation facility. A three electrode cell assembly was used. The working electrode was carbon steel. A SCE was the reference electrode. Platinum was the counter electrode. From polarization study, corrosion parameters such as corrosion potential (E_{corr}), corrosion current (I_{corr}), Tafel slopes anodic = b_a and cathodic = b_c were calculated and linear polarization study (LPR) was done. The scan rate (V/S0.01. Hold time at (E_{fcs}) was zero and quiet time (s) was two.

2.5 Surface examination study:

The carbon steel specimens were immersed in various test solutions for a period of one day. After one day, the specimens were taken out and dried. The nature of the film formed on the surface of the metal specimen was analyzed for surface analysis technique by FTIR spectra.

2.6 Fourier transform infrared spectra:

These spectra were recorded in a Perkin-Elmer-1600 spectrophotometer using KBr pellet. The FTIR spectrum of the protective film was recorded by carefully removing the film, mixing it with KBr and making the pellet.

3. Results and Discussion

3.1 Analysis of the results of weight loss method

The values of IE for different concentrations of PD in the absence and presence of Zn^{2+} in sea water for a period of one day obtained from the weight loss method are given in Table 3.1. It can be seen that Zn^{2+} alone has some inhibitive properties. IE increases as the concentration of PD increases. As the concentration of Zn^{2+} increases, IE also increases. Upon addition of 10 mL of PD, IE dereases. This is due to the fact that the complex (Fe^{2+} -active principle in PD) formed on the metal surface dissolves and goes into solution. Similar observation has been made in the case of corrosion inhibition by Henna extract . However, it is observed that when the concentration of Zn^{2+} increases from 25 ppm to 50 ppm, the IE slightly decreases. This may be due to the fact that, when the concentration of Zn^{2+} increases, the Zn^{2+} - PD complex formed is precipitated in the bulk of the solution. Hence PD is not transported towards the metal surface. So, the IE decreases. The formulation consisting of 10 mL of PD and 25 ppm of Zn^{2+} has 92% IE. Therefore, mixture of inhibitors shows better IE than individual inhibitors. This suggests a synergistic effect existing between PD and Zn^{2+} .

Table.3.1 Inhibition efficiency (IE) of PD-Zn^{2+} system in the corrosion of carbon steel immersed in sea water (Immersion period-1 day)

PD (mL)	Zn^{2+} (ppm)		
	0	25	50
	CR (mm/y)	CR (mm/y)	CR (mm/y)
0	0.1576	0.1323	0.0835
2	0.0788	0.0472	0.0394
4	0.0740	0.0394	0.0362
6	0.0709	0.0236	0.0299
8	0.0630	0.0173	0.0252
10	0.0583	0.0126	0.0236

Table.3.2 corrosion rates (CR) in millimeter per year (mm/y) of carbon steel immersed in sea water in the presence of PD-Zn^{2+} system (Immersion period-1 day)

PD (mL)	Zn^{2+} (ppm)		
	0	25	50
	IE (%)	IE (%)	IE (%)
0	-	16	47
2	50	70	70
4	53	75	72
6	55	85	81
8	60	89	84
10	63	92	85

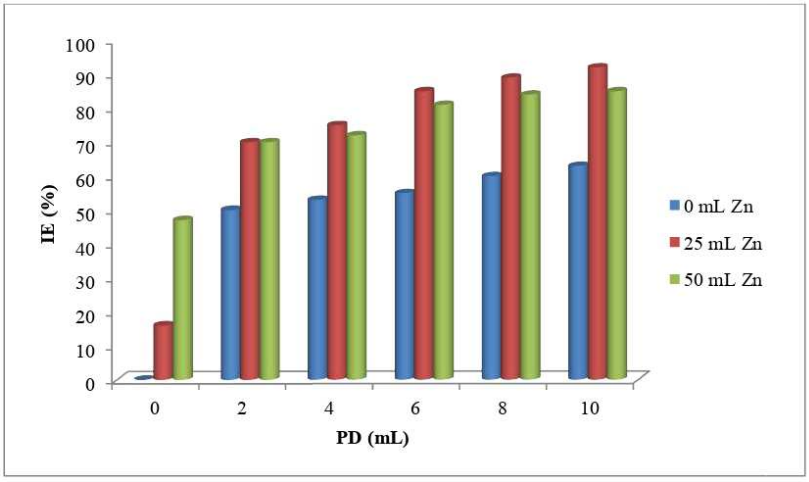

Fig.3.1 Graph of inhibition efficiency (IE) of PD – Zn^{2+} system in the corrosion of carbon steel immersed in sea water (Immersion period – 1 day)

3.2 Synergism parameter (S_I)

Synergism parameter is calculated to evaluate the synergistic effect existing between inhibitors . The synergism parameter (S_I) can be calculated using the relationship given by Aramaki and Hackermann .

$$S_I = 1-\theta_{1+2} / 1-\theta'_{1+2} \quad \ldots\ldots$$

Where

θ_{1+2} = $(\theta_1+\theta_2) -(\theta_1 \times \theta_2)$

θ_1 = surface coverage of inhibitor (PD)

θ_2 = surface coverage of inhibitor (Zn^{2+})

θ'_{1+2} = combined surface coverage of inhibitors (PD) and (Zn^{2+})

Surface coverage = IE%/100

S_I approaches 1 when no interaction exists between the two inhibitors. When $S_I > 1$, synergistic effect exists between the two inhibitors. In the case of $S_I < 1$, negative interaction takes place between the two inhibitors, (i.e, CR increase) The calculated synergism parameter values are given in Table 3.2a and 3.2b. The S_I value is found to be greater than one indicating synergistic effect existing between Zn^{2+} of concentrations 25 ppm and 50 ppm with various concentrations of PD . Thus the enhancement of the IE caused by the addition of Zn^{2+} ions to PD is due to the synergistic effect. The above result is in accordance with the interpretations made by Sangeetha et al. while discussing the values of S_I are slightly smaller in the case of 25 ppm of Zn^{2+} when compared with 50 ppm of Zn^{2+}. This is in line with the inhibition efficiencies obtained by weight loss method. Thus the values of synergism parameters given have quantitative value of synergism existing between the two inhibitors.

Table 3.2a Synergism parameters for PD-Zn^{2+} (25 ppm) system, when carbon steel immersed in sea water (Immersion period-1 day)

PD (mL)	θ_1	θ_2	θ'_{1+2}	S_I
2	0.50	0.16	0.70	1.4
4	0.53	0.16	0.75	1.5792
6	0.55	0.16	0.85	2.52
8	0.60	0.16	0.89	3.0545
10	0.63	0.16	0.92	3.885

Table 3.2b Synergism parameters for PD-Zn^{2+} (50 ppm) system, when carbon steel immersed in sea water (Immersion period-1 day)

PD (mL)	θ_1	θ_2	θ'_{1+2}	S_I
2	0.50	0.47	0.75	1.06
4	0.53	0.47	0.77	1.0830
6	0.55	0.47	0.81	4.0078
8	0.60	0.47	0.84	1.325
10	0.63	0.47	0.85	1.3073

3.3 Analysis of results of potentiodynamic polarization study for the PD-system

Polarization study has been used to detect the formation of protective film on the metal surface during corrosion inhibition process. The potentiodynamic polarization curves obtained for carbon steel in sea water without and with inhibitors (10 mL of PD + 25 ppm Zn^{2+}) are shown in Fig.3.2. The cathodic branch represents the oxygen reduction reaction, while the anodic branch represents the iron dissolution reaction. The electrochemical parmmeters such as corrosion potential (E_{corr}), corrosion current (I_{corr}), Tafel solpes (b_a and b_c), linear polarization resistance (LPR) are given in Table 3.3.

When carbon steel is immersed in sea water, the corrosion potentials is -816 mV vs SCE. The inhibitor system shifts the corrosion potential to -815 mV vs SCE. The corrosion potential shift is very small. This suggests that the PD-Zn^{2+} formulation functions as a mixed inhibitor controlling the anodic reaction and cathodic reaction, to the same extent

The corrosion current value and LPR value for sea water are 6.354×10^{-6} A/cm^2 and 6.500 x 10^3 ohm cm^2. In the presence of the inhibitors, the corrosion current value has decreased to 5.848 x 10^{-6} A/cm^2, and the LPR value is increased to 6.988 x 10^3 ohm cm^2.This indicates that a protective film is formed on the metal surface, LPR value increases and corrosion current value decreases .

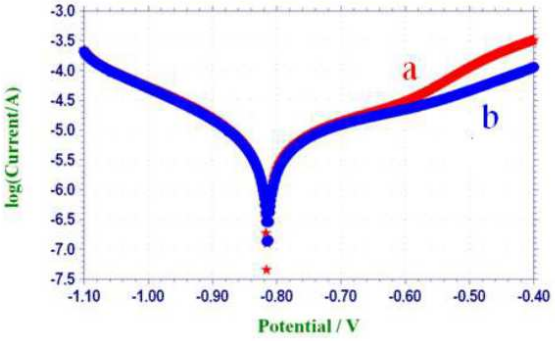

Fig..3.2 Polarization curves of carbon steel immersed in various test solutions

(a) Sea water

(b) Sea water containing 10mL of PD and 25 ppm of Zn^{2+}

Table3.3 Corrosion parameter of carbon steel immersed in sea water in the absence and presence of inhibitor system (PD-Zn^{2+}) obtained from polarization method

Inhibitor PD mL	**Zn^{2+} ppm**	**E_{corr} mVvs SCE**	**I_{corr} A/cm^2**	**b_a mV/dec**	**b_c mV/dec**	**LPR ohm cm^2**
0	0	-816	6.354×10^{-6}	239	157	6.500×10^3
10	25	-815	5.848×10^{-6}	239	154	6.988×10^3

3.4 Analysis of FTIR spectra

The main constituent of pippali dye is pipperine. The grey colour of the extract is due to Pipperine. The structure of pipperineis shown in Scheme 3.1 .The pippali dye extract was evaporated to dryness to get a solid mass. Its FTIR spectrum of the solid mass is shown in Fig 5.4.6a.The –OH stretching frequency appears at 3418cm^{-1}. The C=O stretching frequency appears at 1710cm^{-1}. Thus, Pippali dye was characterized by IR spectroscopy. The FTIR spectrum of the protective film formed on the surface of the metal after immersed in the solution containing 25 ppm of Zn^{2+} and 10mL of PD shown in Fig3.3.. It is found that the -OH has shifted from 3418 cm^{-1} to 3437 cm^{-1}. The C=O stretching frequency has decreased from 1710cm^{-1} to 1630cm^{-1}. It was inferred that PD has coordinated with Fe^{2+} through the phenolic oxygen and carbonyl oxygen, resulting in the formation of the Fe^{2+} - PD complex on the anodic sites of the metal surface. The peak at 1367cm^{-1} is due to Zn-O band. The peak at 3437cm^{-1} is due to –OH stretching. Hence it is confirmed that $Zn(OH)_2$ is formed on the cathodic sites of the metal surface.Thus, the FTIR spectral study leads to the conclusion that the protective film consists of the Fe^{2+}- PD complex and $Zn(OH)_2$ [6-25].

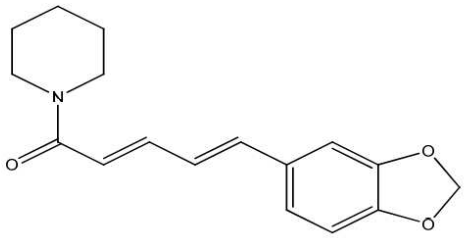

Piperine

Scheme.3.1. Structure of piperine

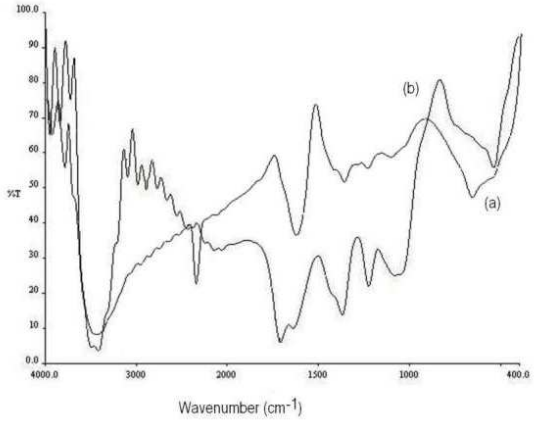

Fig.3.3 FTIR spectra

a) Pure PD

b) Film formed on metal surface after immersion in sea water containing 10mL of PD – 25 ppm Zn^{2+}

3.5 Mechanism of corrosion inhibition

In order to explain the corrosion inhibition of carbon steel immersed in sea water containing PD (10 mL)-Zn^{2+} (25 ppm) the following mechanism may be proposed.

- When the formulation consists of PD (10 mL)- Zn^{2+} (25 ppm) in sea water there is formation of Zn^{2+} -piperine complex in solution.
- When carbon steel is immersed in this solution piperine -Zn^{2+} complex diffuses from the bulk of the solution towards the metal surface.
- Piperine -Zn^{2+} complex is converted into piperine - Fe^{2+} complex on the anodic sites of the metal surface with the release of Zn^{2+} ion.

- Zn^{2+}- piperine + Fe^{2+} → Fe^{2+}- piperine + Zn^{2+}
- The released Zn^{2+} combines with OH^- to form $Zn(OH)_2$ on the cathodic sites of the metal surface.

  $$Zn^{2+} + 2OH^- \rightarrow Zn(OH)_{2\downarrow}$$

- Thus the protective film consists of piperine -Fe^{2+} complex and $Zn(OH)_2$.
- AFM images confirm the formation of protective layer on the metal surface.

References

[1] Raja P.B., Sethuraman M.G., Natural products as corrosion inhibitor for metal in corrosive Media – a review, Mater. Lett., 62, 113 -116 (2008)

[2] El Hosary A.A., Saleh R.M., Shams El Din A.M., Corrosion inhibition by naturally occurring Substances.I. Effect of Hibiscus subdariffa (karkade) extract on the dissolution of aluminum and Zinc, Corros. Sci., 12, 897-904 (1972)

[3] Saleh R.M., Ismail A.A., El Hosary A.A., Corrosion inhibition by naturally occurring Substances. V11. The effect of aqueous extracts of some leaves and fruit peels on the Corrosion of steel, aluminium, zinc and copper in acids, Br. Corros. J., 17, 131- 135 (1982)

[4].Saleh R.M., Ismail A.A., El Hosary A.A., Corrosion inhibition by naturally occurring Substances. V11. The effect of aqueous extracts of some seeds, leaves, fruits peels on the Corrosion of aluminium in sodium hydroxide, Corrs. Sci., 23, 1239 - 1241 (1983)

[5]. Ekpe U.J., Ebenso E.E., Ibok U.J., Inhibitory action of Azadirachta leaves extract on Corrosion of mild steel in tetraoxosulphate (VI) acid, J. West African Assoc., 37, 13-30 (1994)

[6]. C.A. Loto The effect of Vernonia amygdalina (bitter leaf) solution extract on the Corrosion inhibition of mild steel, Nig. Cor. J., 19, 20-28 (1998)

[7] S. Rajendran, M. Agasta, R. Bama Devi, B. Shyamala Devi, K. Rajam and J. Jayasundari, Zastita Materijala, 50 (2009) 77.

[8] T. Umamathi, J. Arockia Selvi, S. Agnesia Kanimozhi, S. Rajendran and A. John Amalraj, Indian J.Chem. Technol.,15 (2008) 560.

[9] Y.Y. Thangam, M. Kalanithe, C.M. Anbarasi and S. Rajendran, Arabian J. Sci. Engg., 34 (2009) 49.

[10] S.Rajendran, B.R.E.J. Peter, A.P.P. Regis, A.J. Amalraj and M.Sundaravadivelu, Transactions of the SAEST., 38 (2003) 11.

[11] S. Rajendran, S.M. Reinkala, N. Anthony and R. Ramaraj, *Corros Sci.,* **44** (2002)449.

[12] J. Sathyabama, S. Rajendran, J.A. Selvi and S. Jeyasundari, *Bulg. Chem. Commun.,* **41 (2009)** 374.

[13] Xianghong Li, Shuduan Deng, Hui Fu and Guannan Mu, *Corros. Sci.,* **50 (2008)** 2635.

[14] G.K. Gomma, *Mater. Chem. Phys.,* **55 (1998)** 241.

[15] K. Aramaki and Hackermann, J. Electrochem. Soc., 116 (1969).

[16] D. Gopi, S. Manimozhi, K.M. Govindaraju, P. Manisankar and S. Rajeswari, J. Appl. Electrochem.,37 (2007) 439.

[17] C.A. Loto, R.T. Loto and A.P.I. Popoola, Intl. J. Electrochem. Sci., 6 (2011) 3830.

[18] X.Li, S. Deng, H. Fu and G. Mu, Corros. Sci., 52 (2010) 1167.1

[19] M.Sangeetha, S. Rajendra4n, J. Sathiyabama, A.Krishnaveni, P. Shanthy, N. Manimaran, B. Shyamaladevi, Portugaliae Electrochim. Acta., 29 (2011) 429.

[20] S.Rajendran, A. Raji, J.Arockia Selvi, A.Rosaly and S.Thangasamy, *J. Mater.Edun.,* **29 (2007)** 245.

[21] S.Rajendran, A. Raji, J. Arockia Selvi, A. Rosaly and S. Thangasamy, *Edutracks.*, 6 **(2007)** 30.

[22] S.Merah, L. Larabi, O. Benali and Y. Harek, *Pigment Resin Technol.*, **37**(5) **(2008)** 291.

[23] H.Benita Sherine, A. Jamal Abdul Nasser and S. Rajendran, *In. J. Eng. Sci. Technol.*,**24 (2010)** 341.

[24] SS. Agnesia Kanimozhi and S. Rajendran, *Arab. J. Sci. Eng.*, **34 (2009)** 37.

[25] C.Mary Anbarasi and S. Rajendran. *J. Electrochem. Sci. Eng.*, **1(2011)** 15.

Received-10-09-2016

Accepted-16-09-2016

E. Amutha, Assistant Professor of Mathematics	International Journal of Current Research in Science and Technology	-	On Counting g-β Continues Functions	-	-	International 2394-5745	2017

International Journal of Current Research in Science and Technology
Volume 3, Issue 2 (2017), 1–11.
ISSN: 2394-5745
Available Online: http://ijcrst.in/

International Journal of Current Research in Science and Technology

On Contra $g\beta$-Continuous Functions

Research Article

K.Amutha[1], K.M.Dharmalingam[2] and O.Ravi[3]*

1 Department of Mathematics, Madurai Kamaraj University, Madurai, Tamil Nadu, India.
2 Department of Mathematics, The Madura College, Madurai, Tamil Nadu, India.
3 Department of Mathematics, P.M.Thevar College, Usilampatti, Madurai, Tamil Nadu, India.

Abstract: In this paper, we introduce and investigate the notion of contra $g\beta$-continuous functions by utilizing $g\beta$-closed sets [33]. We obtain fundamental properties of contra $g\beta$-continuous functions and discuss the relationships between contra $g\beta$-continuity and other related functions.

MSC: 54C08, 54C10, 54C05.

Keywords: $g\beta$-closed set, $g\beta$-continuous function, contra $g\beta$-continuous function, contra $g\beta$-graph, $g\beta$-normal space.

1. Introduction

In 1996, Dontchev [9] introduced a new class of functions called contra-continuous functions. He defined a function f : X → Y to be contra-continuous if the pre image of every open set of Y is closed in X. In 2007, Caldas et al. [4] introduced and investigated the notion of contra g-continuity. In 1968, Zaitsev [36] introduced the notion of π-open sets as a finite union of regular open sets. This notion received a proper attention and some research articles came to existence. Dontchev and Noiri [10] introduced and investigated π-continuity and πg-continuity. Ekici and Baker [11] studied further properties of πg-closed sets and continuities. In 2007, Ekici [12] introduced and studied some new forms of continuities. In [17], Kalantan introduced and investigated π-normality. The digital n-space is not a metric space, since it is not T_1. But recently Takigawa and Maki [34] showed that in the digital n-space every closed set is π-open. Recently, Ekici [13] introduced and studied contra πg-continuous functions. In 2010, Caldas et. al. [7] introduced and studied contra πgp-continuity.

In this paper, we present a new generalization of contra-continuity called contra $g\beta$-continuity. It turns out that the notion of contra $g\beta$-continuity is a weaker form of contra β-continuity and a stronger form of contra $\pi g\beta$-continuity [28].

2. Preliminaries

Throughout this paper, spaces (X, τ) and (Y, σ) (or simply X and Y) always mean topological spaces on which no separation axioms are assumed unless explicitly stated. Let A be a subset of a space X. The closure of A and the interior of A are denoted by cl(A) and int(A), respectively. A subset A of X is said to be regular open [31] (resp. regular closed [31]) if A

* *E-mail: siingam@yahoo.com*

= int(cl(A)) (resp. A = cl(int(A))). The finite union of regular open sets is said to be π-open [36]. The complement of a π-open set is said to be π-closed [36].

Definition 2.1. *A subset A of a space X is said to be*

(1) pre-closed [21] if cl(int(A)) ⊆ A;

(2) α-open [23] if A ⊆ int(cl(int(A)));

(3) semi-open [18] if A ⊆ cl(int(A));

(4) β-open [1] if A ⊆ cl(int(cl(A)));

(5) β-closed [1] if int(cl(int(A))) ⊆ A;

(6) g-closed [19] if cl(A) ⊆ U whenever A ⊆ U and U is open in X;

(7) gp-closed [26] if pcl(A) ⊆ U whenever A ⊆ U and U is open in X;

(8) gβ-closed [33] if βcl(A) ⊆ U whenever A ⊆ U and U is open in X;

(9) πgp-closed [27] if pcl(A) ⊆ U whenever A ⊆ U and U is π-open in X;

(10) πgβ-closed [32] if βcl(A) ⊆ U whenever A ⊆ U and U is π-open in X.

The complements of the above closed sets are called their respective open sets. The complements of the above open sets are called their respective closed sets. The intersection of all pre-closed (resp. β-closed) sets containing A is called pre-closure (resp. β-closure) of A and is denoted by pcl(A) (resp. βcl(A)). The family of all gβ-open (resp. gβ-closed, closed) sets of X containing a point x ∈ X is denoted by GβO(X, x) (resp. GβC(X, x), C(X, x)). The family of all gβ-open (resp. gβ-closed, closed, semi-open, β-open) sets of X is denoted by GβO(X) (resp. GβC(X), C(X), SO(X), βO(X)). Let A be a subset of a space (X, τ). The set $\bigcap \{U \in \tau : A \subseteq U\}$ is called the kernel of A [22] and is denoted by ker(A).

Lemma 2.2 ([16]). *The following properties hold for subsets U and V of a space (X, τ).*

(1) x ∈ ker(U) if and only if U ∩ F ≠ ∅ for any closed set F ∈ C(X, x);

(2) U ⊆ ker(U) and U = ker(U) if U is open in X;

(3) If U ⊆ V, then ker(U) ⊆ ker(V).

3. Contra $g\beta$-continuous Functions

Definition 3.1. *Let A be a subset of a space (X, τ).*

(1) The set $\bigcap \{F : F$ is gβ-closed in $X : A \subseteq F\}$ is called the gβ-closure of A and is denoted by gβ-cl(A).

(2) The set $\bigcup \{F : F$ is gβ-open in $X : A \supseteq F\}$ is called the gβ-interior of A and is denoted by gβ-int(A).

Lemma 3.2. *Let A be a subset of a space (X, τ), then*

(1) gβ-cl(X−A) = X−gβ-int(A);

(2) x ∈ gβ-cl(A) if and only if A ∩ U ≠ ∅ for each U ∈ GβO(X, x);

(3) If A is $g\beta$-closed in X, then A = $g\beta$-cl(A).

Remark 3.3. *If A = $g\beta$-cl(A), then A need not be a $g\beta$-closed.*

Example 3.4. *Let X = {a, b, c} and τ = {$\emptyset$, X, {a}}. Take A = {a}. Clearly $g\beta$-cl(A) = A but A is not $g\beta$-closed.*

Definition 3.5. *A function f : X → Y is called contra $g\beta$-continuous if $f^{-1}(V)$ is $g\beta$-closed in X for every open set V of Y.*

Theorem 3.6. *The following are equivalent for a function f : X → Y :*

(1) f is contra $g\beta$-continuous;

(2) The inverse image of every closed set of Y is $g\beta$-open in X;

(3) For each x ∈ X and each closed set V in Y with f(x) ∈ V, there exists a $g\beta$-open set U in X such that x ∈ U and f(U) ⊆ V;

(4) f($g\beta$-cl(A)) ⊆ ker(f(A)) for every subset A of X;

(5) $g\beta$-cl($f^{-1}(B)$) ⊆ f^{-1}(ker(B)) for every subset B of Y.

Proof.
(1) ⇒ (2): Let U be any closed set of Y. Since Y/U is open, then by (1), it follows that f^{-1}(Y/U) = X/f^{-1}(U) is $g\beta$-closed. This shows that f^{-1}(U) is $g\beta$-open in X.
(1) ⇒ (3): Let x ∈ X and V be a closed set in Y with f(x) ∈ V. By (1), it follows that f^{-1}(Y/V) = X/f^{-1}(V) is $g\beta$-closed and so f^{-1}(V) is $g\beta$-open. Take U = f^{-1}(V), we obtain that x ∈ U and f(U) ⊆ V.
(3) ⇒ (2): Let V be a closed set in Y with x ∈ f^{-1}(V). Since f(x) ∈ V, by (3) there exists a $g\beta$-open set U in X containing x such that f(U) ⊆ V. It follows that x ∈ U ⊆ f^{-1}(V). Hence f^{-1}(V) is $g\beta$-open.
(2) ⇒ (4): Let A be any subset of X. Let y ∉ ker(f(A)). Then by Lemma 2.2, there exist a closed set F containing y such that f(A) ∩ F = $\emptyset$. We have A ∩ f^{-1}(F) = $\emptyset$ and since f^{-1}(F) is $g\beta$-open then we have $g\beta$-cl(A) ∩ f^{-1}(F) = $\emptyset$. Hence we obtain f($g\beta$-cl(A)) ∩ F = $\emptyset$ and y ∉ f($g\beta$-cl(A)). Thus f($g\beta$-cl(A)) ⊆ ker(f(A)).
(4) ⇒ (5): Let B be any subset of Y. By (4), f($g\beta$-cl(f^{-1}(B))) ⊆ ker(B) and $g\beta$-cl(f^{-1}(B)) ⊆ f^{-1}(ker(B)).
(5) ⇒ (1): Let B be any open set of Y. By (5), $g\beta$-cl(f^{-1}(B)) ⊆ f^{-1}(ker(B)) = f^{-1}(B) and $g\beta$-cl(f^{-1}(B)) = f^{-1}(B). So we obtain that f^{-1}(B) is $g\beta$-closed in X. □

Definition 3.7. *A function f : X → Y is said to be*

(1) completely continuous [2] if $f^{-1}(V)$ is regular open in X for every open set V of Y;

(2) contra-continuous [9] (resp. contra pre-continuous [15], contra β-continuous [5]) if $f^{-1}(V)$ is closed (resp. pre-closed, β-closed) in X for every open set V of Y;

(3) contra g-continuous [4] (resp. contra gp-continuous [7]) if $f^{-1}(V)$ is g-closed (resp. gp-closed) in X for every open set V of Y;

(4) contra π-continuous [7] (resp. contra πgp-continuous [7], contra $\pi g\beta$-continuous [28] if $f^{-1}(V)$ is π-closed (resp. πgp-closed, $\pi g\beta$-closed) in X for every open set V of Y.

For the functions defined above, we have the following implications:

$$
\begin{array}{ccc}
\textbf{\textit{contra } π\textit{-continuity}} & & \\
\downarrow & & \\
\textbf{\textit{contra-continuity}} & \longrightarrow & \textbf{\textit{contra pre-continuity}} \\
\downarrow & & \downarrow \\
\textbf{\textit{contra } g\textit{-continuity}} & & \textbf{\textit{contra } β\textit{-continuity}} \\
\downarrow & & \downarrow \\
\textbf{\textit{contra } gp\textit{-continuity}} & \longrightarrow & \textbf{\textit{contra } $g\beta$\textit{-continuity}} \\
\downarrow & & \downarrow \\
\textbf{\textit{contra } πgp\textit{-continuity}} & \longrightarrow & \textbf{\textit{contra } $\pi g\beta$\textit{-continuity}}
\end{array}
$$

Remark 3.8. *None of these implications is reversible as shown by the following Examples and the related papers [5, 7, 28].*

Example 3.9. *Let $X = \{a, b, c\}$, $\tau = \{\emptyset, X, \{a\}\}$ and $\sigma = \{\emptyset, X, \{a\}, \{a, b\}\}$. Then the identity function $f : (X, \tau) \to (X, \sigma)$ is contra $\pi g\beta$-continuous but not contra $g\beta$-continuous.*

Example 3.10. *Let $X = \{a, b, c\}$, $\tau = \{\emptyset, X, \{a\}\}$ and $\sigma = \{\emptyset, X, \{a, b\}\}$. Then the identity function $f : (X, \tau) \to (X, \sigma)$ is contra $g\beta$-continuous but not contra β-continuous.*

Definition 3.11. *A function $f : X \to Y$ is said to be*

(1) $g\beta$-semiopen if $f(U) \in SO(Y)$ for every $g\beta$-open set U of X;

(2) contra-I($g\beta$)-continuous if for each $x \in X$ and each $F \in C(Y, f(x))$, there exists $U \in G\beta O(X, x)$ such that $int(f(U)) \subseteq F$.

(3) $g\beta$-continuous [6] if $f^{-1}(F)$ is $g\beta$-closed in X for every closed set F of Y.

Theorem 3.12. *If a function $f : X \to Y$ is contra-I($g\beta$)-continuous and $g\beta$-semiopen, then f is contra $g\beta$-continuous.*

Proof. Suppose that x ∈ X and F ∈ C(Y, f(x)). Since f is contra-I($g\beta$)-continuous, there exists U ∈ $G\beta O$(X, x) such that int(f(U)) ⊆ F. By hypothesis f is $g\beta$-semiopen, therefore f(U) ∈ SO(Y) and f(U) ⊆ cl(int(f(U))) ⊆ F. This shows that f is contra $g\beta$-continuous. □

Lemma 3.13. *For a subset A of (X, τ), the following statements are equivalent.*

(1) A is open and $g\beta$-closed;

(2) A is regular open.

Proof.
(1) ⇒ (2): Since A is open and $g\beta$-closed, βcl(A) ⊆ A. It implies that int(cl(int(A))) ⊆ A. Also, since A is α-open, A ⊆ int(cl(int(A))). Hence int(A) = A = int(cl(int(A))). Thus A is regular open.
(2) ⇒ (1): Since A is regular open, A is open and int(A) = A = int(cl(int(A))). Since int(cl(int(A))) ⊆ A, A is β-closed and so $g\beta$-closed. □

Theorem 3.14. *For a function $f : X \to Y$, the following statements are equivalent.*

(1) f is contra $g\beta$-continuous and continuous;

(2) f is completely continuous.

Proof.

(1) ⇒ (2): Let U be an open set in Y. Since f is contra $g\beta$-continuous and continuous, $f^{-1}(U)$ is $g\beta$-closed and open, by Lemma 3.13, $f^{-1}(U)$ is regular open. Then f is completely continuous.

(2) ⇒ (1): Let U be an open set in Y. Since f is completely continuous, $f^{-1}(U)$ is regular open, by Lemma 3.13, $f^{-1}(U)$ is $g\beta$-closed and open. Then f is contra $g\beta$-continuous and continuous. □

Definition 3.15.

(1) A subset A of a topological space X is said to be Q-set [20] if int(cl(A)) = cl(int(A)).

(2) Let $f : X \to Y$ be a function. Then f is called Q-continuous [35] (resp. perfectly continuous [24]) if $f^{-1}(U)$ is Q-set (resp. clopen) in X for each open set U of Y.

Lemma 3.16. *For a subset A of X, the following statements are equivalent:*

(1) A is clopen,

(2) A is open, Q-set and $g\beta$-closed.

Proof.

(1) ⇒ (2): Since A is clopen, A is open and closed. Thus A is Q-set. Since A is closed, A is $g\beta$-closed.

(2) ⇒ (1): Since A is open and $g\beta$-closed, by Lemma 3.13, A is regular open. Since A is regular open and Q-set, A = int(cl(A)) = cl(int(A)). Hence A is regular closed and so closed. Since A is open and closed, A is clopen. □

Theorem 3.17. *For a function $f : X \to Y$, the following statements are equivalent.*

(1) f is perfectly continuous;

(2) f is continuous, Q-continuous and contra $g\beta$-continuous.

Proof. It is obtained from the above Lemma. □

Theorem 3.18. *If a function $f : X \to Y$ is contra $g\beta$-continuous and Y is regular, then f is $g\beta$-continuous.*

Proof. Let x be an arbitrary point of X and U be an open set of Y containing f(x). Since Y is regular, there exists an open set W in Y containing f(x) such that cl(W) ⊆ U. Since f is contra $g\beta$-continuous, there exists $V \in G\beta O(X, x)$ such that f(V) ⊆ cl(W). Then f(V) ⊆ cl(W) ⊆ U. Hence f is $g\beta$-continuous. □

Theorem 3.19. *Let $\{X_i : i \in \Omega\}$ be any family of topological spaces. If a function $f : X \to \prod X_i$ is contra $g\beta$-continuous, then $Pr_i \ o \ f : X \to X_i$ is contra $g\beta$-continuous for each $i \in \Omega$, where Pr_i is the projection of $\prod X_i$ onto X_i.*

Proof. For a fixed $i \in \Omega$, let V_i be any open set of X_i. Since Pr_i is continuous, $Pr_i^{-1}(V_i)$ is open in $\prod X_i$. Since f is contra $g\beta$-continuous, $f^{-1}(Pr_i^{-1}(V_i)) = (Pr_i \ o \ f)^{-1}(V_i)$ is $g\beta$-closed in X. Therefore, Pr_i *o* f is contra $g\beta$-continuous for each $i \in \Omega$. □

Theorem 3.20. *Let $f : X \to Y$ and $g : Y \to Z$ be a function. Then the following hold:*

(1) If f is contra $g\beta$-continuous and g is continuous, then $g \ o \ f : X \to Z$ is contra $g\beta$-continuous;

(2) If f is $g\beta$-continuous and g is contra-continuous, then $g \ o \ f : X \to Z$ is contra $g\beta$-continuous;

(3) If f is contra $g\beta$-continuous and g is contra-continuous, then $g \ o \ f : X \to Z$ is $g\beta$-continuous.

Definition 3.21. *A space (X, τ) is called $g\beta$-$T_{1/2}$ if every $g\beta$-closed set is β-closed.*

Theorem 3.22. *Let $f : X \to Y$ be a function. Suppose that X is a $g\beta$-$T_{1/2}$ space. Then the following are equivalent.*

(1) f is contra $g\beta$-continuous;

(2) f is contra β-continuous.

Definition 3.23. *For a space (X, τ), ${}_g\tau^\beta = \{U \subseteq X : g\beta\text{-}cl(X\backslash U) = X\backslash U\}$.*

Theorem 3.24. *Let (X, τ) be a space. Then*

(1) Every $g\beta$-closed set is β-closed (i.e. (X, τ) is $g\beta$-$T_{1/2}$) if and only if ${}_g\tau^\beta = \beta O(X)$;

(2) Every $g\beta$-closed set is closed if and only if ${}_g\tau^\beta = \tau$.

Proof.
(1) Let $A \in {}_g\tau^\beta$. Then $g\beta$-cl(X\A) = X\A. By hypothesis, βcl(X\A) = $g\beta$-cl(X\A) = X\A and hence $A \in \beta O(X)$. Conversely, let A be a $g\beta$-closed set. Then $g\beta$-cl(A) = A and hence $X\backslash A \in {}_g\tau^\beta = \beta O(X)$, i.e. A is β-closed.
(2) Similar to (1). □

Theorem 3.25. *If ${}_g\tau^\beta = \tau$ in X, then for a function $f : X \to Y$ the following are equivalent:*

(1) f is contra $g\beta$-continuous;

(2) f is contra gp-continuous;

(3) f is contra g-continuous;

(4) f is contra-continuous.

Theorem 3.26. *If ${}_g\tau^\beta = \tau$ in X, then for a function $f : X \to Y$ the following are equivalent:*

(1) f is contra $g\beta$-continuous;

(2) f is contra β-continuous;

(3) f is contra pre-continuous;

(4) f is contra-continuous.

4. Properties of Contra $g\beta$-continuous Functions

Definition 4.1. *A space X is said to be $g\beta$-T_1 if for each pair of distinct points x and y in X, there exist $g\beta$-open sets U and V containing x and y respectively, such that $y \notin U$ and $x \notin V$.*

Definition 4.2. *A space X is said to be $g\beta$-T_2 if for each pair of distinct points x and y in X, there exist $U \in G\beta O(X, x)$ and $V \in G\beta O(X, y)$ such that $U \cap V = \emptyset$.*

Theorem 4.3. *Let X be a topological space. Suppose that for each pair of distinct points x_1 and x_2 in X, there exists a function f of X into a Urysohn space Y such that $f(x_1) \neq f(x_2)$. Moreover, let f be contra $g\beta$-continuous at x_1 and x_2. Then X is $g\beta$-T_2.*

Proof. Let x_1 and x_2 be any distinct points in X. Then suppose that there exist an Urysohn space Y and a function f : X → Y such that $f(x_1) \neq f(x_2)$ and f is contra $g\beta$-continuous at x_1 and x_2. Let $w = f(x_1)$ and $z = f(x_2)$. Then $w \neq z$. Since Y is Urysohn, there exist open sets U and V containing w and z, respectively such that $cl(U) \cap cl(V) = \emptyset$. Since f is contra $g\beta$-continuous at x_1 and x_2, then there exist $g\beta$-open sets A and B containing x_1 and x_2, respectively such that $f(A) \subseteq cl(U)$ and $f(B) \subseteq cl(V)$. So we have $A \cap B = \emptyset$ since $cl(U) \cap cl(V) = \emptyset$. Hence, X is $g\beta$-T_2. □

Corollary 4.4. *If f is a contra $g\beta$-continuous injection of a topological space X into a Urysohn space Y, then X is $g\beta$-T_2.*

Proof. For each pair of distinct points x_1 and x_2 in X and f is contra $g\beta$-continuous function of X into a Urysohn space Y such that $f(x_1) \neq f(x_2)$ because f is injective. Hence by Theorem 4.3, X is $g\beta$-T_2. □

Definition 4.5. *A space (X, τ) is said to be $g\beta$-connected if X cannot be expressed as the disjoint union of two non-empty $g\beta$-open sets.*

Remark 4.6. *Every $g\beta$-connected space is connected.*

Theorem 4.7. *For a space X, the following are equivalent:*

(1) X is $g\beta$-connected;

(2) The only subsets of X which are both $g\beta$-open and $g\beta$-closed are the empty set $\emptyset$ and X;

(3) Each contra $g\beta$-continuous function of X into a discrete space Y with at least two points is a constant function.

Proof. (1) ⇒ (2): Suppose $S \subset X$ is a proper subset which is both $g\beta$-open and $g\beta$-closed. Then its complement $X - S$ is also $g\beta$-open and $g\beta$-closed. Then $X = S \cup (X - S)$, a disjoint union of two non-empty $g\beta$-open sets which contradicts the fact that X is $g\beta$-connected. Hence, $S = \emptyset$ or X.

(2) ⇒ (1): Suppose $X = A \cup B$ where $A \cap B = \emptyset$, $A \neq \emptyset$, $B \neq \emptyset$ and A and B are $g\beta$-open. Since $A = X - B$, A is $g\beta$-closed. But by assumption $A = \emptyset$ or X, which is a contradiction. Hence (1) holds.

(2) ⇒ (3): Let f : X → Y be contra $g\beta$-continuous function where Y is a discrete space with at least two points. Then $f^{-1}(\{y\})$ is $g\beta$-closed and $g\beta$-open for each $y \in Y$ and $X = \bigcup \{f^{-1}(y) : y \in Y\}$. By hypothesis, $f^{-1}(\{y\}) = \emptyset$ or X. If $f^{-1}(\{y\}) = \emptyset$ for all $y \in Y$, then f is not a function. Also there cannot exist more than one $y \in Y$ such that $f^{-1}(\{y\}) = X$. Hence there exists only one $y \in Y$ such that $f^{-1}(\{y\}) = X$ and $f^{-1}(\{y_1\}) = \emptyset$ where $y \neq y_1 \in Y$. This shows that f is a constant function.

(3) ⇒ (2): Let P be a non-empty set which is both $g\beta$-open and $g\beta$-closed in X. Suppose f : X → Y is a contra $g\beta$-continuous function defined by $f(P) = \{a\}$ and $f(X \backslash P) = \{b\}$ where $a \neq b$ and $a, b \in Y$. By hypothesis, f is constant. Therefore $P = X$. □

Definition 4.8. *A subset A of a space (X, τ) is said to be $g\beta$-clopen if A is both $g\beta$-open and $g\beta$-closed.*

Theorem 4.9. *If f is a contra $g\beta$-continuous function from a $g\beta$-connected space X onto any space Y, then Y is not a discrete space.*

Proof. Suppose that Y is discrete. Let A be a proper non-empty open and closed subset of Y. Then $f^{-1}(A)$ is a proper non-empty $g\beta$-clopen subset of X which is a contradiction to the fact that X is $g\beta$-connected. □

Theorem 4.10. *If $f : X \to Y$ is a contra $g\beta$-continuous surjection and X is $g\beta$-connected, then Y is connected.*

Proof. Suppose that Y is not a connected space. There exist non-empty disjoint open sets U_1 and U_2 such that $Y = U_1 \cup U_2$. Therefore U_1 and U_2 are clopen in Y. Since f is contra $g\beta$-continuous, $f^{-1}(U_1)$ and $f^{-1}(U_2)$ are $g\beta$-open in X. Moreover, $f^{-1}(U_1)$ and $f^{-1}(U_2)$ are non-empty disjoint and $X = f^{-1}(U_1) \cup f^{-1}(U_2)$. This shows that X is not $g\beta$-connected. This contradicts that Y is not connected assumed. Hence Y is connected. □

Definition 4.11. *The graph G(f) of a function $f : X \to Y$ is said to be contra $g\beta$-graph if for each $(x, y) \in (X \times Y) \backslash G(f)$, there exist a $g\beta$-open set U in X containing x and a closed set V in Y containing y such that $(U \times V) \cap G(f) = \emptyset$.*

Lemma 4.12. *A graph G(f) of a function $f : X \to Y$ is contra $g\beta$-graph in $X \times Y$ if and only if for each $(x, y) \in (X \times Y) \backslash G(f)$, there exist a $U \in G\beta O(X)$ containing x and $V \in C(Y)$ containing y such that $f(U) \cap V = \emptyset$.*

Theorem 4.13. *If $f : X \to Y$ is contra $g\beta$-continuous and Y is Urysohn, G(f) is contra $g\beta$-graph in $X \times Y$.*

Proof. Let $(x, y) \in (X \times Y) \backslash G(f)$. It follows that $f(x) \neq y$. Since Y is Urysohn, there exist open sets V and W such that $f(x) \in V$, $y \in W$ and $cl(V) \cap cl(W) = \emptyset$. Since f is contra $g\beta$-continuous, there exist a $U \in G\beta O(X, x)$ such that $f(U) \subseteq cl(V)$ and $f(U) \cap cl(W) = \emptyset$. Hence G(f) is contra $g\beta$-graph in $X \times Y$. □

Theorem 4.14. *Let $f : X \to Y$ be a function and $g : X \to X \times Y$ the graph function of f, defined by $g(x) = (x, f(x))$ for every $x \in X$. If g is contra $g\beta$-continuous, then f is contra $g\beta$-continuous.*

Proof. Let U be an open set in Y, then $X \times U$ is an open set in $X \times Y$. It follows that $f^{-1}(U) = g^{-1}(X \times U) \in G\beta C(X)$. Thus f is contra $g\beta$-continuous. □

Definition 4.15. *A space (X, τ) is said to be submaximal [3] if every dense subset of X is open in X and extremally disconnected [25] if the closure of every open set is open.*

Note that (X, τ) is submaximal and extremally disconnected if and only if every β-open set in X is open [14].

Theorem 4.16. *If A and B are $g\beta$-closed sets in submaximal and extremally disconnected space (X, τ), then $A \cup B$ is $g\beta$-closed.*

Proof. Let $A \cup B \subseteq U$ and U be open in (X, τ). Since $A, B \subseteq U$ and A and B are $g\beta$-closed, $\beta cl(A) \subseteq U$ and $\beta cl(B) \subseteq U$. Since (X, τ) is submaximal and extremally disconnected, $\beta cl(F) = cl(F)$ for any set $F \subseteq X$. Now $\beta cl(A \cup B) = \beta cl(A) \cup \beta cl(B) \subseteq U$. Hence $A \cup B$ is $g\beta$-closed. □

Lemma 4.17. *Let (X, τ) be a topological space. If $U, V \in G\beta O(X)$ and X is submaximal and extremally disconnected space, then $U \cap V \in G\beta O(X)$.*

Proof. Let $U, V \in G\beta O(X)$. We have $X \backslash U, X \backslash V \in G\beta C(X)$. By Theorem 4.16, $(X \backslash U) \cup (X \backslash V) = X \backslash (U \cap V) \in G\beta C(X)$. Thus, $U \cap V \in G\beta O(X)$. □

Theorem 4.18. *If $f : X \to Y$ and $g : X \to Y$ are contra $g\beta$-continuous, X is submaximal and extremally disconnected and Y is Urysohn, then $K = \{x \in X : f(x) = g(x)\}$ is $g\beta$-closed in X.*

Proof. Let $x \in X \backslash K$. Then $f(x) \neq g(x)$. Since Y is Urysohn, there exist open sets U and V such that $f(x) \in U$, $g(x) \in V$ and $cl(U) \cap cl(V) = \emptyset$. Since f and g are contra $g\beta$-continuous, $f^{-1}(cl(U)) \in G\beta O(X)$ and $g^{-1}(cl(V)) \in G\beta O(X)$. Let $A = f^{-1}(cl(U))$ and $B = g^{-1}(cl(V))$. Then A and B contains x. Set $C = A \cap B$. C is $g\beta$-open in X. Hence $f(C) \cap g(C) = \emptyset$ and $x \notin g\beta\text{-}cl(K)$. Thus K is $g\beta$-closed in X. □

Definition 4.19. *A subset A of a topological space X is said to be $g\beta$-dense in X if $g\beta\text{-}cl(A) = X$.*

Theorem 4.20. *Let $f : X \to Y$ and $g : X \to Y$ be contra $g\beta$-continuous. If Y is Urysohn and $f = g$ on a $g\beta$-dense set $A \subseteq X$, then $f = g$ on X.*

Proof. Since f and g are contra $g\beta$-continuous and Y is Urysohn, by Theorem 4.18, K = {x ∈ X : f(x) =g(x)} is $g\beta$-closed in X. We have f = g on $g\beta$-dense set A ⊆ X. Since A ⊆ K and A is $g\beta$-dense set in X, then X = $g\beta$-cl(A) ⊆ $g\beta$-cl(K) = K. Hence, f = g on X. □

Definition 4.21. *A space X is said to be weakly Hausdroff [29] if each element of X is an intersection of regular closed sets.*

Theorem 4.22. *If $f : X \to Y$ is a contra $g\beta$-continuous injection and Y is weakly Hausdroff, then X is $g\beta$-T_1.*

Proof. Suppose that Y is weakly Hausdroff. For any distinct points x_1 and x_2 in X, there exist regular closed sets U and V in Y such that $f(x_1) \in U$, $f(x_2) \notin U$, $f(x_1) \notin V$ and $f(x_2) \in V$. Since f is contra $g\beta$-continuous, $f^{-1}(U)$ and $f^{-1}(V)$ are $g\beta$-open subsets of X such that $x_1 \in f^{-1}(U)$, $x_2 \notin f^{-1}(U)$, $x_1 \notin f^{-1}(V)$ and $x_2 \in f^{-1}(V)$. This shows that X is $g\beta$-T_1. □

Theorem 4.23. *Let $f : X \to Y$ have a contra $g\beta$-graph. If f is injective, then X is $g\beta$-T_1.*

Proof. Let x_1 and x_2 be any two distinct points of X. Then, we have $(x_1, f(x_2)) \in (X \times Y) \backslash G(f)$. Then, there exist a $g\beta$-open set U in X containing x_1 and $F \in C(Y, f(x_2))$ such that $f(U) \cap F = \emptyset$. Hence $U \cap f^{-1}(F) = \emptyset$. Therefore, we have $x_2 \notin U$. This implies that X is $g\beta$-T_1. □

Definition 4.24. *A topological space X is said to be Ultra Hausdroff [30] if for each pair of distinct points x and y in X, there exist clopen sets A and B containing x and y, respectively such that $A \cap B = \emptyset$.*

Theorem 4.25. *Let $f : X \to Y$ be a contra $g\beta$-continuous injection. If Y is an Ultra Hausdroff space, then X is $g\beta$-T_2.*

Proof. Let x_1 and x_2 be any distinct points in X, then $f(x_1) \neq f(x_2)$ and there exist clopen sets U and V containing $f(x_1)$ and $f(x_2)$ respectively, such that $U \cap V = \emptyset$. Since f is contra $g\beta$-continuous, then $f^{-1}(U) \in G\beta O(X)$ and $f^{-1}(V) \in G\beta O(X)$ such that $f^{-1}(U) \cap f^{-1}(V) = \emptyset$. Hence, X is $g\beta$-T_2. □

Definition 4.26. *A topological space X is said to be*

(1) $g\beta$-normal if each pair of non-empty disjoint closed sets can be separated by disjoint $g\beta$-open sets.

(2) Ultra normal [30] if for each pair of non-empty disjoint closed sets can be separated by disjoint clopen sets.

Theorem 4.27. *If $f : X \to Y$ is a contra $g\beta$-continuous, closed injection and Y is Ultra normal, then X is $g\beta$-normal.*

Proof. Let F_1 and F_2 be disjoint closed subsets of X. Since f is closed and injective, $f(F_1)$ and $f(F_2)$ are disjoint closed subsets of Y. Since Y is Ultra normal, $f(F_1)$ and $f(F_2)$ are separated by disjoint clopen sets V_1 and V_2, respectively. Hence $F_i \subseteq f^{-1}(V_i)$, $f^{-1}(V_i) \in G\beta O(X, x)$ for i = 1, 2 and $f^{-1}(V_1) \cap f^{-1}(V_2) = \emptyset$ and thus X is $g\beta$-normal. □

References

[1] M.E.Abd El-Monsef, S.N.El-Deeb and R.A.Mahmoud, *β-open sets and β-continuous mappings*, Bull. Fac. Sci. Assiut Univ., 12(1983), 77-90.

[2] S.P.Arya and R.Gupta, *On strongly continuous mappings*, Kyungpook Math. J., 14(1974), 131-143.

[3] N.Bourbaki, *General topology*, Part I, Reading, Ma: Addison wesley, Paris, (1966).

[4] M.Caldas, S.Jafari, T.Noiri and M.Simoes, *A new generalization of contra-continuity via Levine's g-closed sets*, Chaos Solitons and Fractals, 32(2007), 1597-1603.

[5] M.Caldas and S.Jafari, *Some properties of contra-β-continuous functions*, Mem. Fac. Sci. Kochi Univ. (Math.)., 22(2001), 19-28.

[6] M.Caldas and S.Jafari, *On rarely $g\beta$-continuous functions*, An. Stiint. Univ. Al. I. Cuza Iasi, Ser. Noua, Mat., 60(2005), 337-344.

[7] M.Caldas, S.Jafari, K.Viswanathan and S.Krishnaprakash, *On contra πgp-continuous functions*, Kochi J. Math., 5(2010), 67-78.

[8] R.Devi, K.Balachandran and H.Maki, *Semi-generalized closed maps and generalized semi-closed maps*, Mem. Fac. Kochi Univ. Ser. A. Math., 14(1993), 41-54.

[9] J.Dontchev, *Contra-continuous functions and strongly S-closed spaces*, Internat. J. Math. and Math. Sci., 19(1996), 303-310.

[10] J.Dontchev and T.Noiri, *Quasi-normal spaces and πg-closed sets*, Acta Math. Hungar., 89(3)(2000), 211-219.

[11] E.Ekici and C.W.Baker, *On πg-closed sets and continuity*, Kochi J. Math., 2(2007), 35-42.

[12] E.Ekici, *On (g, s)-continuous and (πg, s)-continuous functions*, Sarajevo J. Math., 3(15)(2007), 99-113.

[13] E.Ekici, *On contra πg-continuous functions*, Chaos Solitons and Fractals, 35(2008), 71-81.

[14] M.Ganster and D.Andrijevic, *On some questions concerning semi-preopen sets*, J. Inst. Math. Compu. Sci. Math., 1(1988), 65-75.

[15] S.Jafari and T.Noiri, *On contra precontinuous functions*, Bull. Malaysian Math. Sci. Soc., 25(2002), 115-128.

[16] S.Jafari and T.Noiri, *Contra-super-continuous functions*, Ann. Univ. Sci. Budapest. Eotvos Sect. Math., 42(1999), 27-34.

[17] L.N.Kalantan, *π-normal topological spaces*, Filomat., 22(1)(2008), 173-181.

[18] N.Levine, *Semi-open sets and semi-continuity in topological spaces*, Amer. Math. Monthly, 70(1963), 36-41.

[19] N.Levine, *Generalized closed sets in topology*, Rend. Circ. Mat. Palermo, 19(2)(1970), 89-96.

[20] N.Levine, *On the commutivity of the closure and interior operator in the topological spaces*, Amer. Math. Monthly, 68(1961), 474-477.

[21] A.S.Mashour, M.E.Abd El-Monsef and S.N.El-Deeb, *On precontinuous and weak precontinuous mappings*, Proc. Math. Phys. Soc. Egypt., 53(1982), 47-53.

[22] M.Mrsevic, *On pairwise R_0 and pairwise R_1 bitopological spaces*, Bull. Math. Soc. Sci. Math RS Roumanie. (N.S) 30(78)(2)(1986), 141-148.

[23] O.Njastad, *On some classes of nearly open sets*, Pacific J. Math., 15(1965), 961-970.

[24] T.Noiri, *Super-continuity and some strong forms of continuity*, Indian J. Pure Appl. Math., 15(1984), 241-250.

[25] T.Noiri, *Characterizations of extremally disconnected spaces*, Indian J. Pure Appl. Math., 19(4)(1988), 325-329.

[26] T.Noiri, H.Maki and J.Umehara, *Generalized preclosed functions*, Mem. Fac. Sci. Kochi Univ. Ser. A Math., 19(1998), 13-20.

[27] J.H.Park, M.J.Son and B.Y.Lee, *On πgp-closed sets in topological spaces*, Indian J. Pure Appl. Math., (In press).

[28] O.Ravi, S.Margaret Parimalam, A.Pandi and S.Murugesan, *On contra $\pi g\beta$-continuous functions*, Submitted.

[29] T.Soundararajan, *Weakly Hausdroff spaces and the cardinality of topological spaces*, 1971 General Topology and its Relation to Modern Analysis and Algebra. III, (Proc. Conf. Kanpur, 1968). Academia. Prague 1971, 301-306.

[30] R.Staum, *The algebra of bounded continuous functions into a nonarchimedean field*, Pacific J. Math., 50(1974), 169-185.

[31] M.H.Stone, *Applications of the theory of Boolean rings to general topology*, Trans. Amer. Math. Soc., 41(1937), 375-481.

[32] S.Tahiliani, *On $\pi g\beta$-closed sets in topological spaces*, Note Di Mat., 30(1)(2010), 49-55.

[33] S.Tahiliani, *Generalized β-closed functions*, Bull. Cal. Math. Soc., 98(4)(2006), 367-376.

[34] S.Takigawa and H.Maki, *Every nonempty open set of the digital n-space is expressible as the union of finitely many nonempty regular open sets*, Sci. Math. Jpn., 67(2008), 365-376.

[35] K.V.Tamil Selvi, P.Thangaraj and O.Ravi, *On contra $g\gamma$-continuous functions*, Submitted.

[36] V.Zaitsev, *On certain classes of topological spaces and their bicompactifications*, Dokl. Akad. Nauk. SSSR, 178(1968), 778-779.

E. Amutha, Assistant Professor of Mathematics	International Journal of Current Research in Science and Technology	-	Weakly g-w Closed sets	-	-	International 2394-5745	2017

International Journal of Current Research in Science and Technology
Volume 3, Issue 3 (2017), 9–14.
ISSN: 2394-5745
Available Online: http://ijcrst.in/

International Journal of Current Research in Science and Technology

Weakly g-ω-closed Sets

Research Article

K.Amutha[1], K.M.Dharmalingam[2] and O.Ravi[3]*

1 Department of Mathematics, Madurai Kamaraj University, Madurai, Tamil Nadu, India.
2 Department of Mathematics, The Madura College, Madurai, Tamil Nadu, India.
3 Department of Mathematics, P.M.Thevar College, Usilampatti, Madurai, Tamil Nadu, India.

Abstract: In this paper, another generalized class of τ called weakly g-ω-closed sets is studied and the notion of weakly g-ω-open sets in topological spaces is also studied. The relationships of weakly g-ω-closed sets with various other sets are investigated.

MSC: 54A05, 54A10.

Keywords: τ, generalized class, weakly g-ω-closed set, topological space, generalized closed set, g-ω-closed set, preclosed set, preopen set.

1. Introduction

The first step of generalizing closed sets (briefly, g-closed sets) was done by Levine in 1970 [6]. He defined a subset S of a topological space (X, τ) to be g-closed if its closure is contained in every open superset of S. As the weak form of g-closed sets, the notion of weakly g-closed sets was introduced and studied by Sundaram and Nagaveni [11]. Sundaram and Pushpalatha [12] introduced and studied the notion of strongly g-closed sets, which are weaker than closed sets and stronger than g-closed sets. Park and Park [9] introduced and studied the notion of mildly g-closed sets, which is properly placed between the class of strongly g-closed sets and the class of weakly g-closed sets. Moreover, the relations with other notions directly or indirectly connected with g-closed sets were investigated by them. The notion of ω-open sets in topological spaces introduced by Hdeib [4] has been studied in recent years by a good number of researchers like Noiri et al [8], Al-Omari and Noorani [1, 2] and Khalid Y. Al-Zoubi [5]. The main aim of this paper is to study another generalized class of τ called weakly g-ω-open sets in topological spaces. Moreover, this generalized class of τ generalize g-ω-open sets and weakly g-ω-open sets. The relationships of weakly g-ω-closed sets with various other sets are discussed.

2. Preliminaries

Throughout this paper, $\mathbb{R}$ (resp. $\mathbb{Q}$, $(\mathbb{R}-\mathbb{Q})$, $(\mathbb{R}-\mathbb{Q})_-$ and $(\mathbb{R}-\mathbb{Q})_+$) denotes the set of real numbers (resp. the set of rational numbers, the set of irrational numbers, the set of negative irrational numbers and the set of positive irrational numbers). In this paper, (X, τ) represents a topological space on which no separation axioms are assumed unless explicitly stated. The closure and interior of a subset G of a topological space (X, τ) will be denoted by $cl(G)$ and $int(G)$, respectively.

* *E-mail: siingam@yahoo.com*

Definition 2.1. *A subset G of a topological space (X, τ) is said to be*

(1). g-closed [6] if $cl(G) \subseteq H$ whenever $G \subseteq H$ and H is open in X;

(2). g-open [6] if $X \backslash G$ is g-closed;

(3). weakly g-closed [11] if $cl(int(G)) \subseteq H$ whenever $G \subseteq H$ and H is open in X;

(4). strongly g-closed [12] if $cl(G) \subseteq H$ whenever $G \subseteq H$ and H is g-open in X.

Definition 2.2 ([14]). *In a topological space (X, τ), a point p in X is called a condensation point of a subset H if for each open set U containing p, $U \cap H$ is uncountable.*

Definition 2.3 ([4]). *A subset H of a topological space (X, τ) is called ω-closed if it contains all its condensation points. The complement of an ω-closed set is called ω-open.*

It is well known that a subset W of a topological space (X, τ) is ω-open if and only if for each $x \in W$, there exists $U \in \tau$ such that $x \in U$ and $U - W$ is countable. The family of all ω-open sets, denoted by τ_ω, is a topology on X, which is finer than τ. The interior and closure operator in (X, τ_ω) are denoted by int_ω and cl_ω respectively.

Lemma 2.4 ([4]). *Let H be a subset of a topological space (X, τ). Then*

(1). H is ω-closed in X if and only if $H = cl_\omega(H)$.

(2). $cl_\omega(X \backslash H) = X \backslash int_\omega(H)$.

(3). $cl_\omega(H)$ is ω-closed in X.

(4). $x \in cl_\omega(H)$ if and only if $H \cap G \neq \phi$ for each ω-open set G containing x.

(5). $cl_\omega(H) \subseteq cl(H)$.

(6). $int(H) \subseteq int_\omega(H)$.

Lemma 2.5 ([5]). *If A is an ω-open subset of a space (X, τ), then $A - C$ is ω-open for every countable subset C of X.*

Definition 2.6. *A subset G of a topological space (X, τ) is said to be*

(1). preopen [7] if $G \subseteq int(cl(G))$.

(2). preclosed [7] if $X \backslash G$ is preopen (or) $cl(int(G)) \subseteq G$.

(3). g-ω-closed [13] if $cl(G) \subseteq H$ whenever $G \subseteq H$ and H is ω-open in (X, τ).

(4). regular closed [10] if $G = cl(int(G))$.

Definition 2.7 ([3]). *In a topological space (X, τ), a subset G of X is said to be weakly g-ω-closed if $cl(int(G)) \subseteq H$ whenever $G \subseteq H$ and H is ω-open in X.*

Example 2.8 ([3]). *In $\mathbb{R}$ with the topology $\tau = \{\phi, \mathbb{R}, \mathbb{Q}\}$,*

(1). For $G = \mathbb{R} - \mathbb{Q}$, if H is any ω-open subset of $\mathbb{R}$ such that $G \subseteq H$, then $cl(int(G)) = cl(\phi) = \phi \subseteq H$ and hence G is weakly g-ω-closed in X.

(2). $K = \mathbb{Q} \subseteq \mathbb{Q}$, $\mathbb{Q}$ being ω-open whereas $cl(int(\mathbb{Q})) = cl(\mathbb{Q}) = \mathbb{R} \nsubseteq \mathbb{Q}$ which implies $K = \mathbb{Q}$ is not weakly g-ω-closed in X.

Definition 2.9 ([3]). *A subset G in a topological space (X,τ) is said to be weakly g-ω-open if $X\backslash G$ is weakly g-ω-closed.*

Theorem 2.10 ([3]). *In a topological space (X,τ), a subset G of X is weakly g-ω-closed $\Leftrightarrow cl(int(G)) \subseteq G$.*

Proposition 2.11 ([3]). *In a topological space (X,τ), every g-ω-closed set is weakly g-ω-closed but not conversely.*

Theorem 2.12 ([13]). *In a topological space (X,τ), a subset G is closed if and only if it is g-ω-closed.*

Theorem 2.13 ([13]). *In a topological space (X,τ), every g-ω-closed set is g-closed but not conversely.*

3. Properties of Weakly g-ω-closed Sets

Theorem 3.1. *In a topological space (X,τ), for a subset G of X, the following properties are equivalent.*

(1). G is weakly g-ω-closed;

(2). $cl(int(G))\backslash G = \phi$;

(3). $cl(int(G)) \subseteq G$;

(4). G is preclosed.

Proof.
(1) $\Leftrightarrow$ (2) G is weakly g-ω-closed $\Leftrightarrow cl(int(G)) \subseteq G$ by Theorem 2.10 $\Leftrightarrow cl(int(G))\backslash G = \phi$.
(2) $\Leftrightarrow$ (3) $cl(int(G))\backslash G = \phi \Leftrightarrow cl(int(G)) \subseteq G$.
(3) $\Leftrightarrow$ (4) $cl(int(G)) \subseteq G \Leftrightarrow G$ is preclosed by (2) of Definition 2.6. □

Theorem 3.2. *In a topological space (X,τ), if G is weakly g-ω-closed, then $G \cup (X - cl(int(G)))$ is weakly g-ω-closed.*

Proof. Since G is weakly g-ω-closed, $cl(int(G)) \subseteq G$ by Theorem 2.10. Then $X - G \subseteq X - cl(int(G))$ and $G \cup (X - G) \subseteq G \cup (X - cl(int(G)))$. Thus $X \subseteq G \cup (X - cl(int(G)))$ and so $G \cup (X - cl(int(G))) = X$. Hence $G \cup (X - cl(int(G)))$ is weakly g-ω-closed. □

Theorem 3.3. *In a topological space (X,τ), the following properties are equivalent:*

(1). G is a closed and an open set,

(2). G is a regular closed and an open set,

(3). G is a weakly g-ω-closed and an open set.

Proof.
(1) $\Rightarrow$ (2): Since G is closed and open, $G = cl(G)$ and $G = int(G)$. Thus $G = cl(int(G))$ and $G = int(G)$. Hence G is regular closed and open.
(2) $\Rightarrow$ (3): Since G is regular closed and open, $G = cl(int(G))$. Thus $cl(int(G)) \subseteq G$. By Theorem 2.10, G is weakly g-ω-closed and open.
(3) $\Rightarrow$ (1): Since G is weakly g-ω-closed, $cl(int(G)) \subseteq G$ by Theorem 2.10. Again G is open implies $cl(G) = cl(int(G)) \subseteq G$. Thus G is closed and open. □

Theorem 3.4. *In a topological space (X,τ), every closed set is weakly g-ω-closed.*

Proof. If A is closed, then A is g-ω-closed by Theorem 2.12. By Proposition 2.11, A is weakly g-ω-closed. □

Remark 3.5. *The converse of Theorem 3.4 is not true follows from the following example.*

Example 3.6. *In $\mathbb{R}$ with the topology $\tau = \{\phi, \mathbb{R}, \{1\}\}$, for $G = \mathbb{R} - \mathbb{Q}$, if H is any ω-open subset of $\mathbb{R}$ such that $G \subseteq H$, then $cl(int(G)) = cl(\phi) = \phi \subseteq H$ and hence G is weakly g-ω-closed. But G is not closed for $cl(G) = \mathbb{R} - \{1\} \nsubseteq G$.*

Remark 3.7. *The following example shows that the concepts of g-closedness and weakly g-ω-closedness are independent of each other.*

Example 3.8. *In $\mathbb{R}$ with the topology $\tau = \{\phi, \mathbb{R}, \mathbb{R} - \mathbb{Q}\}$,*

(1). for $G = (\mathbb{R} - \mathbb{Q})_+ =$ the set of positive irrationals, $int(G) = \phi$. So $cl(int(G)) = cl(\phi) = \phi \subseteq G$ and thus G is weakly g-ω-closed by Theorem 2.10. But G is not g-closed for $G \subseteq (\mathbb{R} - \mathbb{Q}) \in \tau$ whereas $cl(G) = \mathbb{R} \nsubseteq \mathbb{R} - \mathbb{Q}$.

(2). for $H = (\mathbb{R} - \mathbb{Q}) \cup \{1\}$, $\mathbb{R}$ is the only open set containing H. Hence H is g-closed. But H is not weakly g-ω-closed for $cl(int(H)) = cl(\mathbb{R} - \mathbb{Q}) = \mathbb{R} \nsubseteq H$.

Remark 3.9. *In a topological space (X, τ), the following relations hold for a subset G of X.*

$$closed \leftrightarrow g\text{-}\omega\text{-}closed \rightarrow weakly\ g\text{-}\omega\text{-}closed \nleftrightarrow g\text{-}closed$$

Where $A \longleftrightarrow B$ means A implies and is implied by B, $A \rightarrow B$ means A implies B but not conversely and $A \nleftrightarrow B$ means A and B are independent.

Theorem 3.10. *In a topological space (X, τ), $cl(A)$ is always weakly g-ω-closed for every subset A of X.*

Proof. Since $cl(cl(A)) \subseteq cl(A)$, $cl(A)$ is closed. Hence $cl(A)$ is g-ω-closed by Theorem 2.12 and weakly g-ω-closed by Proposition 2.11. □

4. Further Properties

Theorem 4.1. *In a topological space (X, τ), if G is weakly g-ω-closed and H is a subset such that $G \subseteq H \subseteq cl(int(G))$, then H is weakly g-ω-closed.*

Proof. Since G is weakly g-ω-closed, $cl(int(G)) \subseteq G$ by (3) of Theorem 3.1. Thus by assumption, $G \subseteq H \subseteq cl(int(G)) \subseteq G$. Then $G = H$ and so H is weakly g-ω-closed. □

Corollary 4.2. *Let (X, τ) be a topological space. If G is a weakly g-ω-closed set and an open set, then $cl(G)$ is weakly g-ω-closed.*

Proof. Since G is open in X, $G \subseteq cl(G) \subseteq cl(G) = cl(int(G))$. G is weakly g-ω-closed implies $cl(G)$ is weakly g-ω-closed by Theorem 4.1. □

Theorem 4.3. *In a topological space (X, τ), a nowhere dense subset is weakly g-ω-closed.*

Proof. If G is a nowhere dense subset in X then $int(cl(G)) = \phi$. Since $int(G) \subseteq int(cl(G))$, $int(G) = \phi$. Hence $cl(int(G)) = cl(\phi) = \phi \subseteq G$. Thus, G is weakly g-ω-closed in (X, τ) by Theorem 2.10. □

Remark 4.4. *The converse of Theorem 4.3 is not true in general as shown in the following example.*

Example 4.5. *In Example 3.8, $G = (\mathbb{R} - \mathbb{Q})_+$ is weakly g-ω-closed. On the other hand, $int(cl(G)) = int(\mathbb{R}) = \mathbb{R} \neq \phi$ and thus $G = (\mathbb{R} - \mathbb{Q})_+$ is not nowhere dense in X.*

Remark 4.6. *In a topological space (X,τ), the intersection of two weakly g-ω-closed subsets is weakly g-ω-closed.*

Proof. Let A and B be weakly g-ω-closed subsets in (X,τ). Then $cl(int(A)) \subseteq A$ and $cl(int(B)) \subseteq B$ by Theorem 2.10. Also $cl[int(A \cap B)] \subseteq cl[int(A)] \cap cl[int(B)] \subseteq A \cap B$. This implies that $A \cap B$ is weakly g-ω-closed by Theorem 2.10. □

Remark 4.7. *In a topological space (X,τ), the union of two weakly g-ω-closed subsets need not be weakly g-ω-closed.*

Example 4.8. *In Example 3.8, for $A = (\mathbb{R}-\mathbb{Q})_+$ = the set of positive irrationals and $B = (\mathbb{R}-\mathbb{Q})_-$ = the set of negative irrationals, $int(A) = \phi$ and $int(B) = \phi$ respectively. So $cl(int(A)) = cl(\phi) = \phi \subseteq A$ and thus A is weakly g-ω-closed by Theorem 2.10. Similarly B is also weakly g-ω-closed. But $int(A \cup B) = int(\mathbb{R}-\mathbb{Q}) = \mathbb{R}-\mathbb{Q}$. So $cl[int(A \cup B)] = cl(\mathbb{R}-\mathbb{Q}) = \mathbb{R} \nsubseteq \mathbb{R}-\mathbb{Q} = A \cup B$. Hence $A \cup B$ is not weakly g-ω-closed.*

Theorem 4.9. *In a topological space (X,τ), a subset G is weakly g-ω-open if and only if $G \subseteq int(cl(G))$.*

Proof. G is weakly g-ω-open $\Leftrightarrow X \backslash G$ is weakly g-ω-closed $\Leftrightarrow X \backslash G$ is preclosed by (4) of Theorem 3.1 $\Leftrightarrow G$ is preopen $\Leftrightarrow G \subseteq int(cl(G))$. □

Theorem 4.10. *In a topological space (X,τ), if the subset G is weakly g-ω-closed, then $cl(int(G)) \backslash G$ is weakly g-ω-open in (X,τ).*

Proof. Since G is weakly g-ω-closed, $cl(int(G)) \backslash G = \phi$ by (2) of Theorem 3.1. Thus $cl(int(G)) \backslash G$ is weakly g-ω-open in (X,τ). □

Theorem 4.11. *In a topological space (X,τ), if G is weakly g-ω-open, then $int(cl(G)) \cup (X-G) = X$.*

Proof. Since G is weakly g-ω-open, $G \subseteq int(cl(G))$ by Theorem 4.9. So $(X-G) \cup G \subseteq (X-G) \cup int(cl(G))$ which implies $X = (X-G) \cup int(cl(G))$. □

Theorem 4.12. *In a topological space (X,τ), if G is weakly g-ω-open and H is a subset such that $int(cl(G)) \subseteq H \subseteq G$, then H is weakly g-ω-open.*

Proof. Since G is weakly g-ω-open, $G \subseteq int(cl(G))$ by Theorem 4.9. By assumption $int(cl(G)) \subseteq H \subseteq G$. This implies $G \subseteq int(cl(G)) \subseteq H \subseteq G$. Thus $G = H$ and so H is weakly g-ω-open. □

Corollary 4.13. *In a topological space (X,τ), if G is a weakly g-ω-open set and a closed set, then $int(G)$ is weakly g-ω-open.*

Proof. Let G be a weakly g-ω-open set and a closed set in (X,τ). Then $int(cl(G)) = int(G) \subseteq int(G) \subseteq G$. Thus, by Theorem 4.12, $int(G)$ is weakly g-ω-open in (X,τ). □

Definition 4.14. *A subset H of a topological space (X,τ) is called a W-set if $H = M \cup N$ where M is ω-closed and N is preopen.*

Proposition 4.15. *Every preopen (resp. ω-closed) set is a W-set.*

Remark 4.16. *The separate converses of Proposition 4.15 are not true in general as shown in the following example.*

Example 4.17.

(1). Let $\mathbb{R}$ and τ be as in Example 2.8 and $G = \mathbb{R}-\mathbb{Q}$. Since G is closed, it is ω-closed and hence a W-set. But $int(cl(G)) = int(G) = \phi \supsetneq G$. Hence $G = \mathbb{R}-\mathbb{Q}$ is not preopen.

(2). In Example 3.8, for $G = \mathbb{R} - \mathbb{Q}$, $int(cl(G)) = int(\mathbb{R}) = \mathbb{R} \supseteq G$. Thus G is preopen and hence a W-set. But G is not ω-closed for any $x \in \mathbb{Q}$ is a condensation point of G and $x \notin G$.

Remark 4.18. *The following example shows that the concepts of preopenness and ω-closedness are independent of each other.*

Example 4.19. *In Example 4.17(1), $G = \mathbb{R} - \mathbb{Q}$ is ω-closed but not preopen. In Example 4.17(2), $G = \mathbb{R} - \mathbb{Q}$ is preopen but not ω-closed.*

References

[1] A.Al-Omari and M.S.M.Noorani, *Contra-ω-continuous and Almost contra-ω-continuous*, Intern. J. Math. Math. Sci., 2007(2007), Artical ID 40469, 13 Pages.

[2] A.Al-Omari and M.S.M.Noorani, *Regular generalized ω-closed sets*, Intern. J. Math. Math. Sci., 2007(2007), Article ID 16292, 11 Pages.

[3] K.Banumathi, I.Rajasekaran and O.Ravi, *Mildly g-ω-closed sets*, Submitted.

[4] H.Z.Hdeib, *ω-closed mappings*, Revista Colomb. De Matem., 16(1-2)(1982), 65-78.

[5] Khalid Y.Al-Zoubi, *On generalized ω-closed sets*, Intern. J. Math. Math. Sci., 13(2005), 2011-2021.

[6] N.Levine, *Generalized closed sets in topology*, Rend. Cir. Math. Palermo, 19(2)(1970), 89-96.

[7] A.S.Mashhour, M.E.Abd El-Monsef and S.N.El-Deeb, *On precontinuous and weak precontinuous mappings*, Proc. Math. Phys. Soc. Egypt, 53(1982), 47-53.

[8] T.Noiri, A.Al-Omari and M.S.M.Noorani, *Weak forms of ω-open sets and decompositions of continuity*, Eur. J. Pure Appl. Math., 2(1)(2009), 73-84.

[9] J.K.Park and J.H.Park, *Mildly generalized closed sets, almost normal and mildly normal spaces*, Chaos, Solitons and Fractals, 20(2004), 1103-1111.

[10] M.H.Stone, *Applications of the theory of Boolean rings to general topology*, Trans. Amer. Math. Soc., 41(1937), 375-481.

[11] P.Sundaram and N.Nagaveni, *On weakly generalized continuous maps, weakly generalized closed maps and weakly generalized irresolute maps in topological spaces*, Far East J. Math. Sci., 6(6)(1998), 903-1012.

[12] P.Sundaram and A.Pushpalatha, *Strongly generalized closed sets in topological spaces*, Far East J. Math. Sci., 3(4)(2001), 563-575.

[13] R.Umamaheswari, R.Premkumar and O.Ravi, *g-ω-closed sets*, Submitted.

[14] S.Willard, *General Topology*, Addison-Wesley, Reading, Mass, USA, (1970).

P. Poongodi Assistant Professor of Mathematics	International Journal for Scientific Research & Development|	-	Note on Domination in Graphs with Bounded Degree	-	-	International ISSN (online): 2321-0613	2017

Note on Domination in Graphs with Bounded Degrees

P. Poongodi[1] S.A. Kiruthika[2]
[1]Assistant professor [2]Research Scholar
[1,2]Department of Mathematics
[1,2]Sakthi College of Arts and Science for Women, Oddanchatram – 624 619.

Abstract— Let G be a graph and D a set of vertices such that every vertex in G is in D or adjacent to at least one vertex in D. Then D is called a dominating set of G and the smallest cardinality of such a dominating set of G is known as the domination number of G, denoted by $\gamma(G)$. This paper is a study of the domination number in graphs with bounds on both the minimum and maximum degrees.

Key words: Domination set, Domination Graphs, Bounded Degrees, Domination Number, Minimum Degrees, Maximum Degrees

I. Introduction

In this section, we define the necessary concepts that will be used throughout this paper and give a brief overview of the history of domination theory and define the necessary domination concepts that will be used.

A. Preliminary definitions:

A graph G is a finite nonempty set of objects called vertices (the singular is vertex), together with a (possibly empty) set of unordered pairs of distinct vertices of G called edges. The vertex set of G is denoted by $V(G)$ (or V if no confusion is likely), while the edge set of G is denoted by $E(G)$ (or E).

The number of vertices in $V(G)$ is denoted by $n(G)$ which is also known as the order of the graph G, while the number of edges in $E(G)$ is denoted by $m(G)$. A graph G is trivial if $n(G)=1$ and non – trivial if $n(G)\geq 2$. For a graph G, if $n(G)=n$ and $m(G)=m$, then G is called an (n,m) graph. Unless otherwise specified, the symbols n and m $(or\ n(G)\ and\ m(G))$ will be reserved exclusively for the order and number of edges respectively of a graph G. By $G=(V,E)$ we will imply the graph G with vertex set V and edge set E.

The edge $e=uv$ is said to join the vertices u and v. If $e=uv$ is an edge of G, then u and v are adjacent vertices, while u and e are incident as are v and e. Furthermore, if e_1 and e_2 are distinct edges of G incident with a common vertex, then e_1 and e_2 are adjacent edges.

A simple graph G is a graph that has at most one edge between every pair of distinct vertices and there is no edge in $E(G)$ joining any vertex in $V(G)$ to itself. Throughout the text we will only consider simple undirected graphs.

The compliment $\overline{G}$ of a graph G is the graph with vertex set $V(G)$ and such that two vertices are adjacent in $\overline{G}$ if and only if these vertices are not adjacent in G.

B. Domination in Graphs:

Let G be a graph and D a set of vertices such that every vertex in G is in D or adjacent to at least one vertex in D. Then D is called a dominating set of G, and the smallest cardinality of such a dominating set of G is known as the domination number of G, denoted by $\gamma(G)$. A minimal dominating set of G is a dominating set of G such that no proper subset $S'\subset S$ is a dominating set.

II. Domination in Graphs with Minimum Degree Two

For any graph G, consider any subset $S\subseteq V$. Then $G(S)$ denotes the subgraph of G induced by S. Furthermore, E(S) denotes the edge set of $G(S)$. For $J\subseteq\{xy / x, y\in V\}$ we form the graph G – J (resp. $G\cup J$) $=(V, E-J(resp.\ E\cup J))$ where V and $E-J(resp.\ E\cup J)$ denotes the vertex and edge set (respectively). If J = {uv}, then G – J (resp. $G\cup J$) is replaced by G – uv (resp. G + uv). We define the graph (G – S) – J as the graph G(V – S) – J.

Let G = (V, E) be any graph and $0<c\leq 1$, then we say G is c – dominated if $\gamma(G)\leq c|V|$ and D is c – dominating set and $|D|\leq c|V|$. Furthermore, if S and T are subsets of V, then we say that S is a dominating set of $G(S\cup T)$.

Now let B(G) be the set that consists of all vertices in G that have degree not equal to two. i.e ,

$$B(G)=\{v\in V / \deg(v)\neq 2\}.$$

For $v\in B(G)$, the connected component of $G-(B(G)-v)$ containing v is said to be the 2 – graph of v. If $\delta(G)\geq 2$, then each vertex of the 2 – graph has degree two in G, except for v itself. The 2 – graph consists of edge disjoint cycles through v (2 – graph cycles) and paths starting at v (2 – graph paths).

III. Domination in Graphs with Maximum Degree Three

The aim of this chapter is to show that a graph G with n vertices, e edges, i isolated vertices and maximum degree

at most three has $\gamma(G) \le \frac{1}{4}(3n - e + i)$.....(1). this is an exact result for the infinite family of graphs depicted in figure 3.1 (the circled vertices denote vertices in a minimum dominating set of G). These graphs are known as the corona's of C_3, C_4, C_5 etc. to show that equality in (1) holds for the corona C_n^c of an n – cycle C_n we first note that by Ore [12], $\gamma(C_n^c) \le \frac{n(C_n^c)}{2}$, furthermore since C_n^c has twice as many vertices as C_n we have that $\frac{n(C_n^c)}{2} = \frac{1}{2}2n = n \le \gamma(C_n^c)$. therefore since $\gamma(C_n^c) = \frac{n(C_n^c)}{2}$. secondly we note that $n(C_n^c) = m(C_n^c)$. Hence we obtain equality in (1) as follows: $\gamma(C_n^c) = \frac{n(C_n^c)}{2} = \frac{1}{4}(3n(C_n^c) - m(C_n^c) + 0)$ (note that a corona has no isolated vertices).

The other seven known graphs satisfying equality in (1) are given in figure 3.2. Note that graphs G_i $(i = 2,...7)$ are connected. Clearly any graph whose components are the graphs in figure 3.2, has $\gamma(G) \le \frac{1}{4}(3n - e + i)$.

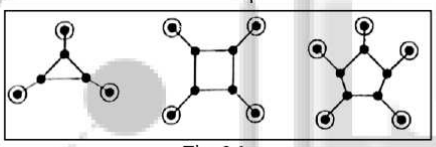

Fig. 3.1:

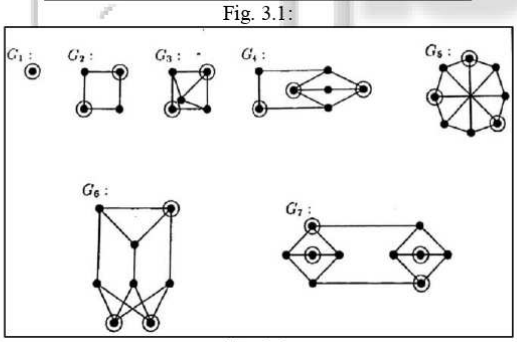

Fig. 3.2:

If v is a vertex of a graph and deg $v = k$, we say that v is a k – *vertex* or that v is a k – neighbour of a neighbouring vertex.

A. The Main Result:

Theorem 3.1.1 A graph G with n vertices, e edges, i 0 – vertices, and maximum degree at most three has

$$\gamma(G) \le \frac{1}{4}(3n - e + i).$$

Proof: The proof is by induction on the order of G. For $G \equiv K_1$, the equality in (1) holds. Consider a graph G' with n' vertices, e' edges and i' 0 – vertices. We assume that $\gamma(G') \le \frac{1}{4}(3n' - e' + i')$. for every graph G' with $n' < n$. Let $\hat{n} = n - n'$, $\hat{e} = e - e'$, $\hat{i} = i - i'$ and let $\hat{\gamma}$ be a member such that $\hat{\gamma} = \gamma(G) - \gamma(G')$ and $\gamma(G') \le \frac{1}{4}(3n' - e' + i')$ renders

$$\gamma(G) = \gamma(G') + \hat{\gamma}$$
$$\le \frac{1}{4}(3n' - e' + i') + \hat{\gamma}$$
$$= \frac{1}{4}\left(3(n - \hat{n}) - (e - \hat{e}) + (i + \hat{i})\right) + \hat{\gamma}$$
$$= \frac{1}{4}(3n - e + i) + \frac{1}{4}(-3\hat{n} + \hat{e} + \hat{i}) + \hat{\gamma}$$
$$= \frac{1}{4}(3n - e + i) + \frac{1}{4}(4\hat{\gamma} - 3\hat{n} + \hat{e} + \hat{i})$$

Therefore G satisfies the theorem if $\sigma = (4\hat{\gamma} - 3\hat{n} + \hat{e} + \hat{i}) \le 0$ for a smaller graph G'. Note that if $\hat{G}$ denotes $G - G'$, and then $\sigma \le 0$ is equivalent to $\gamma(G) \le \frac{1}{4}(3n - e + i)$.

Let $G' = G - N[v]$ for vertex v, unless otherwise stated

CASE 1: $\delta(G) = 0$

If is a 0 – vertex, then

$$\sigma = 4\hat{\gamma} - 3\hat{n} + \hat{e} + \hat{i}$$
$$= 4.1 - 3.1 + 0 + (-1)$$
$$= 0$$

CASE 2: $\delta(G) = 1$

Case 2a: **Two 1 – vertices are adjacent.**

The two 1 – vertices form a component isomorphic to K_2. Let $G' = G - K_2$ then

$$\sigma = 4\hat{\gamma} - 3\hat{n} + \hat{e} + \hat{i}$$
$$= 4.1 - 3.2 + 1 + 0$$
$$= -1$$

Continuous same way we get different σ

IV. An Upper Bound for the k – Domination Number of a Graph

The domination number of a graph G, denoted $\gamma_k(G)$ by to be the least cardinality of a set U of vertices such that any other vertex is adjacent to at least k vertices of U. It will be shown that if each vertex has degree at least k, then $\gamma_k(G) \le kn/(k+1)$ where n is the order of G

REFERENCES

[1] J.F Fink and M.S Jacobson, On n – domination, n – dependence and forbidden sub graphs submitted.
[2] D.C Fisher, K. Fraughnaugh and S.M Seager, Domination of graphs with maximum degree three. Preprint
[3] T.W Haynes, S.T Hedetniemi, and P.J Slater, Fundamentals of Domination in Graphs, Marcel Dekker, New York.
[4] B. Reed, paths, stars and the number three. Preprint.

S. Kavitha, Assistant Professor of Computer Science	International Journal of Computer Science Trends and Technology (IJCST)	-	Edge Shield Static Median Filter for Removing Noise on Various Types of Images	-	-	International ISSN: 2347-8578	March 2017

International Journal of Computer Science Trends and Technology (IJCST) – Volume 5 Issue 2, Mar – Apr 2017

RESEARCH ARTICLE OPEN ACCESS

Edge Shield Static Median Filter for Removing Noise on Various Types of Images

M.Chitradevi [1], S.Kavitha [2]
Research Scholar [1], Head & Assistant Professor [2]
Department of Computer Science
Sakthi College of Arts and Science
For Women, Oddanchatram
Tamil Nadu - India

ABSTRACT
An image could represent luminance of objects in a scene, the absorption characteristics of the body tissue, the radar cross section of the target, the temperature profile of the region or the gravitational field in an area. In general, any two dimensional function that bears information can be considered an image. An important consideration in image representation is the fidelity or intelligibility criteria for measuring the quality of an image or the Performance of processing technique. Specification of such measures requires models of perception of contrast, spatial frequencies, and colors and so on. The fundamental requirement of digital processing is that images be sampled and quantized. The sampling rate has to be large enough to preserve the useful information in an image. It is determined by the bandwidth of the image.

Keywords:- Image Processing, Image acquisition, Median Filter.

I. INTRODUCTION

Image processing is a rapidly growing area of computer science. Its growth has been fueled by technological advances in digital imaging, computer processors and mass storage devices. Fields which traditionally used analog imaging are now switching to digital systems, for their flexibility and affordability. Important examples are medicine, film and video production, photography, remote sensing, and security monitoring. These and other sources produce huge volumes of digital image data every day, more than could ever be examined manually. A digital image differs from a photo in that the *x, y,* and *f(x,y)* values are all discrete. Usually they take on only integer values, so the image will have *x* and *y* ranging from 1 to 256 each, and the brightness values also ranging from 0 (black) to 255 (white). A digital image can be considered as a large array of discrete dots, each of which has a brightness associated with it. These dots are called picture elements, or more simply pixels. The pixels surrounding a given pixel constitute its neighborhood. A neighborhood can be characterized by its shape in the same way as a matrix. Except in very special circumstances, neighborhoods have odd number of rows and columns; this ensures that the current pixel is in the Centre of the neighborhood.

An image is digitized to convert it to a form which can be stored in a computer's memory or on some form of storage media such as a hard disk or CD-ROM. This digitization procedure can be done by a scanner, or by a video camera connected to a frame grabber board in a computer. Once the image has been digitized, it can be operated upon by various image processing operations. Image processing operations can be roughly divided into three major categories, Image Compression, Image Enhancement and Restoration, and Measurement Extraction. Image compression is involves reducing the amount of memory needed to store a digital image. Image defects which could be caused by the digitization process or by faults in the imaging set-up (for example, bad lighting) can be corrected using Image Enhancement techniques. Once the image is in good condition, the Measurement Extraction operations can be used to obtain useful information from the image.

Digital image processing is concerned primarily with extracting useful information from images. Ideally, this is done by computers, with little or no human intervention. Image processing algorithms may be placed at three levels. At the lowest level are those techniques which deal directly with the raw, possibly noisy pixel values, with denoising and edge detection being good examples. In the middle are algorithms which utilize low level results for further means, such as segmentation and edge linking. At the highest level are those methods which attempt to extract semantic meaning from the information provided by the lower levels, for example, handwriting recognition.

Image acquisition is the process of obtaining a digitized image from a real world source. Each step in the acquisition process may introduce random changes into the values of pixels in the image. These changes are called *noise*. Assume you want to send a photo of your new house to a friend over the Internet. This may be achieved by taking a photograph with a conventional camera, having the film made into a print, scanning the print into a computer, and finally emailing it to your friend. Figure-1 shows the many potential sources of noise.

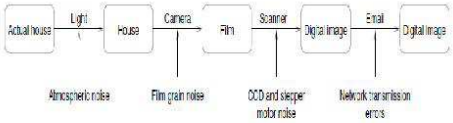

Figure-1: noise may be introduced at each step in the acquisition process.

The air between the photographer and the house may contain dust particles which interfere with the light reaching the camera lens. The silver-halide crystals on the _lm vary in size and are discontinuous, resulting in film grain noise in the printing process. Most scanners use a CCD array to scan a row of the print, which may introduce photo-electronic noise. The scanner's CCD array is controlled by a fine stepper motor. This motor has some degree of vibration and error in its movement, which may cause pixels to be misaligned. The scanner also quantizes the CCD signal, introducing quantization noise. Transmitting the image over the Internet is nearly always a bit preserving operation thanks to error checking in network protocols. However, an image transmitted to Earth from a remote space probe launched in the 1970's is almost guaranteed to contain errors.

II. VARIOUS SORCES OF NOISE IN IMAGES

Noise is a random variation of image Intensity and visible as grains in the image. It may arise in the image as effects of basic physics-like photon nature of light or thermal energy of heat inside the image sensors. It may produce at the time of capturing or image transmission. Noise means, the pixels in the image show different intensity values instead of true pixel values. Noise removal algorithm is the process of removing or reducing the noise from the image. The noise removal algorithms reduce or remove the visibility of noise by smoothing the entire image leaving areas near contrast boundaries. But these methods can obscure fine, low contrast details. The common types of noise that arises in the image are a) Impulse noise, b) Additive noise [1], c) Multiplicative noise. Different noises have their own characteristics which make them distinguishable from others.

Noise is introduced in the image at the time of image acquisition or transmission. Different factors may be responsible for introduction of noise in the image. The number of pixels corrupted in the image will decide the quantification of the noise. The principal sources of noise in the digital image are:

a) The imaging sensor may be affected by environmental conditions during image acquisition.
b) Insufficient Light levels and sensor temperature may introduce the noise in the image.
c) Interference in the transmission channel may also corrupt the image.
d) If dust particles are present on the scanner screen, they can also introduce noise in the image.

Noise is the undesirable effects produced in the image. During image acquisition or transmission, several factors are responsible for introducing noise in the image. Depending on the type of disturbance, the noise can affect the image to different extent. Generally our focus is to remove certain kind of noise. So we identify certain kind of noise and apply different algorithms to remove the noise. Image noise can be classified as Impulse noise (Salt-and-pepper noise), Amplifier noise (Gaussian noise), Shot noise, Quantization noise (uniform noise), Film grain, on-isotropic noise, Multiplicative noise (Speckle noise) and Periodic noise.

A. Impulse Noise (Salt and Pepper Noise)

The term impulse noise is also used for this type of noise [2]. Other terms are spike noise, random noise or independent noise. Black and white dots appear in the image [5] as a result of this noise and hence salt and pepper noise. This noise arises in the image because of sharp and sudden changes of image signal. Dust particles in the image acquisition source or over heated faulty components can cause this type of noise. Image is corrupted to a small extent due to

noise. Figure-3 Show the effect of this noise on the original image (Figure-2).

Figure-2: Original image without noise

Figure-3: Image with 30% salt & pepper noise

B. Gaussian Noise (Amplifier Noise)

The term normal noise model is the synonym of Gaussian noise. This noise model is additive in nature [4] and follow Gaussian distribution. Meaning that each pixel in the noisy image is the sum of the true pixel value and a random, Gaussian distributed noise value. The noise is independent of intensity of pixel value at each point. The PDF of Gaussian random variable is given by: $P(x) = 1/ (\sigma\sqrt{2\pi}) *e(x-\mu)2 / 2\sigma 2$ $-\infty < 0 <\infty$ Where: P(x) is the Gaussian distribution noise in image; μ and σ is the mean and standard deviation respectively. Figure-4, shows the effect of adding Gaussian noise to Figure-2, with zero mean.

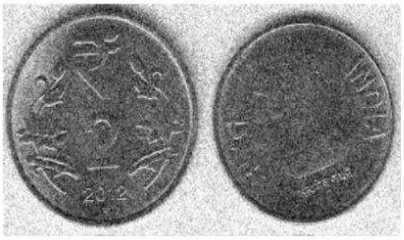

Figure-4: Gaussian noise with zero mean

C. Poisson Noise (Photon Noise)

Poisson or shot photon noise is the noise that can cause, when number of photons sensed by the sensor is not sufficient to provide detectable statistical information [4]. This noise has root mean square value proportional to square root intensity of the image. Different pixels are suffered by independent noise values. At practical grounds the photon noise and other sensor based noise corrupt the signal at different proportions [3]. Figure-5 shows the result of adding Poisson noise.

Figure-5: Image with Poisson noise

D. Speckle Noise

This noise can be modeled by random value multiplications with pixel values of the image and can be expressed as

$$J = I + n*I$$

Where, J is the speckle noise distribution image, I is the input image and n is the uniform noise image by mean o and variance v. This noise deteriorates the quality of active radar and Synthetic aperture radar (SAR) [4] images. This noise is

originated because of coherent processing of back scattered signals from multiple distributed points. In conventional radar system this type of noise is noticed when the returned signal from the object having size less than or equal to a single image processing unit, shows sudden fluctuations. Mean filters are good for Gaussian noise and uniform noise. Figure-6, shows the effect of adding speckle noise.

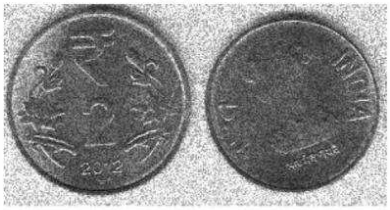

Figure-6: Image with speckle noise

III. IMAGE DE-NOISING

Image de-noising is very important task in image processing for the analysis of images. Ample image de-noising algorithms are available, but the best one should remove the noise completely from the image, while preserving the details. De-noising methods can be linear as well as non-linear. Where linear methods are fast enough, but they do not preserve the details of the images, whereas the non- linear methods preserve the details of the images. Broadly speaking, De-noising filters can be categorized in the following categories:

- Averaging filter
- Order Statistics filter
- Adaptive filter

A. Mean filter

Mean filter is an averaging linear filter [6]. Here the filter computes the average value of the corrupted image in a pre-decided area. Then the center pixel intensity value is replaced by that average value. This process is repeated for all pixel values in the image.

B. Median Filter

Median filter is a best order static, non- linear filter, whose response is based on the ranking of pixel values contained in the filter region. Median filter is quite popular for reducing certain types of noise. Here the center value of the pixel is replaced by the median of the pixel values under the filter region [9] [10].

Median filter is good for salt and pepper noise. These filters are widely used as smoothers for image processing, as well as in signal processing. A major advantage of the median filter over linear filters is that the median filter can eliminate the effect of input noise values with extremely large magnitudes.

C. Order Statistics Filter

Order-Statistics filters are non-linear filters whose response depends on the ordering of pixels encompassed by the filter area. When the center value of the pixel in the image area is replaced by 100th percentile, the filter is called max-filter. On the other hand, if the same pixel value is replaced by 0th percentile, the filter is termed as minimum filter.

D. Adaptive Filter

These filters change their behavior on the basis of statistical characteristics of the image region, encompassed by the filter region.BM3D is an adaptive filter. It is a nonlocal image modeling technique based on adaptive, high order group-wise models.

IV. RESEARCH METHODOLOGY

Research methodology is a systematic way to solve a problem. It is a science of studying how research is to be carried out. Essentially, the procedures by which researchers go about their work of describing, explaining and predicting phenomena are called research methodology. It is also defined as the study of methods by which knowledge is gained. Its aim is to give the work plan of research.

Research flow shows the entire flow the research. And it carries the problem into proper way to find the solution. Number of steps is followed to achieve the desired result.

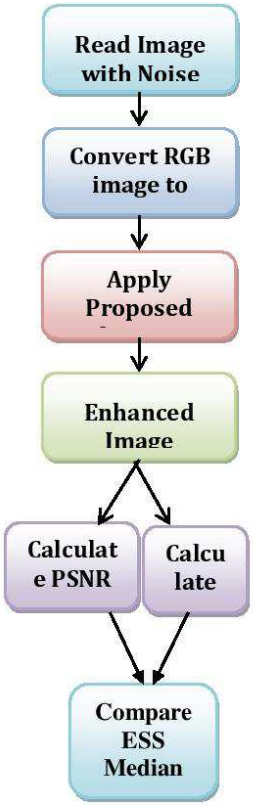

Figure-7: Research Flow

The Figure-7 shows the flow of the research carried. Initial step of the research flow is reading the image with noise. The image used here is true color images which have the RGB values. Then the image is converted into gray scale image with noise for processing with Edge shield static median filter. After the conversion the Edge shield static filter is applied to remove the noise from images. Finally image quality metrics PSNR and MSE is calculated to Enhanced image. After the calculation of PSNR and MSE values of ESS median filter, compare these values with existing median filters.

V. READING IMAGE

Reading Image is an initial task in image processing. An image can me read with the file format with image's name and corresponding directory where the image stored. The image can be either gray scale or color image. The first step in MATLAB image processing is to understand that a digital image is composed of a two or three dimensional matrix of pixels. Individual pixels contain a number or numbers representing what grayscale or color value is assigned to it. Color pictures generally contain three times as much data as grayscale pictures, depending on what color representation scheme is used. Therefore, color pictures take three times as much computational power to process.

Here images are read with noise. Noise is the dust particle of image which degrades the image quality. The type noise here taken to process is Gaussian noise. Noise is introduced into images usually while transferring and acquiring them. The main type of noise added while image acquisition is called Gaussian noise while Impulsive noise is generally introduced while transmitting image data over an unsecure communication channel, while it can also be added by acquiring.

VI. RESULTS AND DISCUSSION

Still images are visual representations that do not move. Text is ideal for transmitting information in a highly articulate manner that can be consistently interpreted irrespective of the user. Still images, however, allow the content creator to convey information which can be more freely interpreted by the user. A picture does indeed paint a thousand words but the meaning of the picture will vary from user to user. Images can be acquired from clip art collections on CDROM or through the use of a scanner. Noise is occurring in still images during the acquisition process. Noises are the unwanted dust particles, filters are used to remove those noises in images. Proposed Edge Shield Static Median filter is used to remove the Gaussian noise that occurs on the image

. The effect of the proposed Edge Shield Static Median filter in still images is noticeable. A number of still images are taken and evaluated with the use of Edge Shield Static Median filter. Some of the results are shown in Table-1.

IMAGE	NOISY IMAGE		EDGE SHIELD STATIC MEDIAN FILTER	
STILL	MSE	PSNR	MSE	PSNR
Baby	281.5493	23.6353	246.1405	24.2190
Charlie	254.4840	24.0742	188.1981	25.3847
Dog	343.8284	22.7674	298.7554	23.3776
Entrance	373.4400	22.4086	329.2497	22.9556
Girl	336.5572	22.8602	292.8767	23.4640
Monkey	347.0654	22.7267	289.8590	23.5089
Remote	326.9327	22.9862	268.9243	23.8345
Tower	370.0080	22.4487	327.4097	22.9799
Women	246.8843	24.2059	204.2118	25.0300
Fly	293.1277	23.4602	266.4666	23.8744
Bear	292.3745	23.4714	268.3916	23.8431

Table-1: PSNR And MSE Values Of Processed Still Images

The table-1 shows the result of different images processed with Edge Shield Static Median filter. The PSNR values are improved in decimal vise and error rate is decreased noticeably.

In baby image, noisy image have the PSNR value 23.635 and wiener filter have the value as 23.7082. After applying the Edge Shield Static Median filter PSNR value increased as 24.2190. The difference between the image PSNR values is 0.5108. The quality of the image in PSNR vise improved as 0.5 percentages. The other images like fly, entrance, bear, etc... Also have the PSNR value increased by the ratio 0.7%.MSE value of noise image of Charlie is 254.4840, after applying the wiener filter the error rate is reduced by 232.6073 and the Edge Shield Static Median filter reduces the error rate as 188.1981the value of reduced error rate is near 65. By comparing all the images the mean square error is reduced near 45% from the noisy image. The performance of Edge Shield Static Median filter on still image is showed as graph.

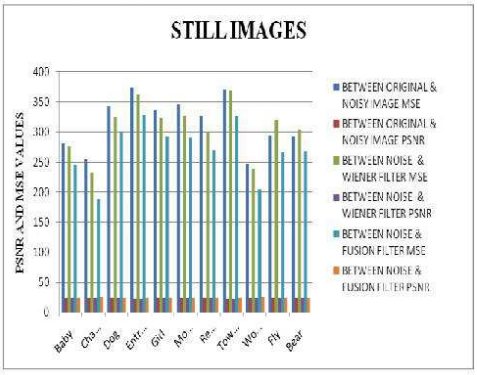

Figure-8: Performance Of Edge Shield Static Median Filter On Still Images

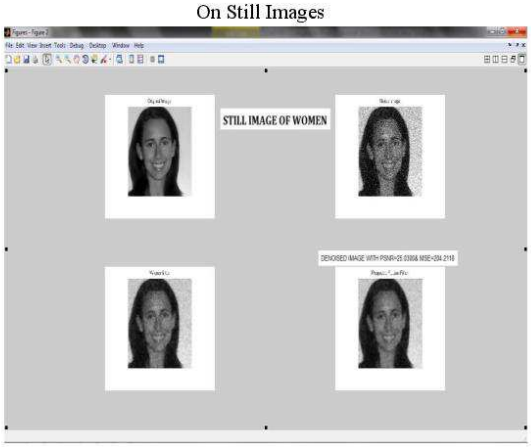

Figure-9: Edge Shield Static Median Filter Applied On An Image Of Women

Result of Edge Shield Static Median filter is Figure-8 shows the graphical representation of processed MSE and PSNR values. The chart shows the MSE and PSNR values of noisy image, MSE and PSNR values of image after applying the wiener filter and Image values after applying the Edge Shield Static Median Filter. The graph visually shows the difference between existing method and proposed method. Figure-9 shows the screen shots of result after applying the wiener and Edge Shield Static Median filter with improved

PSNR and MSE values. The values are calculated between the noisy image and the enhanced image.

VII. CONCLUSION

And the Edge Shield Static Median filter works better in still images than the medical images and satellite images. The obtained results of still images are closed to the original images. Most of noises are removed in all kind of images.

Through the results the proposed Edge Shield Static Median filter produces better results on removing the Gaussian noise on images. And Edge Shield Static Median filter produces improved results on still images. In still images PSNR values are increased by 0.7 % overall and the MSE values is decreased by 45%. In medical MRI images PSNR values are increased by 0.8 % and the MSE values are decreased by 40%. In X-ray images MSE values are decreased by 35% and the PSNR values are increased by 0.7%. Processed satellite image have PSNR values 0.4% and MSE value is decreased by 20%.The results shows clearly the Edge Shield Static Median filter works effectively on still images. The peak errors are increased in the ratio of below the 1%. So this will not produce any distortion in the images.

REFERENCES

[1] Rafael C. Gonzalez, Richard E. Woods, "Digital Image Processing", 2nd edition, Prentice Hall, 2002.

[2] Maria Petrou, PanagiotaBosdogianni, "Image Processing: The Fundamental", John Wiley & Sons Ltd, 2000.

[3] Jung-Hua Wang, Lian-Da Lin, "Improved median filter using min-max algorithm for image processing", Electronics Letters, vol. 33, no. 16, pp. 1362-1363, July 1997.

[4] Raymond H. Chan, Chung-Wa Ho, Mila Nikolova, "Salt and pepper noise removal by median-type noise detectorsand detail preserving regularization", IEEE Trans. Image Processing, vol. 14, no. 10, pp. 1479-1485, October,2005

[5] ThotaSusmitha., GaneswaraRao M.V, Kumar Dr.P.Rajesh, "FPGA Implementation of Adaptive Median Filter for the Removal of Impulse Noise",International Journal of Electronics & Communication Technology,Vol. 2, SP-1, Dec . 2011.

[6] S. E. Umbaugh, Computer Vision and Image Processing, Prentice-Hall, Englewood Cliffs, NJ,USA, 1998.

[7] R. K. Yang, L. Yin, M. Gabbouj, J. Astola, and Y. Neuvo, "Optimal weighted median filtering under structural constraints," IEEETransactions on Signal Processing, vol. 43, no. 3, pp. 591-604 , 1995.

[8] T. S. Huang, G. J. Yang, and G. Y. Tang, "A fast two-dimensional median filtering algorithm," IEEE Transactions on Acoustics, Speechand Signal Processing, vol. 27, no. 1, pp. 13-18 , 1979.

[9] T.-C. Lin, "A new adaptive center weighted median filter for suppression impulsive noise in images," Information Sciences, vol. 177, no. 4, pp. 1073-1087, 2007.

[10] R. Vijay Kumar, S. Manikandan, P. T. Vanathi, P. Kanagasabapathy, and D. Ebenezer, "Adaptive window length recursive weighted median filter for removing impulse noise in images with details preservation," ECTI Transactions on Electrical Eng., Electronics, and Communications, vol. 6, no.1, pp. 73-80 , 2008.

[11] S.-J. Ko and Y. H. Lee, "Center weighted median filters and their applications to image enhancement," IEEE Transactions on Circuitsand Systems, vol. 38, no. 9, pp. 984-993 , 1991.

[12] T. Sun, "Center weighted median filters: Some properties and their applications in image processing," Signal Processing, vol. 35, no. 3, pp. 213-229 , 1994.

[13] K. Arakawa, "Median filter based on fuzzy rules and its application to image restoration," Fuzzy Sets and Systems, vol. 77, no. 1, pp. 3–13 , 1996.

[14] A. Asano, K. Itoh, and Y. Ichioka, "Optimization of the weighted median filter by learning," Optics Express, vol. 16, no. 3, pp. 168–170 , 1991.

[15] G. R. Arce and J. L. Paredes, "Recursive weighted median filters admitting negative weights and their optimization," IEEE Transactionson Signal Processing, vol. 48, no. 3, pp. 768–779, 2000.

[16] S. J. Ko, and Y. H. Lee, 1991. Center weighted median filters and their applications to image enhancement, IEEE Transactions, pp984-993

S. Kavitha, Assistant Professor of Computer Science	International Journal of Advanced Research Trends in Engineering and Technology	-	Content Based Image Retrieval Using Multi-Dimensional Texture, Edge Orientation Histogram and EDBTC Compression	-	-	International ISSN 2394-3777 (Print) ISSN 2394-3785 (Online)	March 2017

ISSN 2394-3777 (Print)
ISSN 2394-3785 (Online)
Available online at www.ijartet.com

International Journal of Advanced Research Trends in Engineering and Technology (IJARTET)
Vol. 4, Special Issue 5, March 2017

CONTENT BASED IMAGE RETRIEVAL USING MULTI DIMENSIONAL TEXTURE, EDGE ORIENTATION HISTOGRAM AND EDBTC COMPRESSION

Rekha.J 1* , B. Muthu Kumar 2 , Kavitha 3 , S.Prabhakaran 4

1, 3Department of Computer Science, Sakthi College of Arts and Science for Women, TN, India

2 Professor, Department of CSE, Syed Ammal Engineering College, Ramanathapuram, TN, India

4 Department of Information Technology, Kathir College of Engineering

*Corresponding Author: mailto: rekhamsc31@gmail.com

ABSTRACT

The graph based ranking model is proposed for information retrieval area. Our proposed technique concentrates on ranking the Data Manifold Model or Manifold Ranking (MR). The Content Based Image Retrieval (CBIR) gives an extra-ordinary result underlying geometrical structure for the given image database. MR is an expensive one. This approach limits its usefulness for the large database containing new queries. The name for Graph based Ranking model is Efficient Manifold Ranking (EMR). The scalable [8] graph construction and efficient ranking computation are the two views of MR. We specially develop an anchor graph on the database. To increase the speed of ranking adjacency matrix is introduced. EMR is a promising method for real-time retrieval applications.

Keywords: Content based image retrieval (CBIR), classification, segmentation.

1. INTRODUCTION

Graph based ranking model is mainly focused the problem of out of sample retrieval on large scale databases. Most of the image retrieval systems are based on the keyword search such as Google and Yahoo image search. The keyword is matched based on the image titles, manual annotation, web document etc. The problem occurs are shortage of text information and incomplete statement and image. CBIR [1] [3] is the best method to overcome the hurdles. The proposed system sets a trend set for low level features, global features can automatically extracted from images. The researches have been performed for designing more informative low-level features to represent images or better metrics. The performance is restricted due to the sensitive data and conditions. Traditional method concentrates on data features but they ignore the structure information. During the unknown label information at the time they focused the method structure information. The same semantic label is likely to share the

ISSN 2394-3777 (Print)
ISSN 2394-3785 (Online)
Available online at www.ijartet.com

International Journal of Advanced Research Trends in Engineering and Technology (IJARTET)
Vol. 4, Special Issue 5, March 2017

neighbouring data points or belong to the same cluster or manifold. Our aim is to produce a good CBIR system for low level features as well as the intrinsic structure of the image database. The intrinsic geometrical structure collectively revealed by a large number of data. MR [9] [10] works on many applications and produce excellent performance and feasibility on a variety of data types such as the text [11], image [12] [13] and video [14]. He et al. [12] is the first person approached MR to CBIR and improved the performance of image retrieval.

MR has some of the drawbacks such as handle large scale databases cost wise high in both stages graph construction and ranking competition stages. In the existing system they don't know how to handle an out-of-sample query. The original MR [4] is inadequate for a real world CBIR system. We propose a novel framework named Efficient Manifold Ranking (EMR). The technique is based on two stages. The first one is Offline stage used for learning and the latter one is Online stage used for handling a new sample. EMR can handle a database with 1 million images. The online retrieval is used to retrieve within a short time.

The new contributions [13] of our proposed system are as follows:

1) To produce an excellent outsource for an out-of-sample retrieval proposed an efficient approximate method to compute ranking scores for a new query.
2) To test the efficiency of the proposed technique, 1 millions samples in three databases are included.
3) To overcome and design the local weight estimation problem of anchor graph, two various methods are compared.

In Section 2, we describes the related work and Section 3 overviews the MR algorithm. In Section 4, we proposed an EMR approach. Section 5 summarizes the experimental results on many real-time image databases. Section 6 concludes the paper.

2. RELATED WORKS

The problem of ranking has been overcome by information retrieval and machine learning areas. Conventional ranking models are content based models, like the Vector Space Model, BM25, language modelling [15], link structure based models [16] [17] [18] . The rank model [19] [20] is an important category to learn optimize a ranking function that incorporates relevance features and avoids tuning a large number of parameters empirically. The authors present a unified framework for jointly optimizing effectiveness and efficiency. [6] presented an automatic segmentation method which effectively combines Active Contour Model, Live Wire method and Graph Cut approach (CLG). The aim of Live wire method is to provide control to the user on segmentation process during execution. Active Contour Model provides a statistical model of object shape and appearance to a new image which are built during a training phase. In the graph cut technique, each pixel is represented as a node and the distance between those nodes is represented as edges. In graph theory, a cut is a partition of the nodes that divides the graph into two disjoint subsets. For initialization, a pseudo strategy is employed and the organs are

ISSN 2394-3777 (Print)
ISSN 2394-3785 (Online)
Available online at www.ijartet.com

International Journal of Advanced Research Trends in Engineering and Technology (IJARTET)
Vol. 4, Special Issue 5, March 2017

segmented slice by slice through the OACAM (Oriented Active Contour Appearance Model). Initialization provides rough object localization and shape constraints which produce refined delineation. This method is tested with different set of images including CT and MR images especially 3D images and produced perfect segmentation results.

Our aim is to give attention of ranking model, graph-based ranking. This approach successfully applied in link-structure analysis of the web [16] [17], social networks research and multimedia data analysis. Generally, a graph can be denoted as G = (V, E, W), where V is a set of vertices in which each vertex represents a data point, $E \subseteq V \times V$ is a set of edges connecting related vertices, and W is a adjacency matrix recording the pairwise weights between vertices. The importance of a vertex is based on local or global information drawn from the graph and it is achieved by graph-based ranking model.

The model data by a weighted graph, and incorporated this graph structure into the ranking function as a regularizer are recommended by Agarwal. Guan et al. proposed a graph-based ranking algorithm for interrelated multi-type resources to generate personalized tag recommendation. An automatically tag ranking scheme by performing a random walk over a tag similarity graph are proposed by Lieut al. The authors made the music recommendation by ranking on a unified hypergraph [7], combining with rich social information and music content. The graph-based model has been proposed a method namely, hypergraph. The MR has been currently spread over on several works. The authors partitioned the data into several parts and computed the ranking function by a block-wise way.

3. MANIFOLD RANKING REVIEW

In this section, we briefly review the manifold ranking algorithm and make a detailed analysis about its drawbacks. We start form the description of notations.

3.1 Notations and Formulations

Given a set of data $\chi = \{x_1, x2... xn\} \subset R^m$ and build a graph on the data (e.g., kNN graph).

$W \in R^{nxn}$ denotes the adjacency matrix with element w_{ij} saving the weight of the edge between point i and j. Normally the weight can be defined by the heat kernel $w_{ij} = \exp[-d^2(xi,xj)/2\sigma^2)]$ if there is an edge linking x_i and x_j, otherwise $w_{ij} = 0$. Function d (xi,xj) is a distance metric of x_i and x_j defined on χ, such as the Euclidean distance. Let r: $\chi \rightarrow R$ be a ranking function which assigns to each point x_i a ranking score r_i. Finally, we define an initial vector $y = [y_1... y_n]^T$, in which $y_i = 1$ if x_i is a query and $y_i = 0$ otherwise.

The cost function associated with r is defined to be

$$O(r) = \frac{1}{2} \left(\sum_{i,j=1}^{n} w_{ij} \| 1/\sqrt{D}_{ij} r_i - 1/\sqrt{D}_{ij} r_j \|^2 + \mu \sum_{i=1}^{n} \| r_i - y_i \|^2 \right) \quad \text{.....(1)}$$

Where $\mu > 0$ is the regularization parameter and D is a diagonal matrix with $D_{ii} = \sum_{j=1}^{n} w_{ij}$.

The first term in the cost function is a smoothness constraint, which makes the nearby points in the space having close ranking scores. The second term is a fitting constraint, which means the ranking result should fit to the initial label assignment. With more prior knowledge about the relevance or confidence of

ISSN 2394-3777 (Print)
ISSN 2394-3785 (Online)
Available online at www.ijartet.com

International Journal of Advanced Research Trends in Engineering and Technology (IJARTET)
Vol. 4, Special Issue 5, March 2017

each query, we can assign different initial scores to the queries. Minimizing the cost function respect to r results into the following closed form solution

$r* = (I_n - \alpha S)^{-1} y$ ….. (2)

where $\alpha = \frac{1}{1+\mu}$, I_n is an identity matrix with n×n, and S is the symmetrical normalization of W, $S=D^{-1/2}WD^{-1/2}$. In large scale problems, we prefer to use the iteration scheme:

$r(t+1) = \alpha S r(t) + (1-\alpha) y$ …..(3)

During each iteration, each point receives information from its neighbors (first term), and retains its initial information (second term). The iteration process is repeated until convergence. When manifold ranking is applied to retrieval (such as image retrieval), after specifying a query by the user, we can use the closed form or iteration scheme to compute the ranking score of each point. The ranking score can be viewed as a metric of the manifold distance which is more meaningful to measure the semantic relevance.

3.2 ANALYSIS

Manifold ranking has been used in various applications at the same time it has its own disadvantages to handle large scale databases. The first step is to construct graph. The kNN is suitable for MR, which has the ability to capture data's local structure. The construction cost for kNN graph is very high and it is represented as $O(n^2 \log k)$, MR ranking use the adjacency matrix W in their computation. The storage cost of W is denoted as O(kn). So the basic need is to construct a graph in both low cost and small storage memory.

The second, MR has very expensive computational cost because of the matrix inversion operation in equation (2). It is the main problem to apply in large databases. We can use the iteration algorithm temporarily to solve this problem.

4. EFFICIENT MANIFOLD RANKING

We present the disadvantages of original MR from to views. They are scalable graph construction [5] and efficient ranking computation.

4.1 COLOR BASED IMAGE

RGB Color Space

The RGB components are widely used in electronic media like CRT screens, LCDs, or phones that transmit to produce light. By using the type of color receptors in human eye can detect millions of colors. The receptor can relate with the RGB components. The color component value is stored in a byte and the values range between 0 and 255.

HSL & HSV Color Space

The RGB color space to form a cube is a challenging one. To represent a cube or color wheel is very poor. During working process with millions of colors at that time tint of color can't be aligned properly on RGB color space.

ISSN 2394-3777 (Print)
ISSN 2394-3785 (Online)
Available online at www.ijartet.com

International Journal of Advanced Research Trends in Engineering and Technology (IJARTET)
Vol. 4, Special Issue 5, March 2017

Step 1: Convert RGB color space image into HSV color space.

Step 2: Color quantization is carried out using color histogram by assigning 8 level each to hue, saturation and value to give a quantized HSV space with 8x8x8=512 histogram bins.

Step 3: The normalized histogram is obtained by dividing with the total number of pixels.

Step 4: Repeat step1 to step3 on an image in the database.

Step 5: Calculate the similarity matrix of query image and the image present in the database.

Step 6: Repeat the steps from 4 to 5 for all the images in the database.

Step 7: Retrieve the images

4.2 TEXTURE BASED IMAGE

The "uniform texture" is not well defined and the segmentation of texture is hard. The different segmentations are to provide a plausible at different scales of resolution. Each leaf in a tree is segmented as one scale so that the whole tree-top or the whole forest are considered to be individual regions at coarser scales. The retrieval error occurs when the mismatch between query and image descriptors in terms of resolution scales.

Retrieval based on comparing texture segments is usually sensitive to over- and under-segmentation. The changes in spatial texture appearance can cause single textures to be split into smaller segments (over-segmentation). The segmentation algorithm combines small regions of different textures (under-segmentation). The significant size is combined together and scattered image creates the problems in texture images. So that the images can be lost. An example of this phenomenon is an aerial view of a town in a richly vegetated area, in which both buildings and vegetation are made up of numerous but small texture patches.

Step 1: Read the Query input image name.

Step 2: Convert color image into grayscale image.

Step 3: Divide the Query image into 16 by 16 blocks.

Step 4: Calculate the query image feature as mean, max and min.

Step 5: Finally compute the covariance of the Query image.

ISSN 2394-3777 (Print)
ISSN 2394-3785 (Online)
Available online at www.ijartet.com

International Journal of Advanced Research Trends in Engineering and Technology (IJARTET)
Vol. 4, Special Issue 5, March 2017

Step 6: Load Covariance features of the image database.

Step 7: Compare the difference between Query image feature and the features of the image database.

Step 8: Sort the distance of the features of the image database.

Step 9: Retrieves the closest distance images from the image database.

Step 10: Display the retrieval images in the output panel.

4.3 SHAPE BASED IMAGE

The purpose of edge detection is to reduce the amount of data in an image. To preserve the structural properties is used to extract image processing. The aim of JFC was to develop an algorithm that is optimal with regards to the following criteria:

1. *Detection*: The probability of detecting real edge points should be maximized while the probability of falsely detecting non-edge points should be minimized. This corresponds to maximizing the signal-to-noise ratio.

2. Localization: The detected edges should be as close as possible to the real edges.

3. *Number of responses*: One real edge should not result in more than one detected edge (one can argue that this is implicitly included in the first requirement).

With JFC's mathematical formulation of these criteria, Canny's Edge Detector is optimal for a certain class of edges (known as step edges). The images used throughout this worksheet are generated using this implementation.

Step 1: Read the Query input image name.

Step 2: Convert color image into grayscale image.

Step 3: Calculate the edge of the query input image.

Step 4: Compute the moment of the query input image.

Step 5: Integrate the moment features of given images row and column wise.

Step 6: Load moment features of the image database.

Step 7: Compare the difference between moment feature of the query image and moment features of the image database.

Step 8: Retrieve the closest difference images from the image database.

ISSN 2394-3777 (Print)
ISSN 2394-3785 (Online)
Available online at www.ijartet.com

International Journal of Advanced Research Trends in Engineering and Technology (IJARTET)
Vol. 4, Special Issue 5, March 2017

Step 9: Display retrieval images on the output panel.

4.4 EMR for CBIR

The EMR is implemented in CBIR to improve information and extend the data features. The extraction features first done with the low level features of images in the database. To utilize the data points in the graph. The representative points can be select as anchors and weight matrix denoted by Z- with a small neighborhood size s. The offline anchor selection doesn't affect the online process. We cannot frequently update the anchors for stable dataset. At the final stage of uploading images or query the user can specify and extract the low level features and update the weight matrix Z-directly in the ranking score.

4.5 Out of Sample retrieval

For the offline stage the data retrieval sample are constructed by using graph and the calculation are done by matrix inversion. The situation is handled differently for out of sample data. The main drawback of MR is hard to handle the new sample queries. The MR designed a fastest strategy for leaving the original graph unchanged and its used to add a new row and column to W (left picture). The new W is not used for the ranking process but it gives an efficient output. During the online stage new query is not acceptable because of its high computational cost.

The out of sample problem can be solved by listening the nearest neighbors query and that query can be used as a query points. If the database is static the query or not used in the graph. The query can be change initial semantic meaning in a large database. The cost wise is high for the linear search nearest neighbors

We use zt to denote the new column. Then, $D_t = z_t^t$ v and $h_t = z_t D_t^{-1/2}$, where h_t is the new column of H. As we have described, the main step of EMR is Eq.(11). Our goal is to further speedup the computation of Eq.(11) for a new query. Let

5. RESULT AND DISCUSSION

The average precision obtains the value for single query is by using Average Precision method and set of top k items to get the relevant item from the retrieved data. The existing systems does not concentrates on strong, content-specific geometric constraints among different visual words in an image. The large scale content based image cannot be retrieved from this method. The object of a graph-based ranking model has the priority to allocate the importance of a vertex, based on local or global information draw from the graph. The manifold ranking algorithm and make a detailed analysis about its drawbacks. MR can be used in large applications but it has some of the drawbacks such as to handle the large scale database.

ISSN 2394-3777 (Print)
ISSN 2394-3785 (Online)
Available online at www.ijartet.com

International Journal of Advanced Research Trends in Engineering and Technology (IJARTET)
Vol. 4, Special Issue 5, March 2017

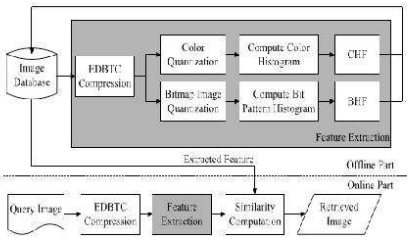

In our proposed method overcome of run out-of-sample retrieval method for ranking scores. It produces an approximate result. The large scale databases can gives the result within a short time. The proposed method gives the outsource under the Corel [2] 100 and Corel 1000 databases. The data can be modelled by a weighted graph, and incorporated this graph structure into the ranking function as a regularizer. An automatically tag ranking scheme by performing a random walk over a tag similarity graph. A projected gradient based algorithm was proposed in to compute weight matrix and in our previous work, a kernel regression method was adopted.

REFERENCES

[1] Zhong Wu Tsinghua Univ., Ctr Adv Study "Scalable Face Image Retrieval with Identity-Based Quantization and Multi-Reference Re-ranking," Asia Lab, 2012.

[2] C.P.Town AT&TLaboratoriesCambridge "Content Based Image Retrieval using Semantic Visual Categories", Cambridge,England-2012.

[3] Behjat Siddiquie University of Maryland, College Park" Image Ranking and Retrieval based on Multi-Attribute Queries" -2012.

[4] J. He, M. Li, H. Zhang, H. Tong, and C. Zhang, "Generalized manifold-ranking-based image retrieval,"IEEE Trans. Image Process., vol. 15, no. 10, pp. 3170–3177, Oct. 2006.

[5] W. Liu, J. He, and S. Chang, "Large graph construction for scalable semi-supervised learning," in Proc. 27th Int. Conf. Mach. Learn.,Haifa, Israel, 2010, pp. 679–686 .

[6] Christo Ananth, S.Santhana Priya, S.Manisha, T.Ezhil Jothi, M.S.Ramasubhaeswari, "CLG for Automatic Image Segmentation", International Journal of Electrical and Electronics Research (IJEER), Vol. 2, Issue 3, Month: July - September 2014, pp: 51-57

[7] J. Yu, D. Tao, and M. Wang, "Adaptive hypergraph learning and its application in image classification," IEEE Trans. Image Process.,vol. 21, no. 7, pp. 3262–3272, Jul. 2012.

[8] W. Liu, J. Wang, and S. Chang, "Robust and scalable graph-based semisupervised learning," Proc. IEEE, vol. 100, no. 9,pp. 2624–2638, Sept. 2012.

[9] D.Zhou,O.Bousquet,T.Lal,J.Weston,andB.Schölkopf, "Learning with local and global consistency," inProc. Adv. NIPS, 2004, pp. 595–602.

[10] D. Zhou, J. Weston, A. Gretton, O. Bousquet, and B. Schölkopf, "Ranking on data manifolds,"Proc.Adv.NIPS, vol. 16. Vancouver, BC, Canada, pp. 169–176, 2004.

[11] X. Wan, J. Yang, and J. Xiao, "Manifold-ranking based topic-focused multi-document summarization," in Proc. 20th IJCAI, vol. 7. San Francisco, CA, USA, 2007, pp. 2903–2908.

[12] J. He, M. Li, H. Zhang, H. Tong, and C. Zhang, "Manifold-ranking based image retrieval," inProc. 12th Annu. ACM Int. Conf. Multimedia, New York, NY, USA, 2004, pp. 9–16.

ISSN 2394-3777 (Print)
ISSN 2394-3785 (Online)
Available online at www.ijartet.com

International Journal of Advanced Research Trends in Engineering and Technology (IJARTET)
Vol. 4, Special Issue 5, March 2017

[13] B. Xu et al., "Efficient manifold ranking for image retrieval," in Proc. 34th Int. ACM SIGIR, New York, NY, USA, 2011, pp. 525–534.

[14] X. Yuan, X. Hua, M. Wang, and X. Wu, "Manifold-ranking based video concept detection on large database and feature pool," in Proc. 14th Annu. ACM Int. Conf. Multimedia, New York, NY, USA, 2006, pp. 623–626.

[15] J. Ponte and W. Croft, "A language modeling approach to infor-mation retrieval," nProc. 21st Annu. Int. ACM SIGIR, Melbourne, VIC, Australia, 1998, pp. 275–281.

[16] S. Brin and L. Page, "The anatomy of a large-scale hypertextual Web search engine,"Comput. Netw. ISDN Syst., vol. 30, no. 1–7, pp. 107–117, 1998.

[17] J. Kleinberg, "Authoritative sources in a hyperlinked environ-ment,"J. ACM, vol. 46, no. 5, pp. 604–632, 1999.

[18] J. Jeon, V. Lavrenko, and R. Manmatha, "Automatic image anno-tation and retrieval using cross-media relevance models," in Proc. 26th Annu. Int. ACM SIGIR, Toronto, ON, Canada, 2003, pp. 119–126.

[19] M. Tsai, T. Liu, T. Qin, H. Chen, and W. Ma, "FRank: A ranking method with fidelity loss," inProc. 30th Annu. Int. ACM SIGIR, Amsterdam, The Netherlands, 2007, pp. 383–390.

[20] W. Gao, P. Cai, K. Wong, and A. Zhou, "Learning to rank only using training data from related domain.

J.Rekha received her MSC(CS) degree from PSGR Krishnammal College for Women, Coimbatore, India in 2013. Now she is currently working toward the M.Phil degree at Sakthi Arts & Science College for women, Oddanchtram, India. Her main research interests include Image Processing, Network Security.

B. Muthu Kumar, Professor, Department of CSE, Syed Ammal Engineering College, Ramanathapuram, TN, India

Kavitha, Professor, Department of Computer Science, Sakthi College of Arts and Science for Women, TN, India

S.Prabhakaran, Department of Information Technology, Kathir College of Engineering, Now he is currently working in Ascox Techno Soft at Madurai, India. Him main research interests include Image Processing, Network Security, Cloud Computing.

S. Kavitha, Assistant Professor of Computer Science	International Journal of Advanced Research Trends in Engineering and Technology	-	Automated Screening System for Acute Myelogenous Leukemia Detection in Blood Microscopic Images	--	-	International ISSN 2394-3777 (Print) ISSN 2394-3785 (Online)	March 2017

ISSN 2394-3777 (Print)
ISSN 2394-3785 (Online)
Available online at www.ijartet.com

International Journal of Advanced Research Trends in Engineering and Technology (IJARTET)
Vol. 4, Special Issue 5, March 2017

AUTOMATED SCREENING SYSTEM FOR ACUTE MYELOGENOUS LEUKEMIA DETECTION IN BLOOD MICROSCOPIC IMAGES

Abirami.V 1* , B. Muthu Kumar 2 , Kavitha 3 , S.Prabhakaran 4

1, 3Department of Computer Science, Sakthi College of Arts and Science for Women, TN, India

2 Professor, Department of CSE, Syed Ammal Engineering College, Ramanathapuram, TN, India

4 Department of Information Technology, Kathir College of Engineering

*Corresponding Author: mailto: abiramibca10@gmail.com

ABSTRACT

The pervasive among the adults are Acute Myelogenous Leukemia (AML) is a sub-type of acute leukemia. The person has AML mostly at the age of 65 years. The current method implements the manual examination of the blood smear during the diagnosis. It needs for the detection of leukemia [11]. It is favor for the operators' ability, accuracy and time consumption. AML is presented a small technique in blood smear. The proposed method includes 1) this approach developed for simplicity 2) classification of complete blood smear images as opposed to sub-images. 3) this algorithm is used to segment and detect nucleated cells. The computer simulation is under the testers comparing the impact of Hausdorff [7] dimension on the system before and after the influence of local binary pattern. The sub-images and the whole images performance and the results are compared to the existing system and proposed system. Our aim is to achieve 98% accuracy for the localization of the lympho [14] blast cells. Already the microscopic blood images are tested.

Keywords: Acute Myelogenous Leukemia (AML), classification, segmentation.

1. INTRODUCTION

Our goal is to a) illustrate that the classification of peripheral blood smear images containing multiple nuclei can be fully automated b) the hold-out cross validation method is used to validate and segment the images c) this method estimates around a 50 set of images (25 abnormal samples and 25 normal samples) from American Society of Hematology. The segmentation and classification of AML based on complete microscopic blood images is our proposed method. The term classification [13] of leukemia is mostly finding the problem accurately.

In our proposed system, it can extract the shape based approaches like lines, sheets from the 3-D biomedical images. The ellipsoidal model is considered as thin structures. In existing system, Gaussian filter method are implemented to simplify and for getting segmentation results. Using CIELAB color space and various edge detection

ISSN 2394-3777 (Print)
ISSN 2394-3785 (Online)
Available online at www.ijartet.com

International Journal of Advanced Research Trends in Engineering and Technology (IJARTET)
Vol. 4, Special Issue 5, March 2017

algorithms, the segmentation is performed. The edge detection methods consolidated are Sobel, Prewitt, Roberts, Laplacian of Gaussian and Canny edge detectors [17]. The best detection technique is canny edge detectors.

The canny implements two different threshold values to identify the strong and weak edges. The weak edges are identified only if they are connected to strong edges. A new method is implemented for segmentation is Gabor filters for extraction and segmentation of tagged cardiac images. The designs of adaptive filters for different local regions are implemented by Gabor filters. Because the wavelets [12] are like local filters in spatial domain. The advantage of Gabor filter is they can combine with Gaussian envelopes. The minimum space bandwidth is achieved by these filters. Gabor filters are used widely in image processing applications like texture segmentation and edge detection. Gabor filters are used widely in image processing applications like texture segmentation and edge detection. [5] proposed a system which uses intermediate features of maximum overlap wavelet transform (IMOWT) as a pre-processing step. The coefficients derived from IMOWT are subjected to 2D histogram Grouping. This method is simple, fast and unsupervised. 2D histograms are used to obtain Grouping of color image. This Grouping output gives three segmentation maps which are fused together to get the final segmented output. This method produces good segmentation results when compared to the direct application of 2D Histogram Grouping. IMOWT is the efficient transform in which a set of wavelet features of the same size of various levels of resolutions and different local window sizes for different levels are used. IMOWT is efficient because of its time effectiveness, flexibility and translation invariance which are useful for good segmentation results.

2. RELATED WORKS

SEGMENTATION OF 4D CARDIAC MRI: AUTOMATED METHOD BASED ON SPATIO-TEMPORAL WATERSHED CUTS

J. COUSTY; L. NAJMAN

A new automated and fast procedure method is proposed to segment the left ventricular myocardium in 4D MRI sequences. The quantitative and qualitative evaluations [20] are provided. The discrete mathematical morphology is used and the time efficiency is high. The ability of the method to compute reliable characteristics of the LV (ejection fraction and left ventricular mass); the temporal continuity of the resulting automated segmentation and the time-efficiency (about 3' to segment a sequence of 25 3D-images on a low-end computer) of the proposed method is checked for the accuracy. The cardiac segmentation [3] method is difficult to design. For that, the watershed [1] cuts, a notion of watershed in edge-weighted graphs which is optimal in a sense equivalent to minimum spanning trees is introduced. The watershed-cuts in 4-dimensional spaces are proposed. Our second goal is to improve the ability of both the spatial and temporal gradient of the images. The segmentation produced the spatially as well as temporal consistent.

The proposed method can be fairly used to assess model-based segmentation schemes and the results are compared with the non-model based segmentation. The proposed method is used to register generic physiological models of the heart to real patient specific cardiac images. It can be

ISSN 2394-3777 (Print)
ISSN 2394-3785 (Online)
Available online at www.ijartet.com

International Journal of Advanced Research Trends in Engineering and Technology (IJARTET)
Vol. 4, Special Issue 5, March 2017

easily register a model to a binary segmentation than directly to images. The successive segmentations obtained over the time take into account spatio-temporal properties of the images. The proposed scheme does not permit the direct derivation of deformation parameters. The accuracy is improved by registration with other modalities such as delayed enhanced MRI and CT scan.

A REVIEW OF SEGMENTATION METHODS IN SHORT AXIS CARDIAC MR IMAGES

The fully and semi-automated methods performing segmentation in short axis images using a cardiac cine MRI [4] sequence is discussed. To tackle the ventricle segmentation in cardiac MRI, an image-driven is proposed. These methods require either minimal or user intervention. The image based and the pixel classification-based frameworks are incorporating strong prior, straightforward extensions of deformable models. The next section presents strong prior for heart segmentation. It can be generated by manually segmenting an image or by integrating information from multiple segmented images from different individuals. Strong prior based methods overcome the segmentation problems. We have proposed a categorization for these methods, highlighting the key role of the type of prior information used during segmentation, and has distinguished three levels of information:

i. No information is used.
ii. Weak prior i.e, low level information.
iii. Strong prior information.

CARDIAC LV AND RV SEGMENTATION USING MUTUAL CONTEXT INFORMATION

In this paper, a graph cut based method is implemented to segment the cardiac right ventricle (RV) and left ventricle (LV) by using mutual context information. It includes a 'context penalty' for the RV by learning its geometrical relationship with respect to the LV. Similarly, the RV provides geometrical context information for LV [2] segmentation. The smoothness cost is formulated for the learned context and captures the geometric relationship between the RV and LV. The mutual context information method is to segment the RV and LV. The geometric relationship is used for the shapes in the form of relative orientations. The RV and LV are manually segmented and they are learned from a set of training images. The learned information is encoded on a graphical model of the image as weights between pixel nodes and terminal nodes. Graph cuts are used to find the final labels in an iterative fashion. This paper makes the following contributions:

1) We encode context information for each pixel as well as between pixels. The Graph cuts do not need the sub-modular graphs. The distance information is not needed.

2) The RV and LV is used to segment the individual organs.

The RV and LV are used to improve segmentation accuracy. Context information was modeled in the form of relative orientation of the two organs from a set of training images. The two penalties and smoothness cost leads to improve the segmentation performance.

ISSN 2394-3777 (Print)
ISSN 2394-3785 (Online)
Available online at www.ijartet.com

International Journal of Advanced Research Trends in Engineering and Technology (IJARTET)
Vol. 4, Special Issue 5, March 2017

3. CLUSTERING BASED SEGMENTATION

Clustering means measurement of points or patterns are grouped together. This technique implements in data of n-dimension. This n represents arbitrary number i.e it can be two, three or more. The cluster technique is a best suit for sparse type of images. This technique includes methods like k-means, fuzzy [8] c-means etc. SubrajeetMohapatra & DeeptiPatra proposed an automated nucleus segmentation method. For segmentation two steps are performed to segment a WBC nucleus [10] from the rest of the image objects. The first step, the segmentation is performed by executing a semi-supervised k-means clustering. The second step of segmentation is performed by nearest neighbor classification in L*a*b space.

In blood microscopic [9] images and the white blood cells [16] are segmented by using a cluster method. In our proposed system, the first step to convert the images into Lab color space. In fuzzy, k-means clustering is to divide the images into three clusters. At the same time, automatic histogram is performed on the Lab color image. The results of clusters and the reference image are compared, selected and performs a logical AND operation.

In the proposed approach first the RGB image is converted to Smith's HSI transformation. Then a membership function is assigned to each color pattern. After obtaining the membership degree for color patterns, pixel classification is carried out for segmentation purposes. A fuzzy approach [19] for leukemia detection is proposed.

3.1 INPUT CELL IMAGE

The input is taken as blood cell image. Basically the data are collected from the outside sources. If the blood cell is visible size then the refraction effects are almost negligible. The disc function is used to approximate the real images. Comparing to MRI images, the disc approximation is enough for testing images. The 3-D geometric information is used to identify in-focus subjects by getting the local blood cell [15] images for testing samples.

3.2 EVALUATE CELL FEATURES

In image processing, feature extraction [6] method is used to redefine a large set of redundant data and a set of features from reduced dimension. The input data are transformed to the set of features is called feature extraction. This method influences the classifier performance and it is very crucial to select the correct one. To give an effective feature set we have to analyze several published articles and methods are absorbed. The features are widely used for a good classification and in our proposed method implements the features on whole images. It is used to boost the classifier performance. This technique is implemented on a segmented image to identify the location and size of complete non-overlapping cells in a microscopic image.

3.3 SEGMENTATION USING k-MEANS ALGORITHM

The least squares partitioning method that divide a collection of objects is called k-means or k-groups. The algorithm follows the below steps:

1. Compute the mean of each cluster.
2. Compute the distance of each point from each cluster by computing its distance

ISSN 2394-3777 (Print)
ISSN 2394-3785 (Online)
Available online at www.ijartet.com

International Journal of Advanced Research Trends in Engineering and Technology (IJARTET)
Vol. 4, Special Issue 5, March 2017

from the corresponding cluster mean. The each nearest point is assigned to the cluster.

Initially the clusters are used to assign randomly. This iteration implements to minimum the sum, overall groups, squared within the group errors. These are the distance of the points to the respective group means. Convergent occurs when it reach the residual sum of squares cannot be lowered any more. The roots obtained the geometrically compact as possible around their respective means.

3.4 ARCHITECTURE

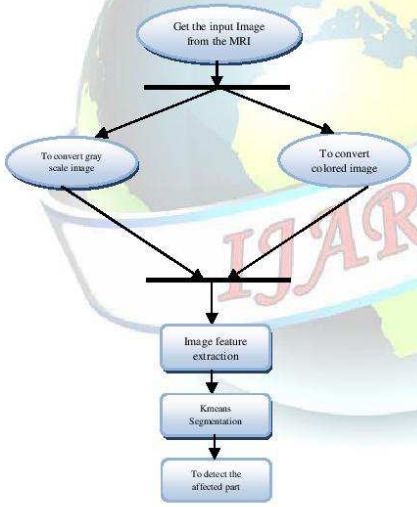

3.5 FEATURE CLASSIFICATION

The classification algorithm includes the identification of images and the assumption of images in depicts one or more features for classifying the system or spectral regions in the case of remote sensing. This feature belongs to several distinct and exclusive classes. The classes are specified on a priori by an analyst on in supervised classified and unsupervised [18] classification. The set of prototype classes are specified the number of desired categories.

3.5.1 PROCESS

The classification of algorithm employ the two phases of processing are training and testing. The training phase includes the typical image features are isolated and unique classification category. The motivating criteria for constructing training classes are that they are:

- *independent*, *i.e.* a change in the description of one training class should not change the value of another,
- *discriminatory*, *i.e.* different image features should have significantly different descriptions, and
- *reliable*, all image features within a training group should share the common definitive descriptions of that group.

3.6 CLASSIFICATION

This classification clear cuts the cancer and non-cancer blood cells to get the spitted part from k-means segmentation. Classification generates the result for k-means cluster and also in support vector machine.

ISSN 2394-3777 (Print)
ISSN 2394-3785 (Online)
Available online at www.ijartet.com

International Journal of Advanced Research Trends in Engineering and Technology (IJARTET)
Vol. 4, Special Issue 5, March 2017

4. METHODOLOGY

4.1 k-MEANS ALGORITHM

The k-means clustering algorithm was developed by J.MacQueen(1967) and then by J.A.Hartigan and M.A.Wong around 1975. This algorithm is to classify or to group the objects based on attributes/features into K groups. After an initial random assignment of data points to k clusters, the centers of clusters are computed. The data points are allocated to the clusters with the closest centers. This process continues until the cluster centers do not significantly change.

The data set of each cluster's architecture is updated. During the updation of clusters, data points are removed from one cluster and added to another. The updating clusters changes the values of the centroids. This change is a reflection of the current cluster data points.

When the cluster is not change, the training of the k-means algorithm is complete. The 'k' cluster centroids are created and it is ready to classify the patient's statuses as normal, hyperthyroid and/or hypothyroid function.

The process gives a easy way to classify the data set through a certain number of clusters (assume k clusters) fixed a priori. The aim is to define k centroids by assigning one to each cluster. These centroids should be placed in a crafty way to avoid location problem. The next step is to check with the given data set and associate it to the nearest centroid. It is necessary to re-calculate k new centroids.

After obtaining k new centroids, a new binding has to be done between the same data points and the nearest new centroid. The loop may change their location step by step until no more changes are to perform in the k centroids.

The objective function

$$J = \sum_{j=1}^{k} \sum_{i=1}^{n} \| x_i^{(j)} - c_j \|^2 \quad (1)$$

Where$\|x_i^{(j)}-c_j\|^2$ is a chosen distance measure between a data point x_i^j and the cluster center c_j is an indicator of the distance of the *n* data points from their respective cluster centers.

The k-means algorithm can be run multiple times to reduce this effect. This algorithm is used to work for a randomly generated data points. It is used to find the locally minimal solution. The dissimilarity measure is represented as the Euclidean distance.

A set of n vectors X_j, j = 1… n, are to be partitioned into C groups G_i , i=1,…,C. The cost function, based on the Euclidean distance between a vector x_k in group j and the corresponding cluster center C_i , can be defined by:

$$J = \sum_{i=0}^{c} Ji = \sum_{i=1}^{c} \left[\sum_{k,x \in Gi} \| Xk - Ci \|^2 \right] \quad (2)$$

Where $J=\sum^{c}_{k,x\epsilon Gi}\| X_K - C_i \|^2$is a cost function within group i. There are two problems that are inherent to k-means clustering algorithms. The first is determining the initial partition and the second is determining the optimal number of clusters.

If the cluster is in the centre of k-means algorithm is used to run several times with the

ISSN 2394-3777 (Print)
ISSN 2394-3785 (Online)
Available online at www.ijartet.com

International Journal of Advanced Research Trends in Engineering and Technology (IJARTET)
Vol. 4, Special Issue 5, March 2017

different set of initial cluster centre to improve performance.

5. RESULTS AND DISCUSSION

5.1 PROBLEM IDENTIFICATION

Detection accuracy is low so that segmentation task is complex. The major problem occurs are Image processing and pattern recognition problems. The LBP method performs the outsource of existing methods are the linear discriminant analysis and the principal component analysis. In this system performs classification of whole images and also includes the better performance for sub-images. The proposed technique is to achieve an automatic classification system to diagnosis the presence of the acute leukemia from blood microscope images. Comparing segmentation of nucleus to the segmentation of the entire cell is much easier. In the bone marrow, the WBC density is very high. A set of manually segmented images of the nucleus are used to decouple segmentation errors. A microscopic blood image of size 184×138 is considered for evaluation.

Drawbacks

- Accuracy is low
- Cannot provide optimized cancer detect
- Segmentation process have some trouble

5.2 PROBLEM SOLVING

The system implements on peripheral blood smear images obtained from two places. Here the method performs automated processing, including color correlation, segmentation of the nucleated cells, and effective validation and classification.

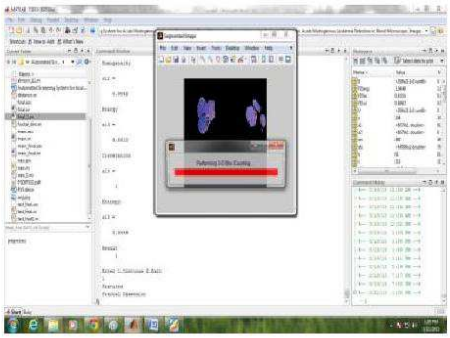

The feature set used to perform the efficient classification among the exploiting shape, color, and texture parameters of a cell. The impact of the LBP operator on the HD proved to be a promising feature for this analysis. A color feature called cell energy was introduced, and results show that this feature presents a good demarcation between cancer and non-cancer cells.

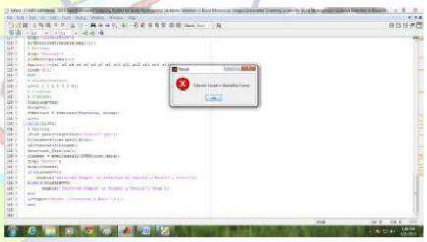

Advantages

- It provides high accuracy
- It provide optimized cancer detect
- No problem on this algorithm
- Here we used K-Means Algorithm for segmentation and classification
- Performance also high

6. CONCLUSION

Our proposed system performs automated processing includes color correlation,

segmentation of the nucleus, effective validation and classification. The shape, color and texture parameters of a cell are utilized from the feature set and to obtain the information and to perform efficient classification. The FD proved promising feature for clustering operator. A color feature called cell energy and they presented good demarcation between cancer and non-cancer cells. The affected part of an MR image is detected. The label information is used to improve the image registration accuracy. It provides useful information for clinicians in cancer disease diagnosis.

REFERENCES

[1] J.Cousty, L.Najman, M. Couprie, S. Clément-Guinaudeau, T. Goissen,And J. Garot, "Segmentation of 4D cardiac MRI: Automated method Based on spatio-temporal watershed cuts,"

[2] M. Jolly, "Fully automatic left ventricle segmentation in cardiac Cine MR Images using registration and minimum surfaces," MIDAS.

[3] M. Lorenzo-Valdés, G. I. Sanchez-Ortiz, A. G. Elkington, R. H. Mohiaddin and D. Rueckert, "Segmentation of 4D cardiac MR images using a probabilistic atlas and the EM algorithm,"

[4] M. Lynch, O. Ghita, and P. F. Whelan, "Segmentation of the left ventricle Of the heart in 3-MRI data using an optimized Non-rigid Temporal model,"

[5] Christo Ananth, A.S.Senthilkani, S.Kamala Gomathy, J.Arockia Renilda, G.Blesslin Jebitha, Sankari @Saranya.S., "Color Image Segmentation using IMOWT with 2D Histogram Grouping", International Journal of Computer Science and Mobile Computing (IJCSMC), Vol. 3, Issue. 5, May 2014, pp-1 – 7

[6] G. Ongun, U. Halici, K. Leblebicioglu, V. Atalay, M. Beksac, and S. Beksac, "Feature extraction and classification of blood cells for an automated differential blood count system," in Proc. IJCNN, 2001, vol. 4, pp. 2461–2466.

[7] S. Mohapatra and D. Patra, "Automated leukemia detection using haus-dorff dimension in blood microscopic images," in Proc. Int. Conf. Emerg. Trends Robot Commun. Technol., 2010, pp. 64–68.

[8] S. Mohapatra, S. Samanta, D. Patra, and S. Satpathi, "Fuzzy based blood image segmentation for automated leukemia detection," inProc. ICDeCom, 2011, pp. 1–5.

[9] S. Mohapatra, D. Patra, and S. Satpathi, "Image analysis of blood microscopic images for acute leukemia detection," inProc. IECR, 2010, pp. 215–219.

[10] S. Mohapatra, D. Patra, and S. Satpathi, "Automated cell nucleus segmentation and acute leukemia detection in blood microscopic images," in Proc. ICSMB, 2010, pp. 49–54.

[11] MedlinePlus: Leukemia.National Institutes of Health. [Online]. Available: http://www.nlm.nih.gov/medlineplus/ency/article/001299.htm

[12] C. Lopez and S. Agaian, "A new set of wavelet- and fractals-based features for Gleason grading of prostate cancer histopathology images," inProc. SPIE, Image Process., Algorithms Syst. XI, 2013, vol. 8655, pp. 865516-1–865516-12.

[13] S. Serbouti, A. Duhamel, H. Harms, U. Gunzer, J. Mary, and R. Beuscart, "Image segmentation and classification methods to detect leukemias," in Proc. Int. Conf. IEEE Eng. Med. Biol. Soc., 1991, pp. 260–261.

[14] D. Foran, D. Comaniciu, P. Meer, and L. A. Goodell, "Computer-assisted discrimination among malignant lymphomas and leukemia using immune phenotyping, intelligent image repositories, and tele

ISSN 2394-3777 (Print)
ISSN 2394-3785 (Online)
Available online at www.ijartet.com

International Journal of Advanced Research Trends in Engineering and Technology (IJARTET)
Vol. 4, Special Issue 5, March 2017

microscopy," IEEE Trans. Inf. Technol. Biomed., vol. 4, no. 4, pp. 265–273, Dec. 2000.

[15] K. S. Kim, P. K. Kim, J. J. Song, and Y. C. Park, "Analyzing blood cell image do distinguish its abnormalities," in Proc. ACM Int. Conf. Multim., 2002, pp. 395–397.

[16] Q. Liao and Y. Deng, "An accurate segmentation method for white blood cell images," in Proc. IEEE Int. Symp. Biomed. Imaging, Atlanta, GA, USA, 2002, pp. 245–248.

[17] K. Panetta, S. Agaian, S. Nercessian, and A. Almunstashri, "Shape-dependent canny edge detector,"Opt. Eng., vol. 50, no. 8, pp. 087008-1–087008-12, Aug. 2011.

[18] P. Bamford and B. Lovell, "Method for accurate unsupervised cell nucleus segmentation," in Proc. Eng. Med. Biol. Soc. Conf., 2001, vol. 3, pp. 2704–2708.

[19] W. Shitong, K. F. L. Chung, and F. Duan, "Applying the improved fuzzy cellular neural network IFCNN to white blood cell detection,"Neurocom-puting, vol. 70, no. 7–9, pp. 1348–1359, Mar. 2007.

[20] M. Oberholzer, M. Ostreicher, H. Christen, and M. Bruhlmann, "Methods in quantitative image analysis," Histochem. Cell Biol., vol. 105, no. 5, pp. 333–355, May 1996.

V.Abirami received her MCA degree from RVS College of Engineering & Technology, Dindigul, India in 2015. Now she is currently working toward the M.Phil degree at Sakthi Arts & Science College for women, Oddanchtram, India. Her main research interests include Image Processing, Network Security.

B. Muthu Kumar, Professor, Department of CSE, Syed Ammal Engineering College, Ramanathapuram, TN, India

Kavitha, Professor, Department of Computer Science, Sakthi College of Arts and Science for Women, TN, India

S.Prabhakaran, Department of Information Technology, Kathir College of Engineering, Now he is currently working in Ascox Techno Soft at Madurai, India. Him main research interests include Image Processing, Network Security, Cloud Computing.

S. Kavitha, Assistant Professor of Computer Science	International Journal of Advanced Research Trends in Engineering and Technology		Biometric Deceit Detection for Secure Authentication Using Deep Learning			International ISSN 2394-3777 (Print) ISSN 2394-3785 (Online)	March 2017

ISSN 2394-3777 (Print)
ISSN 2394-3785 (Online)
Available online at www.ijartet.com

International Journal of Advanced Research Trends in Engineering and Technology (IJARTET)
Vol. 4, Special Issue 5, March 2017

BIOMETRIC DECEIT DETECTION FOR SECURE AUTHENTICATION USING DEEP LEARNING

Udhaya.M 1* , B. Muthu Kumar 2 , Kavitha 3 , S.Prabhakaran 4

1, 3Department of Computer Science, Sakthi College of Arts and Science for Women, TN, India

2 Professor, Department of CSE, Syed Ammal Engineering College, Ramanathapuram, TN, India

4 Department of Information Technology, Kathir College of Engineering

*Corresponding Author: mailto: m.udhaya21@gmail.com

Abstract— Biometrics systems are playing an important role in personal, national and global security to improve person recognition and authentication. However, the deceiving attacks are occurred, it can be overcome by biometric systems. The people are heedless about biometric deceit sensor to derive outstanding deceit detection systems. They are iris, face, and fingerprint techniques based on the approaches of deep learning [13]. The first approach includes of learning each patch in convolutional network architectures and through back propagation the second approach concentrates on learning the weights [18] of the network. The nine biometric deceit specifications each one containing real and fake [20] samples of a given biometric modality and attack type and learn deep representations for each specification by combining and contrasting the two learning approaches. This plan provides better result from the eight out of nine specifications. The outcomes indicate that deceit [22] detection systems based on convolutional networks can be resilient to attacks already known and possibly adapted, with little effort, to image-based attacks.

Index Terms— filter weights learning, back-propagation, deceit detection.

I. INTRODUCTION

BIOMETRICS are used for access control, espionage and also in every security systems by allowing person recognition and authentication based on the features of human. The biometric techniques have been widely applied to person recognition, ranging from traditional fingerprint to face [19], to iris and recently, to vein and blood flow for data acquisition, storage and processing, and also the scientific advances in computer vision, pattern recognition, and machine learning due to technological improvements.

There are various methods to deceit a biometric system. Indeed, previous works show eight different points of attack that can be divided into two main categories: direct and indirect attacks. The possibility to generate synthetic biometric samples is the first exposure of biometric security sensors. The final comprises all the remaining seven attacks and statutory different proportions of knowledge about the system, e.g., the matching algorithm used, the specific feature extraction procedure, database access for manipulation, and also possible weak links in the communication channels within the system.

This is possibly because a number of biometric traits can be easily forged with the use of common equipments and consumer electronics to emulate real biometric readings. Examples are stampers, printers,

ISSN 2394-3777 (Print)
ISSN 2394-3785 (Online)
Available online at www.ijartet.com

International Journal of Advanced Research Trends in Engineering and Technology (IJARTET)
Vol. 4, Special Issue 5, March 2017

displays, audio [4] recorders. The biometric deceit specifications allowed researchers to make steady advance in the beginning of anti-deceit systems. The deceit detection has been investigated are iris, face, and fingerprint techniques. Specifications share the common characteristic of image or video based.

The success of an anti-deceit method is based on the design. It is able to capture acquisition telltales left by specific attacks based on the systems rely on expert knowledge. Small changes in the attack could require the redesign of the entire system.

In this paper, we do not focus on custom-tailored solutions. Instead, inspired by the Deep Learning's success in various tasks, and by the ability of the technique to leverage data concentrates on two general-purpose approaches to build image-based anti-deceit systems with convolution networks for several attack types. [6] proposed a system in which OWT extracts wavelet features which give a good separation of different patterns. Moreover the proposed algorithm uses morphological operators for effective segmentation. From the qualitative and quantitative results, it is concluded that our proposed method has improved segmentation quality and it is reliable, fast and can be used with reduced computational complexity than direct applications of Histogram Clustering. The main advantage of this method is the use of single parameter and also very faster. While comparing with five color spaces, segmentation scheme produces results noticeably better in RGB color space compared to all other color spaces.

The Filter optimization [16] (FO) and Architecture Optimization (AO) are presented on the left and right high-lighten as blue and red.

The practical outcome strongly indicates that convolutional [11] networks can be readily used for brawny deceit detection. In fact, in the research field the data-driven solutions based on deep representations is a valuable direction, allowing the construction of systems with little effort to image-based attack types. The remaining works are classified into five sections. Section II enlightens the previous anti-deceit systems for the three biometric techniques discussed in this paper, while Section III describes the methodology adopted for architecture optimization (AO) and filter optimization (FO) while Section IV presents experiments, results, and comparisons with state-of-the-art methods. Finally, Section V concludes the paper and discusses some possible future works.

II. RELATED WORKS

[1]C. Rathgeb and A. Uhl, The fuzzy commitment scheme has been leveraged as a means of biometric template protection.

Binary templates are replaced by helper data which assist the retrieval of cryptographic keys. Biometric variance is overcome by means of error correction while authentication is performed indirectly by verifying key validities. A statistical attack against the fuzzy commitment scheme is presented. Comparisons of different pairs of binary biometric feature vectors yield binomial distributions, with standard deviations bounded by the entropy of biometric templates. In case error correction consists of a series of chunks helper data becomes vulnerable to statistical attacks. Error correction codewords are bound to separate parts of a binary template among which biometric entropy is dispersed. As a consequence, chunks of the helper data are prone to statistical significant false acceptance. In experiments the proposed attack is applied to different iris-biometric fuzzy commitment schemes retrieving cryptographic keys at alarming low effort.

[2] A. F. Sequeira, H. P. Oliveira, J. C. Monteiro, J. P. Monteiro, and J. S. Cardoso, Biometric

ISSN 2394-3777 (Print)
ISSN 2394-3785 (Online)
Available online at www.ijartet.com

International Journal of Advanced Research Trends in Engineering and Technology (IJARTET)
Vol. 4, Special Issue 5, March 2017

systems based on iris are vulnerable to several attacks, particularly direct attacks consisting on the presentation of a fake iris to the sensor.

The development of iris liveness detection techniques is crucial for the deployment of iris biometric applications in daily life specially in the mobile biometric field. The 1st Mobile Iris Liveness [5] Detection Competition (MobILive) was organized in the context of IJCB2014 in order to record recent advances in iris liveness detection. The goal for (MobILive) was to contribute to the state of the art of this particular subject. This competition covered the most common and simple deceit attack in which printed images from an authorized user are presented to the sensor by a non-authorized user in order to obtain access. The specification dataset was the MobBIOfake database which is composed by a set of 800 iris images and its corresponding fake copies (obtained from printed images of the original ones captured with the same handheld device and in similar conditions). In this paper we present a brief description of the methods and the results achieved by the six participants in the competition.

[3] N. Erdogmus and S. Marcel, The problem of detecting face deceit attacks (presentation attacks) has recently gained a well-deserved popularity.

Mainly focusing on 2D [9] attacks forged by displaying printed photos or replaying recorded videos on mobile devices, a significant portion of these studies ground their arguments on the flatness of the deceit material in front of the sensor. In this paper, we inspect the deceit potential of subject-specific 3D facial masks for 2D face recognition. Additionally, we analyze Local Binary Patterns based countermeasures using both color and depth data, obtained by Kinect. For this purpose, we introduce the 3D Mask Attack Database (3DMAD), the first publicly available 3D deceit database, recorded with a low-cost depth camera. Extensive experiments on 3DMAD show that easily attainable facial masks can pose a serious threat to 2D face recognition systems and LBP is a powerful weapon to eliminate it.

III. METHODOLOGY

3.1 SUPPORT VECTOR MACHINE (SVM)

A Support Vector Machine (SVM) is used to define a separating hyperplane. The output of the hyperplane is classified into two classes. They are horizontal and vertical hyperplanes. The SVM algorithm is used to find the hyperplane. It gives the largest minimum distance. The distance of twice receives the name of the margin within SVM's theory. Optimal are used to separate the .hyperplane and maximize the margin data.

Nonlinear classification

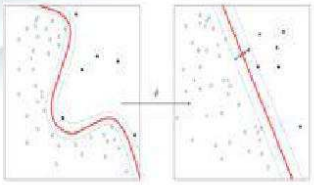

Fig: 3.1 Nonlinear

3.2 Fast Fourier Transform (FFT)

In this figure 3.2 a Fast Fourier transform (FFT) is a systematic algorithm to compute the DFT

ISSN 2394-3777 (Print)
ISSN 2394-3785 (Online)
Available online at www.ijartet.com

International Journal of Advanced Research Trends in Engineering and Technology (IJARTET)
Vol. 4, Special Issue 5, March 2017

for an input vector. Systematic means FFT can compute the DFT of n-element vector in O (n log n) operations contrasts to the O (n^2). FFT exists for vector length n. Parallel FFT developed for advent of parallel computing. FFT are used to represent the sequence of summations or its factorization of transform matrix. FFT is used to transform the function of time into function of frequency. It mainly supports to identify the timing dependent. FFT's major work is to breakdown the complicated signal and converts into simple waves.

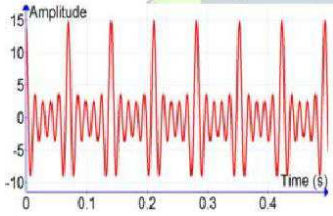

Fig: 3.2 Fast Fourier Transform

Architecture

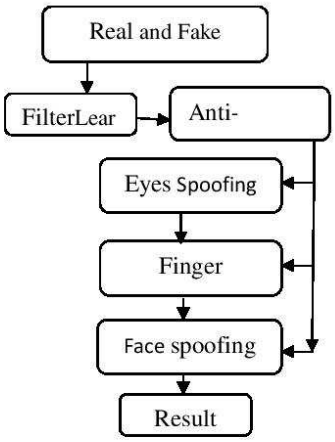

Fig: 3.3 Architecture

3.3 Specular Reflection Features

In figure 3.4 shows specular reflection is like a mirror reflection of light and the light reflects in a single incoming direction and into a single outgoing direction. It reflects the light in the entire same angle. Lights are used to reflect in three possible outcomes such as absorption, transmission and reflection. The light reflected at a definite angle is from a smooth surface. The light reflections are depending upon the smooth surfaces or texture surfaces. To remove specular reflection and normalizing face gleam, specular reflection component image is used. The input face image or video used to separate the technique which is specular reflection component. The assumption is gleam comes from a single source of same color and not over saturated. The face [14] images are captured indoors under relatively controlled gleam and it presents the difference between the genuine face of a specular reflection components and the corresponding deceit face.

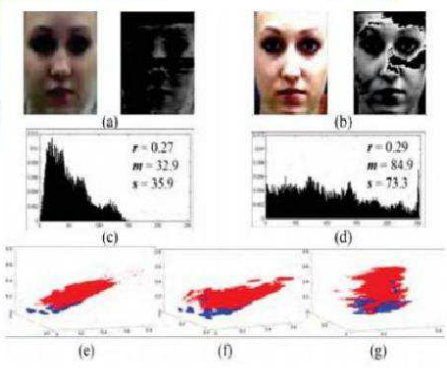

Fig: 3.4 Specular Reflection

ISSN 2394-3777 (Print)
ISSN 2394-3785 (Online)
Available online at www.ijartet.com

International Journal of Advanced Research Trends in Engineering and Technology (IJARTET)
Vol. 4, Special Issue 5, March 2017

3.4 Color Contrast Features

Another important difference between genuine and deceit faces is the color contrast. Genuine faces have opulent colors. This contrast tends to dwindle out in deceit faces due to the color proliferation loss during image/video reseize. In this paper, we follow the method used to measure the image color contrast. Color with 32 steps in the RGB channels is performed on the normalized face image. In this figure 3.5 shows two measurements are then obtained from the color distribution: i) the top 100 most frequently appearing colors, and ii) the number of unique colors appearing in the normalized face image. The dimensionality of the color contrast feature vector is 101.

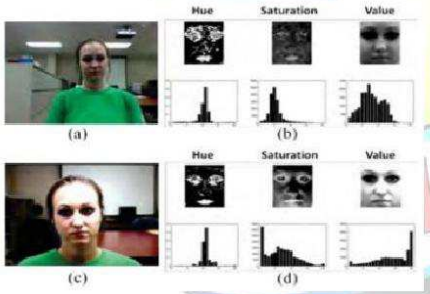

Fig:3.5 Color Contrast

IV. RESULT AND DISSCUISION

The information deals with the face deceit detection problem through texture patterns and image quality metrics.

- By considering the previous problems, Network architecture (figure 3.3) in designed.
- To reduce the problems, deep learning technique is assumed.
- Fingerprint deceit attack detection is a huge problem and the outcome is far away from a perfect classification rate.
- The acquisition sensor is the unshielded [3] part of a system and the attackers mostly focuses on deceit directly.

4.1. Preprocessing

The preprocessing testing was executed on face, Iris [2] and fingerprint images to study the representations properly. In this figure 4.1 & 4.2 preprocessing lead to images with sizes.

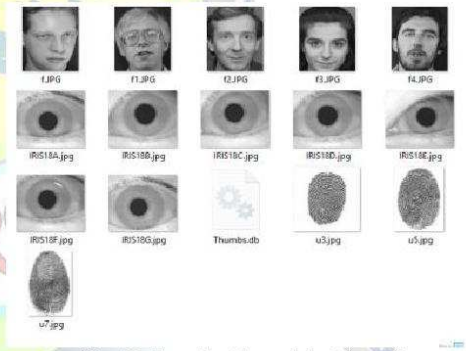

Fig: 4.1 To collect the original face, finger and iris images for store the database.

ISSN 2394-3777 (Print)
ISSN 2394-3785 (Online)
Available online at www.ijartet.com

International Journal of Advanced Research Trends in Engineering and Technology (IJARTET)
Vol. 4, Special Issue 5, March 2017

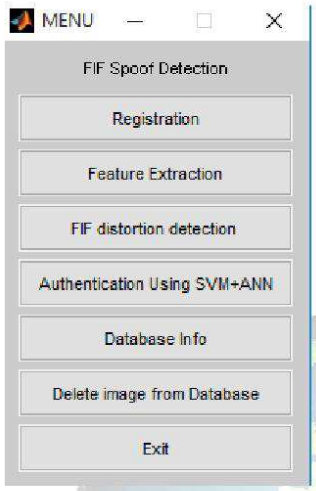

Fig: 4.2 To get menu form after preprocessing

4.2. Iris Deceit Detection

In figure 4.3 iris [1] is a unique modality and it generates the accurate result for recognition [17]. The first algorithm was proposed by Daugman based on iris codes which are used in iris technologies and applications. The several algorithms are also proposed to advance the state-of-art in iris recognition.

Iris deceit is a technique by which one can muddle or mock the identity of a sole. The ways of deceit an iris recognition system is discussed below:

Fig: 4.3 To registered iris image for users from database

1) Pupil dilation: Pupil dilation can occur due to gleam variations, alcohol (substance) consumption, and medicine. As shown by Hollingsworth et al., large pupil dilation can cause iris patterns to be unrecognizable.

2) Textured contact lenses: Several researchers have shown that a colored textured contact [7] lens can block the actual iris patterns and confuse an iris recognition system. Inter-class and intra-class similarities are significantly affected by colored textured contact lenses. Similarly, a lens with a painted iris obfuscates the actual eye patterns and creates a different appearance which is unseen by the iris recognition systems.

3) Print attack: Presenting a printed image of an iris to the scanner/system can help impersonating one's identity. With appropriate printer and paper combination, the quality of printed iris can be substantial enough to mislead an iris recognition system.

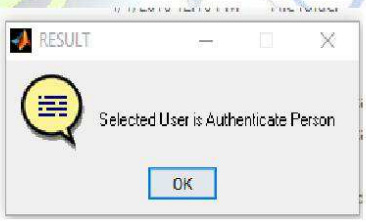

Fig:4.4 Selected user is autherised

ISSN 2394-3777 (Print)
ISSN 2394-3785 (Online)
Available online at www.ijartet.com

International Journal of Advanced Research Trends in Engineering and Technology (IJARTET)
Vol. 4, Special Issue 5, March 2017

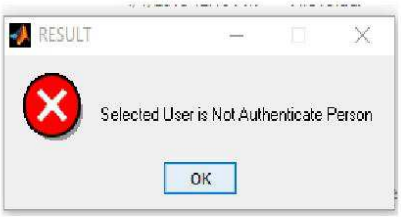

Fig: 4.5 Selected users is not authorized

4.3. Face Deceit Detection

In this dissertation, the problem of face deceit detection, particularly in a cross-database scenario is reviewed. The proposed method is to perform face [8] deceit detection based on Image Distortion Analysis (IDA). The IDA features are classified into specular reflection, blurriness, color moments, and color contrast have been designed to capture the image distortion. The 121-dimensional IDA feature vector is resulted from the four different features joined together. A troupe classifier consists of two constituent SVM features used for the classification of genuine and deceit faces.

Fig: 4.6 To registered face image for users from database

Due to the innate data-driven nature of texture based methods, they can be easily over-fitted to one particular gleam and imagery condition. It does not generalize to databases collected under disparate conditions.

4.4. Fingerprint Deceit Detection

Fingerprint [10] [22] distortion detection problem are classified into two types such as the registered ridge orientation map and period map as the feature vector, which is classified by a SVM classifier.

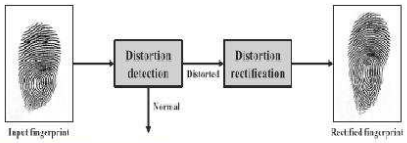

Fig: 4.7 Fingerprint deceit

4.4.1 Reference Fingerprints

To study the fingerprint (figure 4.8) distortion statistics, Tsinghua distorted fingerprint database is used. For data collection, a FTIR fingerprint scanner with video capture functionality was utilized.

Fig: 4.8 To registered iris image for users from database

In this figure 4.9 the fingerprints between training and testing data are different. A large number of references are used to register the various patterns of fingerprints properly. Distorted fingerprints are also used as reference.

ISSN 2394-3777 (Print)
ISSN 2394-3785 (Online)
Available online at www.ijartet.com

International Journal of Advanced Research Trends in Engineering and Technology (IJARTET)
Vol. 4, Special Issue 5, March 2017

Based on the finger's center and direction, a reference fingerprint is registered. The accurate fingerprints results are generated by a Poincare index based algorithm. The upper core point is used as the finger center. For arch fingerprints upper core points are not correctly detected and the centre point is manually estimated.

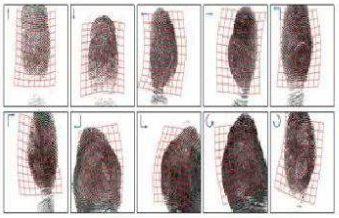

Fig: 4.9 Reference Finger Print

4.5. Evaluation and Implementation

The proposed distortion detection algorithm and the distortion rectification algorithm is evaluated by performing matching experiments on three databases. Finally, we discuss the impact of the number of reference iris, fingerprints, face on distorted iris and face rectification.

The input images are given to Veri-Finger technique. The three experiments are original iris, fingerprints, face, rectified iris, fingerprints, face by Senior and Bolle approach, and rectified iris, fingerprints, face. No burglar matches were conducted because the matching score of Veri-Finger is linked to the false accept rate (FAR).

1FVC2006 DB2_A was used to examine whether distortion rectification may have negative impact on matching accuracy or not in distorted iris, fingerprints, face. The distorted subset of FVC2004 DB1 consists of 89 distorted iris, fingerprints, face and pairing normal iris, fingerprints, face. To clearly evaluate the contribution of distortion rectification to matching distorted iris, fingerprints, face, it was tested separately

V. CONCLUSION & FUTURE WORK

5.1 CONCLUSION

Our networks use classic convolution operations that can be viewed as linear and non-linear image processing operations. The operations are essentially extracted from higher level representations and named as multiband images, whose pixel attributes are joined into high-dimensional feature vectors for later pattern recognition. False non-match rates of fingerprint matchers are very high. By using the security hole in automatic fingerprint recognition system the criminals and terrorists used it in an illegal manner. For this reason, it is necessary to develop a fingerprint distortion detection and rectification algorithms to fill the hole.

Face deceit detection include

i. Understand the characteristics and requirements for face deceit detection.

ii. By considering the user demographics (age, gender, and race) and ambient gleam a large and representative database is collected.

ISSN 2394-3777 (Print)
ISSN 2394-3785 (Online)
Available online at www.ijartet.com

International Journal of Advanced Research Trends in Engineering and Technology (IJARTET)
Vol. 4, Special Issue 5, March 2017

iii. To develop robust, effective, and efficient features (e.g., through feature transformations) for the network.

iv. Consider user-specific training for face deceit detection.

By using the proposed method enhance the biometric modalities such as palm, vein, and gait. In fact, there is an additional research that could take to next step. We imagine the application of deep learning representations on top of pre-processed image feature maps (e.g., LBP-like feature maps, acquisition-based maps exploring noise signatures, visual [15] rhythm representations, etc.). With an n-layer feature representation, we might be able to explore features otherwise not possible using the raw data. In addition, exploring temporal coherence and fusion would be also important for video-based attacks.

REFERENCES

[1] C. Rathgeb and A. Uhl, "Attacking iris recognition: An efficient hill-climbing technique," inProc. IEEE/IAPR 20th Int. Conf. Pattern Recog-nit. (ICPR), Aug. 2010, pp. 1217–1220.

[2] C. Rathgeb and A. Uhl, "Statistical attack against iris-biometric fuzzy commitment schemes," inProc. IEEE Comput. Soc. Conf. Comput. Vis. Pattern Recognit. Workshops (CVPRW), Jun. 2011, pp. 23–30.

[3] J. Galbally, J. Fierrez, and J. Ortega-Garcia, "Vulnerabilities in biometric systems: Attacks and recent advances in liveness detection," Database, vol. 1, no. 3, pp. 1–8, 2007.

[4] N. K. Ratha, J. H. Connell, and R. M. Bolle, "An analysis of minu-tiae matching strength," in Audio- and Video-Based Biometric Person Authentication. Berlin, Germany: Springer-Verlag, 2001, pp. 223–228.

[5] A. F. Sequeira, H. P. Oliveira, J. C. Monteiro, J. P. Monteiro, and J. S. Cardoso, "MobILive 2014—Mobile iris liveness detection competition," in Proc. IEEE Int. Joint Conf. Biometrics (IJCB), Sep./Oct. 2014, pp. 1–6. [Online]. Available: http://mobilive2014. inescporto.pt/

[6] Christo Ananth, A.S.Senthilkani, Praghash.K, Chakka Raja.M., Jerrin John, I.Annadurai, "Overlap Wavelet Transform for Image Segmentation", International Journal of Electronics Communication and Computer Technology (IJECCT), Volume 4, Issue 3 (May 2014), pp-656-658

[7] D. Yadav, N. Kohli, J. S. Doyle, R. Singh, M. Vatsa, and K. W. Bowyer, "Unraveling the effect of textured contact lenses on iris recognition," IEEE Trans. Inf. Forensics Security, vol. 9, no. 5, pp. 851–862, May 2014.

[8] I. Chingovska, A. Anjos, and S. Marcel, "On the effectiveness of local binary patterns in face anti-deceit," inProc. Int. Conf. Biometrics Special Interest Group (BIOSIG), 2012, pp. 1–7.

[9] N. Erdogmus and S. Marcel, "Deceit in 2D face recognition with 3D masks and anti-deceit with Kinect," inProc. IEEE 6th Int. Conf. Biometrics, Theory, Appl., Syst. (BTAS), Sep./Oct. 2013, pp. 1–6.

[10] L. Ghiani et al., "LivDet 2013—Fingerprint liveness detection compe-tition," in Proc. Int. Conf. Biometrics (ICB), 2013, pp. 1–6. [Online].Available: http://prag.diee.unica.it/fldc/

[11] A. Krizhevsky, I. Sutskever, and G. E. Hinton, "ImageNetclas-sification with deep convolutional neural networks," in Advances in Neural Information Processing

ISSN 2394-3777 (Print)
ISSN 2394-3785 (Online)
Available online at www.ijartet.com

International Journal of Advanced Research Trends in Engineering and Technology (IJARTET)
Vol. 4, Special Issue 5, March 2017

Systems. Red Hook, NY, USA: Curran & Associates Inc., 2012.

[12] D. C. Cire¸san, U. Meier, J. Masci, and J. Schmidhuber, "Multi-column deep neural network for traffic sign classification,"NeuralNetw., vol. 32, pp. 333–338, Aug. 2012.

[13] J. Ouyang and X. Wang, "Joint deep learning for pedestrian detection," in Proc. IEEE Int. Conf. Comput. Vis. (ICCV), 2014, pp. 2056–2063.

[14] Y. Taigman, M. Yang, M. Ranzato, and L. Wolf, "DeepFace: Closing the gap to human-level performance in face verification," in Proc. IEEE Int. Conf. Comput. Vis. Pattern Recognit., Jun. 2014, pp. 1701–1708.

[15] N. Pinto, D. Doukhan, J. J. DiCarlo, and D. D. Cox, "A high-throughput screening approach to discovering good forms of biologically inspired visual representation,"PLoSComput. Biol., vol. 5, no. 11, p. e1000579, 2009.

[16] J. Bergstra and Y. Bengio, "Random search for hyper-parameter opti-mization,"J.Mach.Learn.Res., vol. 13, no. 1, pp. 281–305, 2012.

[17] Y. LeCun, L. Bottou, Y. Bengio, and P. Haffner, "Gradient-based learning applied to document recognition," Proc. IEEE, vol. 86, no. 11, pp. 2278–2324, Nov. 1998.

[18] A. M. Saxe, P. W. Koh, Z. Chen, M. Bhand, B. Suresh, and A. Y. Ng, "On random weights and unsupervised feature learning," inProc. 28th Int. Conf. Mach. Learn., 2011, pp. 1–8.

[19] Presentation Attack Detection Algorithm For Face And Iris Biometrics (R. RaghavendraChristoph Busch Norwegian Biometric Laboratory, Gjøvik University College, Norway)

[20]Fake Biometric Detection to Iris, Fingerprint Using Image Quality Assessment (Ms. Kavita H. Waghmode M.E. Student, Signal Processing, BSCOER, Narhe, Pune, India)

M.Udhaya received her MSC(IT) degree from Sri Nagalakshmin Ammal College for Science, Pappunayakanpatti, India in 2015. Now she is currently working toward the M.Phil degree at Sakthi Arts & Science College for women, Oddanchtram, India. Her main research interests include Image Processing, Network Security.

B. Muthu Kumar, Professor, Department of CSE, Syed Ammal Engineering College, Ramanathapuram, TN, India

Kavitha, Professor, Department of Computer Science, Sakthi College of Arts and Science for Women, TN, India

S.Prabhakaran, Department of Information Technology, Kathir College of Engineering, Now he is currently working in Ascox Techno Soft at Madurai, India. Him main research interests include Image Processing, Network Security, Cloud Computing.

S. Kavitha, Assistant Professor of Computer Science	International Journal of Advanced Research Trends in Engineering and Technology		3D Face Identification under Disruption using Masked Projection			International ISSN 2394-3777 (Print) ISSN 2394-3785 (Online)	March 2017

ISSN 2394-3777 (Print)
ISSN 2394-3785 (Online)
Available online at www.ijartet.com

International Journal of Advanced Research Trends in Engineering and Technology (IJARTET)
Vol. 4, Special Issue 5, March 2017

3-D Face Identification under Disruption Using Masked Projection

Anitha.M[1] , B. Muthu Kumar [2] , Kavitha [3] , S.Prabhakaran [4]

[1,3]Department of Computer Science, Sakthi College of Arts and Science for Women, TN, India

[2]Professor, Department of CSE, Syed Ammal Engineering College, Ramanathapuram, TN, India

[4] Department of Information Technology, Kathir College of Engineering

anithamagudeeswaran25@gmail.com

Abstract:

Face has unique identity among all the human beings. Face identification is used to perform on 2-D and 3-D facial data.3-D provides higher accuracy than 2-D especially in high security applications. Considering the disruptions covering the facial surface is a great challenge and so enables the fully automatic security systems. In this proposed system handling two problems such as 1) disruption handling for surface registration, and 2) missing data handling for classification based on subspace analysis techniques. The adaptively-selected-model-based registration technique is implemented for alignment problem, where a face model is selected for an cramped face such that only the valid non-cramped patches are utilized. When the registration stage is completed, disruptions are detected and removed. In the classification stage, masked projection is proposed. It enables the use of subspace analysis scheme with incomplete data. Thedisruption handling is to improve the overall results. The two databasesnamely, the Bosphorus and the UMB-DB are reported in experimental results. The results confirm that registration based on the adaptively selected model together with the masked subspace analysis classification offer adisruption robust face identification system.

Keywords: Disruption, UMB-DB, Bosphorus, Face Identification.

1. INTRODUCTION

Identifying the features of human beings is easily done in biometric systems. The human face is mostly preferred in the biometric identifications. It has the advantage ofcontactless acquisition [13]. It is used in many applications such as public records, authentication, security and safety. In biometric system, the face identification technique is the most trusty and preferable.

This paper is presented as follows: in Section 2, face identification (2-D and 3-D) is discussed. Section 3 describes the advantages of 3-D face identification systems like disruption, ageing effect, gleam and changes in pose. Section 4 gives short description about external and internal objects. In section 5, the review of databases and challenges are summarized.

ISSN 2394-3777 (Print)
ISSN 2394-3785 (Online)
Available online at www.ijartet.com

International Journal of Advanced Research Trends in Engineering and Technology (IJARTET)
Vol. 4, Special Issue 5, March 2017

Section 6 addresses the different approaches of disruption invariant.

2. FACE IDENTIFICATION

A face identification system is used to verify a particular person from a digital image or video source. The human face is used to identify in the society and provides security among the biometric face identification system. In this system, they can capture a face without touching the person and identified. The proposed system is used to control the crime deterrent.Face is classified into many dimensions. Here 2-D and 3-D face is discussed. The surface reflectance is presented by 2-D intensity and the face shape data is given by 3-D depth values.

Based on 3-D or 2-D data, the acquisition, registration and characteristic matching is done for face identification. Identification is enhanced dimensionally by using the parameters like shape and texture channels parallel. 2-D image information is included in texture channel. 3-D has more advantages than 2-D. The variation like gleam [1] [22] affects the shape of the face or the probe. [9] proposed a system in which an automatic anatomy segmentation method is proposed which effectively combines the Active Appearance Model, Live Wire and Graph Cut (ALG) ideas to exploit their complementary strengths. It consists of three main parts: model building, initialization, and delineation. For the initialization (recognition) part, a pseudo strategy is employed and the organs are segmented slice by slice via the OAAM (Oriented Active Appearance method). The purpose of initialization is to provide rough object localization and shape constraints for a latter GC method, which will produce refined delineation. It is better to have a fast and robust method than a slow and more accurate technique for initialization.

3. 3-D FACE IDENTIFICATION

When comparing to 2-D face identification, 3-D is the most preferable because it has higher accuracy rate. In addition, it is robust to obstacles and variations. Example for identification is time dimension[1] [22]. Shape of face plays a major role in 3-D face identification in one's identity. It is resistant to deceit and deception. The effect of gleam and pose from 3-D texture face is eliminated by the shape data. The combination of shape and texture of face processing leads to high performance [1].

During the processing of face, internal factors occur. The appearance and shape of the face is the major problem when ageing occurs. The facial muscles will produce new expressions like smiling, happy, sad, angry etc. Disruption makes problems for identifying the original image of face. Still the disruption variation is a challenging part[1].

4. DISRUPTION

The real-time applications are constrained to work in controlled issues[12]. The information of face provides non neutral facial expressions. The face can be cramped due to hair, hands, phone, scarf, glasses, goggles etc[12] [22]. It hides some part in face[8]. The internal and the external objects[1] [22] are affected due to the presence of 3-D facial information in a large number of acquisitions. Sometimes it loses the

ISSN 2394-3777 (Print)
ISSN 2394-3785 (Online)
Available online at www.ijartet.com

International Journal of Advanced Research Trends in Engineering and Technology (IJARTET)
Vol. 4, Special Issue 5, March 2017

information. There are two types of disruptions. They are 1) disruption due to internal objects and 2) disruption due to external objects.

4.1 DISRUPTION DUE TO INTERNAL OBJECTS

Changes in pose lead to self disruptions. Due to that a part of facial surface hinders acquisition of another region. These disruptions cause missing of information of facial surface [15].

4.2 DISRUPTION DUE TO EXTERNAL OBJECTS

Examples of external objects are hair, hands, phone, scarf, glasses, goggles etc[15]. The problems occurred in partial disruption has found the solution is implications for image processing. The real life examples are iris recognition, identification via ear, medical, hair, hands and goggles. The developed technologies used for hacking and forgery. The disruption system are used to control the intruders misbehave. The people are used tricks to forgery the security systems by covering the face with mask or scarf. The deceiting and deception leads toraising failure rates of the realistic systems in accordance with face identification[8].

5. REVIEW OF DATABASES

The complexity in database is used to recognize the different faces are a realistic challenge. The UMB-DB database and the Bosphorus database are addressed in 3-D face. The large disruption faces are contained in UMB-DB 3-D database. When the face is affected by disruption, the UMB-DB database is used to test the algorithms and systems. In face identification, the disruption is present due to external and internal objects. The UMB-DB consists of 1473 2-D color images and 143 contents of 3-D depth images. The contents include 98 Males and 45 Females. The majority of the people age ranging from 19 to 50. A pair of twins and a child of 4years old age have been additionally included. The contents are included from Caucasian race. The database has captured9 acquisitions which include 1) Three with a neutral expression 2) Three contents with non-neutral facial expressions mainly, Smiling, Angry and Bored 3) Three contents their face cramped by different objects like scarf, hair and hands having random positions.

The UMB-DB database has captured the contents like eyeglasses, holding phones, partially cramped by hair and other objects. The aggregate number of cramped faces is 578. During the time of acquisitions the persons were allowed to cover the some part of face. The UMB-DB database provides an average of 42% and maximum of about 84%. Minolta vivid-900 laser scanner is used to create the dataset. When acquisition occurs every time, seven feature points are noted manually [12].

6. APPROACHES

Alyuz et al [13] have presented a paper about masked projection having face identification with disruption. They illustrates mainly two problems i) Disruption handling for surface registration ii) Based on subspace analysis method handling missing data for

ISSN 2394-3777 (Print)
ISSN 2394-3785 (Online)
Available online at www.ijartet.com

International Journal of Advanced Research Trends in Engineering and Technology (IJARTET)
Vol. 4, Special Issue 5, March 2017

classification. To recover the alignment problem they addressed an adaptively selected model based registration method. This method includes the preliminary handling of 3-D face identification method which consists of registration and removal of disruption steps. Adaptive registration pipeline is classified into conflict techniques. Some of the techniques are nose detection, adaptive model selection and Bosphorus database. The important non-cramped patches are utilized with ICP based approach in adaptive modeling. Disruptions are detected and removed during registration stage. In classification stage masked projection is presented. In the presence of defective data the use of subspace analysis method is enabled in the proposed technique. To improve the performance disruption handling is added in the classification stage.

7. MODELING OF FACIAL SURFACE

With the help of pixel level Gaussian Mixture Model (GMM) facial surface complex model is designed in the proposed technique. Comparing the pixels with the respective mixture model for their fitness. Through the training phase pixels are passed. The pre-aligned faces are obtained by the adaptive registration technique. To give depth images, the facial surfaces are re-sampled after alignment. Comparing to baseline approach our proposed technique delivers best performance. Using UMB-DB database and Bosphorus database, these approaches are tested for detecting disruption[15].

8. RELATED WORKS

The binary segmentation problem from the challenge of face detection with disruption is considered in this approach. It includes the data residing in the neighborhood relations in the form of pixel. The graph is modeled from the regional cues of depth values included with neighborhood cues and acquired surface. The surface pixels are separated into face or disruption with graph cut technique. Comparing to GMM, GC gives outstanding results. The research field is now on encapsulating regional anddetecting neighborhoodinformation [15].

Alyuz et al. [14] have presented the method to disruption handling at the classification stage, known as masking projection. Enabling the use of subspace analysis technique with insufficient data is focused in this paper. They have augmented with regional approach suitable for disruption handling in classification stage. It leads to recognition rate by the use of UMB-DB and Bosphorus Database.

A. Colombo et al. [3] have proposed the tolerant technique against partially cramped faces. The detection algorithm reviews the features on the face. The acquired face of the person is registered. The method which is used to avoid samples including cramping objects is Iterative Closest Point (ICP).The Gappy Principal Component Analysis (PCA) classifier is used to isolate between face and non face. The face detection can be done using UND database. It shows 90.4%accuracy for face identification.

ISSN 2394-3777 (Print)
ISSN 2394-3785 (Online)
Available online at www.ijartet.com

International Journal of Advanced Research Trends in Engineering and Technology (IJARTET)
Vol. 4, Special Issue 5, March 2017

Agrawala et al. [5] have analyzed a framework for detecting 3D faces by comparing, matching and averaging their shapes. Representing facial surfaces with radial curves starting from nose tips is analyzed using elastic shapeto develop a Riemannian frame work. The framework is normal for measuring facial disruption and it is a challenging task for variations in large pose. This approach is experimented from both exact and hypothetical perspectives using three databases FRGC2, GavabDB andBosphorus. They proposed a local representation by utilizing a curved representation of a 3D face and a quality filter for selecting the curves in unrestricted situation.

Bagchi et al. [6]analyzed a robust face recognition system.The system is resistant to pose changes and to disruptions from real time. TheIterative Closest Point (ICP) algorithm is used with the residual distances between aInput Face and gallery model. Theperformance of ICP depends on initial conditions.By considering the threshold of depth map value of the 3-D image, disruptions are removed. Using Bosphorus database, thisdisruption invariant method provides 91.30% accuracy.

9.RESULTS AND DISCUSSION

After analyzing many papers presented by researchers, it is summarized as most of the process done on the basis of masking projection at the classification stage. The techniques which are used in common are ICP, GPCA and PCA. These methods are used to solve the problems like gleam, disruption, variation in pose [4] and expressions. The below table represents the analysis related to the proposed system.

10. CONCLUSION

The research work concentrates on different methods used for disruption invariant 3-D face identification technique.Disruption in 3-D face identification is a challenging task while processing. In this proposed work, 3-D face recognition with challenges of disruptionsarereviewed. Additionally, disruptions due to internal objectsand external objectsare discussed. The maximum number of cramped datasets with large number of information is provided by UMB-DB database.All the approachesfocused are effective for retaining the spatial domain information.In the future robustness of 3-D face identification can be improved to have high disruption invariant.

REFERENCES

[1] Salah, A., Gokberk, B., Akarun, L.2006. 3D Face Recognition.Proceedings of the Fifth GAP Engineering Congress.Şanlıurfa, Turkey.

[2] Dr. Mario I., Chacon M., January 2009. Occlusions in Face Recognition: a 3D Approach. Source: State of the Art in Face Recognition.

[3] A. Colombo, C. Cusanoand R. Schettini, "Gappy PCA classification for occlusion tolerant 3d face detection", Journal of Mathematical Imaging and Vision, 2009.

[4] H. Drira, Ben Amor, B., A.Srivastava, M. Daoudi, R. Slama, Sept. 2013. 3D Face Recognition under Expressions, Occlusions, and Pose Variations, in Pattern Analysis and Machine Intelligence, IEEE Transactions on , vol.35, no.9, pp. 2270-2283. International Journal of Computer Applications (0975 – 8887) National Conference on Advances in Computing (NCAC 2015)29

ISSN 2394-3777 (Print)
ISSN 2394-3785 (Online)
Available online at www.ijartet.com

International Journal of Advanced Research Trends in Engineering and Technology (IJARTET)
Vol. 4, Special Issue 5, March 2017

[5] Agrawala, A. and Singh, Y. N. 2015. Evaluation of Face Recognition Methods in Unconstrained Environments ", International Conference on Intelligent Computing, Communication & Convergence (ICCC-2014).

[6] Bagchi, Bhattacharjee, D. and Nasipuri, M. 2014. Robust 3d face recognition in presence of pose and partial occlusions or missing parts, International Journal in Foundations of Computer Science &Technology (IJFCST), Vol.4, No.4.

[7] Chintalapati, S., Raghunadh, M. V. 2014. Illumination, Expression and Occlusion Invariant Pose-Adaptive Face Recognition System for Real-Time Application.International Journal of Engineering Trends and Technology (IJETT).

[8] Azeem, A., Sharif, M., RazaM., and Murtaza, M. 2014. A Survey: Face Recognition Techniques under Partial Occlusion. The International Arab Journal of Information Technology.

[9] Christo Ananth, G.Gayathri, I.Uma Sankari, A.Vidhya, P.Karthiga, "Automatic Image Segmentation method based on ALG", International Journal of Innovative Research in Computer and Communication Engineering (IJIRCCE), Vol. 2, Issue 4, April 2014,pp- 3716-3721

[10]Jozer, B., Matej, F., Lubos, O., Milos, O., Jarmila, P., "Face recognition under partial occlusion and noise",EUROCON, 2013 IEEE, vol., no., pp.2072, 2079, 1-4 July 2013.

[11] A. S. Gawali and Prof. R. R. Deshmukh,''3D Face Recognition Using Geodesic Facial Curves to Handle Expression, Occlusion and Pose Variations",International Journal of Computer Science and Information Technologies, Vol. 5 (3) , 2014, 4284-4287.

[12] Colombo, A., Cusano, C., and Schettini, R. 2011. UMB-DB: A database of partially occluded 3D faces. In Computer Vision Workshops (ICCV Workshops), 2011 IEEE International Conference on (pp. 2113-2119). IEEE.

[13] Alyuz, N., Gokberk, B., Akarun, L., "3-D Face Recognition Under Occlusion Using Masked Projection," in Information Forensics and Security, IEEE Transactions on , vol.8, no.5, pp.789-802, May 2013.

[14] Alyuz, N.,Gokberk, B., Akarun, L. 23-25 April 2014 Masked projection for 3D face recognition under occlusion. Signal Processing and Communications Applications Conference (SIU).

[15] Alyuz, N., Gokberk, B., Akarun, L. 24-28 Aug. 2014 Detection of Realistic Facial Occlusions for Robust 3D Face Recognition. Pattern Recognition (ICPR), 2014 22nd International Conference.

[16] Alyuz, N., Gokberk, B., Spreeuwers, L., Veldhuis, R.,Akarun, L. 20-22 April 2011.Occlusion-robust 3D face recognition using restoration and local classifiers.In Signal Processing and Communications Applications (SIU), IEEE 19th Conference.

[17] Chintalapati, S., Raghunadh, M.V. 2013. Automated attendance management system based on face recognition algorithms. In Computational Intelligence and Computing Research (ICCIC).IEEE International Conference.

[18] Shyam, R., Singh, Y. N., 2014. Taxonomy of 2D and 3D face recognition methods. In Signal Processing and Integrated Networks (SPIN).International Conference.

[19] Peijiang Liu, Yunhong Wang, Di Huang, Zhaoxiang Zhang. 2012. Recognizing Occluded 3D Faces Using an Efficient ICP Variant. In Multimedia and Expo (ICME).IEEE International Conference.

[20] Colombo, A., Cusano, C., Schettini, R. 2008. Recognizing Faces in 3D Images Even In Presence of

ISSN 2394-3777 (Print)
ISSN 2394-3785 (Online)
Available online at www.ijartet.com

International Journal of Advanced Research Trends in Engineering and Technology (IJARTET)
Vol. 4, Special Issue 5, March 2017

Occlusions. In Biometrics: Theory, Applications and Systems BTAS. IEEE International Conference.

M. Anitha received her MSC(CS) degree from SRI GVG Visalakshmi College for Women, Udumelpet, India in 2015. Now she is currently working toward the M.Phil degree at Sakthi Arts & Science College for women, Oddanchtram, India. Her main research interests include Image Processing, Network Security.

B. Muthu Kumar, Professor, Department of CSE, Syed Ammal Engineering College, Ramanathapuram, TN, India

Kavitha, Professor, Department of Computer Science, Sakthi College of Arts and Science for Women, TN, India

S.Prabhakaran, Department of Information Technology, Kathir College of Engineering,Now he is currently working in Ascox Techno Soft at Madurai, India. Him main research interests include Image Processing, Network Security, Cloud Computing.

S. Yoga, Assistant Professor of Computer Science	International Journal of Innovative Research in Computer and Communication Engineering		An Efficient Image De-Noising Gaussian Noise Using Improved Anis diffusion Filter with DWT in Medical Images			International ISSN(Online): 2320-9801 ISSN (Print): 2320-9798	March 2017

ISSN(Online): 2320-9801
ISSN (Print): 2320-9798

International Journal of Innovative Research in Computer and Communication Engineering
(An ISO 3297: 2007 Certified Organization)
Website: www.ijircce.com
Vol. 5, Issue 3, March 2017

An Efficient Image De-Noising Gaussian Noise Using Improved Anisodiffusion Filter with DWT in Medical Images

A. Karthiga Devi [1], S.Yoga, M.Sc(CS&IT)., M.Phill(CS)., M.Phill (Maths) [2]

M.Phil Scholar, Dept. of Computer science., Sakthi College of Arts and Science For Women, Dindigul, India.

Assistant Professor, Dept. of Computer science., Sakthi College of Arts and Science For Women, Dindigul, India.

ABSTRACT: Image de-noising continues to be an active research topic. Although state-of-the-art de-noising methods are numerically impressive and approach theoretical limits, they suffer from visible artifacts. However, the images obtained from medical imaging techniques (MRI, Ultrasound, CT etc.,) often include imaging noises. Therefore de-noising is an essential and used as a preprocessing process to remove their noises before extracting some meaningful information from these images. In this paper presents an efficient de-noising technique based on Anisodiffusion filter with Discrete Wavelet Transform (DWT) is developed. This proposed method enhances the edges in the de-noised image. The proposed method is tested with MRI, Ultrasound, and CT scan medical images. The performance of this method is compared with the existing standard filters and it has produced good result

KEYWORDS: Image de-noise; DWT; Anisodiffusion filter; Gradient;

I. INTRODUCTION

Medical imaging is one of the technique and process of creating visual representations of the interior of a body for clinical analysis and visual representation of internal structures of human organs [1].There are many imaging techniques available today, among them Magnetic Resonance Imaging (MRI), Ultrasound, Elastography and Computer Tomography (CT) are most widely used imaging techniques. Magnetic Resonance Imaging (MRI) uses most powerful magnets to polarize and excite hydrogen nuclei of water molecules in human tissue, producing a detectable signal which is spatially encoded, resulting in images of the body. Medical ultrasonography is useful for high frequency broadband sound waves in the megahertz range that are reflected by tissue to varying degrees to produce 2D and 3D images. Ultrasound is used for imaging the abdominal organs, heart, breast, muscles, tendons, arteries and veins.

Elastography is one of the relatively new imaging modality that maps the elastic properties of soft tissue. Elastography is useful in medical diagnoses, as elasticity can discern healthy from unhealthy tissue for specific organs and growth. Computed Tomography (CT) scan, produces 2D image of the structures in a thin section of the body. In CT, a beam of X-rays spins around an object being examined and is picked up by sensitive radiation detectors after having penetrated the object from multiple angles. A computer then analyses the information received from the scanner's detectors and constructs a detailed image of the object. However the images produced by these image sources are sensitive to image noise and thus degrade the quality of the image.

Noise is any degradation of the image signal caused by external disturbance [2]. Usually the medical images, are affected by noises due to the disturbance in the imaging process and inclusion of imaging artifacts. These image noises are classified as Amplifier noise (Gaussian noise), Salt-and-pepper noise (Impulse noise), Shot noise, Quantization noise (uniform noise), Film grain noise, Speckle noise (Multiplicative noise) and Periodic noise. Gaussian is an idealized form of white noise, which is caused by random fluctuations in the signal [3]. In Gaussian noise, each pixel of the image will be changed from its original value by a small amount. There are many standard filters are available in the literature to remove the noises form the medical images. The standard Median Filter (MF) is effective filter but works better only at low noise densities [4], that is, if the noise level is above 50%, edge details of original image cannot be preserved by the standard median filter. Similarly, Adaptive Median Filter (AMF) works well at low noise densities [5], but in high level noise the window size has to be increased which leads to produce blurring effect in the image. Also these filters will not take into account the local features, as an outcome of which the edges may not recovered satisfactorily.

ISSN(Online): 2320-9801
ISSN (Print): 2320-9798

International Journal of Innovative Research in Computer and Communication Engineering
(An ISO 3297: 2007 Certified Organization)
Website: www.ijircce.com
Vol. 5, Issue 3, March 2017

The rest of the paper is organized as follows: Related is detailed in Sect. 2. In Sect. 3, Proposed Methodology and the conclusion are in Sect. 5.

II. RELATED WORK

In [3] authors discussed most of the rules relating simple nonlinear threshold values for wavelet-based de-noising have assumptions that the wavelet coefficients are independent values. However, when we talk of natural images, we observe that wavelet coefficients have significant dependency. The phrase Peak Signal to Noise Ratio, often abbreviated PSNR, is an engineering term for the ratio between the maximum possible power of a signal and the power of corrupted noise that affects the fidelity of its representation. In this paper, experimentation is performed to study the effect of Increasing Gaussian noise on PSNR and the corresponding measure. In [5] authors illustrated on two types of image models corrupted by impulse noise, we propose two new algorithms for adaptive median filters. They have variable window size for removal of impulses while preserving sharpness. The first one, called the ranked-order based adaptive median filter (RAMF), is based on a test for the presence of impulses in the center pixel itself followed by a test for the presence of residual impulses in the median filter output. The second one, called the impulse size based adaptive median filter (SAMF), is based on the detection of the size of the impulse. In [6] authors proposed a new definition of scale-space is suggested, and a class of algorithms used to realize a diffusion process is introduced. The diffusion coefficient is chosen to vary spatially in such a way as to encourage intraregional smoothing rather than inter region smoothing. It is shown that the 'no new maxima should be generated at coarse scales' property of conventional scale space is preserved. As the region boundaries in the approach remain sharp, a high-quality edge detector which successfully exploits global information is obtained. In [7] authors discussed a image restoration based on the "mean curvature motion" equation. Existence and uniqueness of the "viscosity" solution of the equation are proved, a stable algorithm is given, experimental results are shown, and the subjacent vision model is compared with those introduced recently by several vision researchers. The algorithm presented appears to be the sharpest possible among the multi-scale image smoothing methods preserving uniqueness and stability.

III. PROPOSED ALGORITHM

The proposed method accepts the image De-noising for Gaussian Noise in Medical Images parameters as input which contains the MATLAB simulation where the improved Anis diffusion Filter with DWT coding based image de-noising algorithm is applied to the noisy image databases. This overall proposed architecture in figure 1 follows a de-noising process flow from the beginning to end state.

A. *Image preprocessing*

MATLAB plays a vital role in Image Processing in order to develop the quality of image. MATLAB is a high-level language and interactive environment for computation of numbers, visualization, and programming. Data can be analysed, algorithms can be developed and models and applications can be created using MATLAB.

The main goal of the pre-processing is to improve the image quality to make it ready to further processing by removing or reducing the unrelated and surplus parts in the background of the medical images are CT and MRI images that complicated to interpret. Hence pre-processing is essential to improve the quality. It will prepare the mammogram for the next two- process segmentation and feature extraction. The noise and high frequency components removed by filters.

B. *Gaussian noise*

Gaussian noise is one of the statistical noise having a probability density function (PDF) equal to that of the normal distribution, which is also known as the Gaussian distribution.

The probability density function p of a Gaussian random variable z is given by

$$PG(z) = \frac{1}{\partial\sqrt{2\pi}} e^{-\frac{(z-\mu^2}{2\partial^2}} \quad \text{eqn. (1)}$$

ISSN(Online): 2320-9801
ISSN (Print): 2320-9798

International Journal of Innovative Research in Computer and Communication Engineering
(An ISO 3297: 2007 Certified Organization)
Website: www.ijircce.com
Vol. 5, Issue 3, March 2017

where, z represents the grey level, μ the mean value and σ the standard deviation.

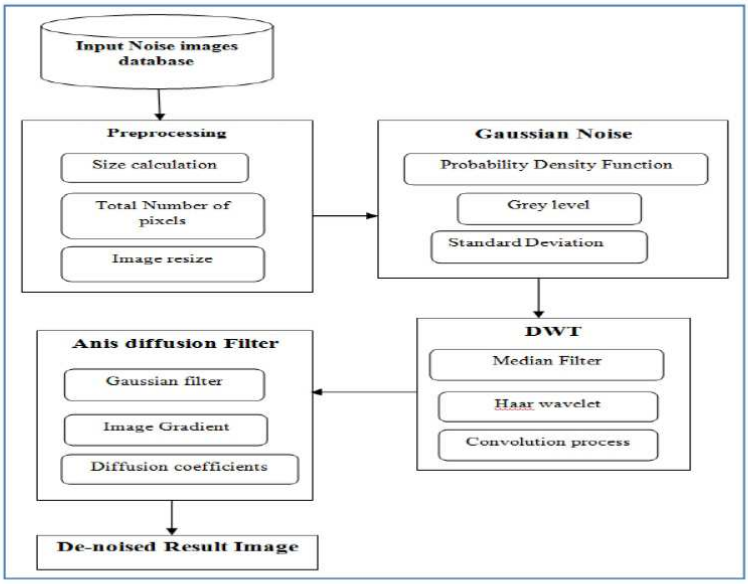

Fig.1. Proposed Framework flow diagram

C. *Discrete Wavelet Transform (DWT)*

The Discrete Wavelet Transform (DWT) of image signals produces a non-redundant image representation, which provides better spatial and spectral localization of image formation, compared with other multi scale representations such as Gaussian and Laplacian pyramid. The DWT can be interpreted as signal decomposition in a set of independent, spatially oriented frequency channels. The signal S is passed through two complementary filters and emerges as two signals, approximation and Details. This is called decomposition or analysis. The components can be assembled back into the original signal without loss of information. This process is called reconstruction or synthesis.

The mathematical manipulation, which implies analysis and synthesis, is called discrete wavelet transform and inverse discrete wavelet transform. An image can be decomposed into a sequence of different spatial resolution images using DWT. In case of a 2D image, an N level decomposition can be performed resulting in 3N+1 different frequency bands namely, LL, LH, HL and HH.

D. *Anisotropic Diffusion Filter*

Anisotropic diffusion, also called Perona-Malik diffusion is a technique to reduce image noise without removing significant parts of the image content, such as edges, lines or other details, which are important to the interpretation of the image. Anisotropic diffusion resembles the process that creates a scale space, where an image generates a parameterized family of successively more and more blurred images based on a diffusion process. Each of the images

ISSN(Online): 2320-9801
ISSN (Print): 2320-9798

International Journal of Innovative Research in Computer and Communication Engineering
(An ISO 3297: 2007 Certified Organization)
Website: www.ijircce.com
Vol. 5, Issue 3, March 2017

resulting in this family is given as a convolution between the image and a 2D isotropic Gaussian filter, where the width of the filter increases with the parameter. This diffusion process is a linear and space-invariant transformation of the original image. Anisotropic diffusion is normally implemented, by means of an approximation of the generalized diffusion equation.

Formally, let $\Omega \subset R^2$ denote subset of the plane and I(. , *t*): $\Omega \rightarrow$ R be a family of gray scale images, then anisotropic diffusion is given by:

$$\frac{\partial I}{\partial t} = div\ c(x, y, t\ \nabla I = \ \nabla c. \nabla I + c(x, y, t, \nabla I) \quad \text{eqn. (2)}$$

where, ∇ denotes the Laplacian, ∇ denotes the gradient, div-(...) is the divergence operator and c(x, y, t) is the diffusion coefficient and it controls the rate of diffusion, usually chosen as a function of the image gradient so as to preserve edges in the image.

Though the Anisodiffusion filter with DWT is an edge preserving filter when it is used as a preprocessing procedure for image segmentation and analysis, the preserved edge details are not enough for accurate segmentation of individual objects present in the images, especially for medical images. Therefore, in this proposed method the edge details are added to the noisy image before applying the de-noising procedure based on the Anisodiffusion filter.

IV. Conclusion and Future Work

In this paper presents a novel image de-noising process using Anis diffusion Filter with DWT coding on medical images to remove the Gaussian noise present in images by preserving the edges. This proposed method is tested with MRI, CT scan and Ultrasound medical images. The performance of this method is also compared with the standard filters, Mean filter, Median filter, Linear filter, Adaptive filter, Gaussian filter, Unsharp filter, Sobel filter. Presently, we have de-noised only the Gaussian noise in the medical images, in future it may be modified to eliminate all types of noises in medical images.

References

1. Rafael C.Gonzalez & Richard E.Woods.,"Digital Image Processing", Second edition, 3, 2005.
2. Alasdair Mcandrew.,"Introduction to digital image processing with MATLAB", Course Technology a part of cengage learing, 2 ,2004.
3. M. Parminder Kaur and Jagroop Singh.,"A Study Effect of Gaussian Noise on PSNR Value for Digital Images", International Journal of Computer and Electrical Engineering, 3, (2), April, 2011.
4. J.Astola and P.Kuosamaneen.,"Fundamentals of nonlinear digital filtering", technology and engineering, 225-288,1997.
5. H.Hawag and R.A Hadded.,"Adaptive median filter: new algorithms and result", International Journal of Computer Engineering and Technology, 4(6), Nov 2013.
6. Pietro Perona and Jiltendra Malik.,"scale space and edge detection using anisotropic diffusion filter", IEEE transactions on pattern analysis and machine intelligence, 12(7), 629-639, July 1990.
7. F.catte, P.L.Lions, J.M mortel., "Image selective smoothing and edge detection by linear diffusion", Society of Industrial and Applied Mathematics, 29(3), 845-866, June 1992.

N. Nanthini, Assistant Professor of Computer Science	International Journal of Innovative Research in Computer and Communication Engineering		A Novel Image Compression on Image Local Patch Extraction Using Run Length Coding			International ISSN(Online): 2320-9801 ISSN (Print): 2320-9798	March 2017

ISSN(Online): 2320-9801
ISSN (Print): 2320-9798

International Journal of Innovative Research in Computer and Communication Engineering
(An ISO 3297: 2007 Certified Organization)
Website: www.ijircce.com
Vol. 5, Issue 3, March 2017

A Novel Image Compression on Image Local Patch Extraction Using Run Length Coding

P. Sathiya [1] , N. Nanthini M.Sc., M.Phil [2]

M.Phil Scholar, Dept. of Computer science., Sakthi College of Arts and Science For Women, Dindigul, India.

Assistant Professor, Dept. of Computer science., Sakthi College of Arts and Science For Women, Dindigul, India.

ABSTRACT: Image compression is currently a prominent topic for both military and commercial researchers. Due to rapid growth of digital media and the subsequent need for reduced storage and to transmit the image in an effective manner Image compression is needed. In this paper presents a novel Image Compression On Image Local Patch Extraction Using Run Length Coding incorporates image compression theory, which is the process of extracting the information from the image features from the unsupervised database. The proposed method presents a framework for digital image compression with patch extraction is to discovering best feature from Noisy image database. By aligning the important image features from the database and by using the matching sequence or its encryption of match, the searching between the data features are determined.

KEYWORDS: Image Compression; Run length coding; patch extraction; JPEG2000;

I. INTRODUCTION

Digital image processing is the use of computer algorithms to perform image processing on digital images. The two types of methods used for Digital Image Processing are Analog and Digital Image Processing. Analog or visual techniques of image processing can be used for the hard copies like printouts and photographs. Image analysts use various fundamentals of interpretation while using these visual techniques. The image processing is not just confined to area that has to be studied but on knowledge of analyst. Association is another important tool in image processing through visual techniques. So analysts apply a combination of personal knowledge and collateral data to image processing.

Along with the standardization or independently, many lossless image compression algorithms have been proposed. Among a variety of algorithms, the most widely used ones may be Lossless JPEG [1], JPEG-LS [2], LOCO-I [3], CALIC [4], JPEG2000 [5] (lossless mode) and JPEG XR [6]. The LOCO-I and CALIC were developed in the process of JPEG standardization, where most ideas in LOCO-I are accepted for the JPEG-LS standard although the CALIC provides better compression performance at the cost of more computations.

Image compression is an application of data compression that encodes the original image with few bits. The objective of image compression is to reduce the redundancy of the image and to store or transmit data in an efficient form. The block diagram of the general image storage system. The main goal of such system is to reduce the storage quantity as much as possible, and the decoded image displayed in the monitor can be similar to the original image as much as can be. Lossless compression is bit preserving compression, where the reconstructed image is numerically identical to the original image. This type of compression is important for applications such as medical and satellites imaging, where distortion or loss of information is unacceptable.

The rest of the paper is organized as follows: Related is detailed in Sect. 2. In Sect. 3, Proposed Methodology and the conclusion are in Sect. 5.

II. RELATED WORK

In [2] authors described the JPEG-2000 is an emerging standard for still image compression. This paper provides a brief history of the JPEG-2000 standardization process, an overview of the standard, and some description of the capabilities provided by the standard. Part I of the JPEG-2000 standard specifies the minimum compliant decoder, while Part II describes optional, value-added extensions. Although the standard specifies only the decoder and bit-stream syntax, in this paper we describe JPEG-2000 from the point of view of encoding. In [3] authors described the standardization committee has been the development of Part I, which could be used on a royalty- and fee-free basis.

ISSN(Online): 2320-9801
ISSN (Print): 2320-9798

International Journal of Innovative Research in Computer and Communication Engineering
(An ISO 3297: 2007 Certified Organization)
Website: www.ijircce.com
Vol. 5, Issue 3, March 2017

This is important for the standard to become widely accepted. The standardization process, which is coordinated by the JTCI/SC29/WG1 of the ISO/IEC has already produced the international standard (IS) for Part I. In this article the structure of Part I of the JPFG 2000 standard is presented and performance comparisons with established standards are reported. In [4] authors formulated national standards for digitization and compression of gray-scale fingerprint images. The compression algorithm for the digitized images is based on adaptive uniform scalar quantization of a discrete wavelet transform subband decomposition, a technique referred to as the wavelet/scalar quantization method. The algorithm produces archival-quality images at compression ratios of around 15 to 1 and will allow the current database of paper fingerprint cards to be replaced by digital imagery. A compliance testing program is also being implemented to ensure high standards of image quality and interchangeability of data between different implementations. In [5] authors present a new and different implementation based on set partitioning in hierarchical trees (SPIHT), which provides even better performance than our previously reported extension of EZW that surpassed the performance of the original EZW. The image coding results, calculated from actual file sizes and images reconstructed by the decoding algorithm, are either comparable to or surpass previous results obtained through much more sophisticated and computationally complex methods. In addition, the new coding and decoding procedures are extremely fast, and they can be made even faster, with only small loss in performance, by omitting entropy coding of the bit stream by the arithmetic code. In [6] authors illustrated a large volumes of fingerprints are collected and stored every day in a wide range of applications, including forensics, access control etc., and are evident from the database of Federal Bureau of Investigation (FBI) which contains more than 70 million finger prints. Wavelet based Algorithms for image compression are the most successful, which result in high compression ratios compared to other compression techniques. Even though wavelet bases are providing good compression ratios, they are not optimal for representing images consisting of different regions of smoothly varying grey-values, separated by smooth boundaries.

III. PROPOSED ALGORITHM

The proposed method accepts the Image Compression parameters as input which contains the MATLAB simulation where the novel Run Length coding based image compression algorithm is applied to the real-world image databases. This overall proposed architecture in figure 1 follows a Compression framework from the beginning to end state.

A. *IMAGE FEATURE EXTRACTION*

Image feature extraction is done without local decision making; the result is often referred to as a feature image. Consequently, a feature image can be seen as an image in the sense that it is a function of the same spatial (or temporal) variables as the original image, but where the pixel values hold information about image features instead of intensity or color. Image pre-processing is an Image mining technique that involves transforming raw data into an understandable format. Real-world data is often incomplete, inconsistent, and/or lacking in certain behaviors or trends, and is likely to contain many errors. Data pre-processing is a proven method of resolving such issues. Data pre-processing prepares raw data for further processing. The two images must be of the same size and are supposed to be associated with indexed images on a common color map.

The input images are first separated into amount of pixels, which are separated into non-overlapping pixels. The image pixel orientation and magnitude are computed for each pixel. An image vectors variation of these bin orientations is formed for each shape. The magnitude of the bin is used as a vote weight. The resulting mean shift grouping pixels are concatenated to form the image descriptor.

ISSN(Online): 2320-9801
ISSN (Print): 2320-9798

International Journal of Innovative Research in Computer and Communication Engineering
(An ISO 3297: 2007 Certified Organization)
Website: www.ijircce.com
Vol. 5, Issue 3, March 2017

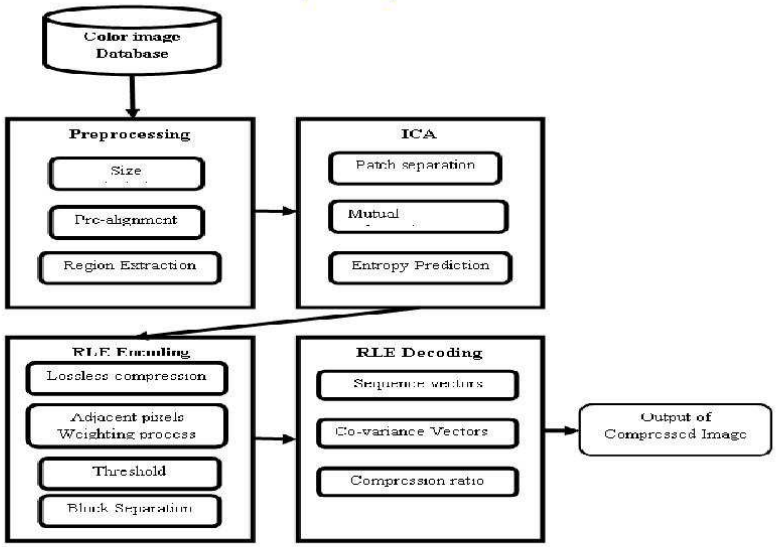

Fig.1. Proposed Framework flow diagram

B. *ICA Transform based Patch Separation*

The ICA Transformation method uses a statistical "latent variables" model. Assume that we observe n linear mixtures x_1, ...,x_n of n independent components,

$$Xj = a_{j1}s_1 + a_{j2}s_2 + \ldots + a_{jn}s_n, \text{ for all } j. \quad \text{eqn. (1)}$$

In the ICA model, we assume that each mixture xj as well as each independent component sk is a random variable, instead of a proper time signal.

Matching Pursuit algorithm is normally use a full frame as a single block. It gives better compression without any blocking artifacts but it is not good for error resilience over noisy channels. Additively, computation is very heavy as MP is an iterative algorithm. To enhance error resilience capability along with reduced computational load, we have processed the image in blocks of 16x16 pixels. These blocks are encoded using variable number of coefficients until either of the stopping criteria is met which are minimum error threshold and maximum number of encoded coefficients.

C. *RLE Encoding Compression*

This encoding method is frequently applied to graphics-type images (or pixels in a scan line) — simple compression algorithm in its own right.

- RLE Approach is given below:
- Sequences of image elements $X_1, X_2, \ldots, X_n$ (Row by Row)
- Mapped to pairs $(c_1, l_1), (c_1, l_2), \ldots, (c_1, l_n)$
- where c_i represent image intensity or colour and li the length of the ith run of pixels.
- (Not dissimilar to zero length suppression above)

ISSN(Online): 2320-9801
ISSN (Print): 2320-9798

International Journal of Innovative Research in Computer and Communication Engineering
(An ISO 3297: 2007 Certified Organization)
Website: www.ijircce.com
Vol. 5, Issue 3, March 2017

The patches have been employed firstly to produce separate streams of DC coefficients (Direct Current. It'll define the basic shade for the whole block. The DC may also refer as constant component). AC coefficients (Alternating Components. The remaining coefficients are called the AC coefficients) and their indexes. The correlation among DC coefficients is exploited by using differential pulse code modulation (DPCM). Similarly indexes of the AC coefficients are also de-correlated by DPCM.

D. *RLE Decoding*

The Run length decoding process is easy: If there aren't control pixel characters the coded symbol just corresponds to the original symbol, and if control pixel count occurred then it must be replaced with characters in a defined number of times. It can be noticed that the process of decoding image pixels. RLE algorithms are practically used in various image compression techniques like the well known BMP, PCX, TIFF, and is also used in PDF file format. Furthermore, RLE also exists as separate compression technique and there is also a file format called RLE (in various brands).

IV. PSEUDO CODE

Step 1: Read the Latent Finger print image.
Step 2: Get the height N and the width M for the image
Step 3: Create an array, let it RLE (N, M) ,each element of this array consists of three fields for image channels.
Step 4: Convert the image to the main array; ICA (N,M).
Step 5: ICA (N, M) image to the main array; RLE (N,M).
Step 6: Let X=RLE (0,0); RLE (0,0) is the first element in an array.
Let TH=10, TH: the threshold.
Step 7: For I= 0 to N-1
Step 8: For J=0 to M-1
Step 9: If X-RLE (I,J) <= TH then
Let C=C+1
Else
Let X=RLE(I, J) and C=0
Step 10: End.

V. CONCLUSION AND FUTURE WORK

In this paper presents a novel image compression on image local patch extraction using run length coding compression ass it is evident from the algorithm, that the exact image data (pixel values) are extracted from the compressed data stream without any loss. This is possible because the compression algorithm does not ignores or discards any original pixel value. Moreover the techniques such as approximate matching and run length encoding technique are intrinsically lossless. This compression technique proves to be highly effective for images with large similar locality of pixel lay out. This technique will find extensive use in medical imaging sector because of its lossless characteristics and the medical images has large area of similar pixel layout pattern, like in color images large area are black. In future the X-Ray image compression system could be an extra option for processing in Latent images.

REFERENCES

1. W. B. Pennebaker and J. L. Mitchell, JPEG Still Image Data Compression Standard. New York, NY, USA: Van Nostrand Reinhold, 1993.
2. Information Technology—Lossless and Near-Lossless Compression of Continuous-Tone Still Images (JPEG-LS), ISO/IEC Standard 14495-1, 1999.
3. M. Weinberger, G. Seroussi, and G. Sapiro, "The LOCO-I lossless image compression algorithm: Principles and standardization into JPEG-LS," IEEE Trans. Image Process., vol. 9, no. 8, pp. 1309–1324, Aug. 2000.
4. X.Wu and N. Memon, "Context-based, adaptive, lossless image coding," IEEE Trans. Commun., vol. 45, no. 4, pp. 437–444, Apr. 1997.
5. Information Technology—JPEG 2000 Image Coding System—Part 1: Core Coding System, INCITS/ISO/IEC Standard 15444-1, 2000.
6. ITU-T and ISO/IEC, JPEG XR Image Coding System—Part 2: Image Coding Specification, ISO/IEC Standard 29199-2, 2011.

P. Alaguthai, Assistant Professor of Computer Science	International Journal of Innovative research in Computer and Communication Engineering		An Optimal Image Fusion Using local Variation and Gradient Reversal Suppression			International ISSN(Online): 2320-9801 ISSN (Print): 2320-9798	March 2017

ISSN(Online): 2320-9801
ISSN (Print): 2320-9798

International Journal of Innovative Research in Computer and Communication Engineering

(An ISO 3297: 2007 Certified Organization)

Website: www.ijircce.com

Vol. 5, Issue 3, March 2017

An Optimal Image Fusion Using Local Variation and Gradient Reversal Suppression

T. Sathya M.Sc(CS&IT).,M.Ed [1], P. Alaguthai M.Sc(CS).,M.Phil[2]

M.Phil Scholar, Dept. of Computer Science, Sakthi College of Arts and Science for Women, Dindigul, India

Assistant Professor, Dept. of Computer Science, Sakthi College of Arts and Science for Women, Dindigul, India

ABSTRACT: The goal of image fusion(IF) is to integrate complementary multi-sensor, multi-temporal and/or multi-view information into one new image containing information the quality of which cannot be achieved otherwise. In this paper presents an optimal Image fusion scheme is novel for capturing a scene by using a standard dynamic range device and synthesizing an image suitable for SDR (Standard Dynamic Range) displays. The captured image series, first calculate the image global luminance levels, which maximize the observable contrasts, and then the scene gradients embedded in these images. The fusion algorithm techniques of diffusion and contrast are implemented. This is done in a multi-resolution of brightness variation in the sequence.

KEYWORDS: Image Fusion; gradient; SDR; Luminance;

I. INTRODUCTION

Image fusion is the process of combining information from two or more images of the same scene so that the resulting image will be more suitable for human and machine perception or further image processing tasks such as segmentation, feature extraction, and target recognition [1]–[4]. It is widely applied into many fields such as computer vision, medical imaging, and remote sensing. For example, in the computer vision field, the technique can be used for overcoming the limited depth-of-focus of optical lenses in charge-coupled devices.

Image fusion methods can be broadly classified into two categories, namely, spatial domain and transform domain. The former, including averaging and principal component analysis (PCA) [2], can directly fuse the source images into the intensity values, whereas the latter, which include the Laplacian pyramid (LAP)-based method [1], discrete wavelet transform (DWT)-based approach [3], and discrete cosine transform (DCT)-based algorithm [4], merge the transform coefficients using the classical weighted average strategy or the choose-max strategy and then obtain the fused result through the inverse transformation of the combined coefficients.

Digital Imaging System has been used in various image processing domains such as satellite and commercial domain like Voter ID. The proposed system uses JPEG images and it supports two-dimensional (2-D) images. The quality of the image is measured using Peak-Signal- Noise Ratio (PSNR) which is measured by decibel (dB). It mainly concentrates on Depth of Field (DOF) of an image. In the proposed work the input images are in the form of sequence of four images which is taken at various situations such as with flash, without flash, with light and without light. Depth of Field is nothing but the distance between the nearest and farthest objects in a scene which appears acceptably sharp in an image. The various steps are carried out and thus the result obtained is a fusion of the images which is clear and the quality of image is good. It shows best result when compared with the existing system.

The fusion algorithm techniques are used for fusion of images based on contrast and gradient level. This is done in a multi-resolution of brightness variation in the sequence. Gaussian filter method and Laplacian methods are used so that up-scaling and down-scaling is done successfully.

The rest of the paper is organized as follows: Related is detailed in Sect. 2. In Sect. 3, Proposed Methodology and the conclusion are in Sect. 5.

II. RELATED WORK

In [2] authors discussed to increase the spatial resolution, a SPOT panchromatic image was combined with the extracted spectral image; merging methods, classic IHS transforms and linear combinations were tested. For these two

ISSN(Online): 2320-9801
ISSN (Print): 2320-9798

International Journal of Innovative Research in Computer and Communication Engineering
(An ISO 3297: 2007 Certified Organization)
Website: www.ijircce.com
Vol. 5, Issue 3, March 2017

steps of image processing, the best results were obtained by respectively using PCA and a selective linear combination. The merging of the SPOT data was done selectively in order to avoid the disturbance of the spectral content of the

Landsat TM image. For this reason, only the PC corresponding to the visible part of the spectral domain was combined with the SPOT. In [3] authors proposed the goal of image fusion is to integrate complementary information from multisensor data such that the new images are more suitable for the purpose of human visual perception and computer-processing tasks such as segmentation, feature extraction, and object recognition. This paper presents an image fusion scheme which is based on the wavelet transform. The wavelet transforms of the input images are appropriately combined, and the new image is obtained by taking the inverse wavelet transform of the fused wavelet coefficients. An area-based maximum selection rule and a consistency verification step are used for feature selection. In [4] authors studied the image fusion techniques in the discrete cosine transform (DCT) domain. A new image fusion technique based on a contrast measure defined in the DCT domain is presented. The performance of our contrast measure based technique is analyzed and compared with other image fusion techniques. In [5] authors presented a tensor modeling and algorithms for computing various tensor decompositions (the Tucker/HOSVD and CP decompositions, as discussed here, most notably) constitute a very active research area in mathematics. Most of this research has been driven by applications. There is also much software available, including MATLAB toolboxes. The objective of this lecture has been to provide an accessible introduction to state of the art in the field, written for a signal processing audience. They believe that there is good potential to find further applications of tensor modeling techniques in the signal processing field. In [6] authors illustrated Two particular tensor decompositions can be considered to be higher-order extensions of the matrix singular value decomposition: CANDECOMP/PARAFAC (CP) decomposes a tensor as a sum of rank-one tensors, and the Tucker decomposition is a higher-order form of principal component analysis.

III. PROPOSED ALGORITHM

The proposed method accepts the Image fusion parameters as input which contains the MATLAB simulation where the novel image fusion based on scene gradient and luminance extraction algorithm is applied to the real-world image databases. This overall proposed architecture in figure 1 follows a from the beginning to end state.

A. *Image separation*

The exposure level of a photo is the total radiant energy integrated by the camera when the shutter is opened. The exposure level can influence significantly the quality of a captured photo because when there are no saturation or thermal noise, a pixel's signal-to-noise ratio (SNR) always increases with higher exposure levels. For this reason, most modern cameras can automate the task of choosing an exposure level that provides high SNR for most pixels and causes little or no saturation.

The exposure level is not affected by the sensor gain, but affects noise properties and saturation are affected by sensor gain. Lens-based camera systems provide only two ways to control exposure level—the diameter of their aperture and the exposure time. All light passing through the aperture will reach the sensor plane, and that the average irradiance is measured over the aperture which is independent of the aperture's diameter. . In this case, the exposure level L satisfies

$$L \propto \tau D^2 \quad \text{eqn. (1)}$$

Where τ is the exposure time and D is the aperture diameter.

For a specified aperture and focus setting, the depth of field is the interval of distances in the scene [*d1, d2*], whose blur diameter is below a maximum acceptable size.

ISSN(Online): 2320-9801
ISSN (Print): 2320-9798

International Journal of Innovative Research in Computer and Communication Engineering
(An ISO 3297: 2007 Certified Organization)
Website: www.ijircce.com
Vol. 5, Issue 3, March 2017

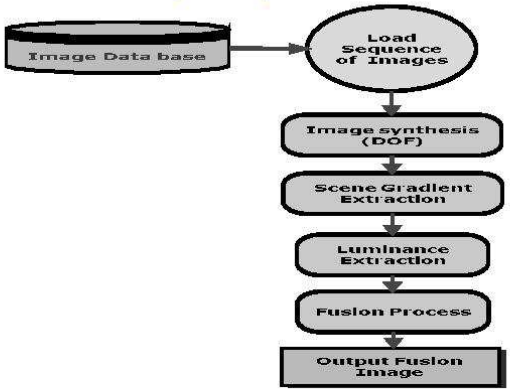

Fig.1. Proposed Framework flow diagram

B. *Scene Gradient Extraction*

A good solution to suppress halos is to apply the scene gradients to adjust the gradient of the synthesized SDR image. The scene gradient information is adaptively captured by setting the different exposure levels, i.e., the scene gradients are captured through the local adaptation to the scene luminance for an window $M \times M$ centered at (x, y). Technically, the scene gradient of a point is reflected by the gradient that is perceivable by human eyes, called visible gradient, and that can be measured by counting the number of visible differences of luminance's between neighboring pixels in the window.

To compute the quantity of the visible gradient $\psi(x, y)$ by

$$\psi(x,y) = \sum_{i=x-\frac{M}{2}}^{x+\frac{M}{2}} \sum_{j=y-\frac{M}{2}}^{y+\frac{M}{2}} T(|c(I_H(x,y).VMAX(\nabla I_H(x,y))|) \quad eqn.(2)$$

These exposure levels lead to different gradient magnitudes because the gradient magnitude depends on the image luminance's and the image luminance depends on the exposure level. The scene gradient extraction is a process to find gradient $G(x, y)$ which maximizes the quantity of the visible gradient,

$$G(x,y) = \arg max_{\nabla I_H(x,y)} \psi(x,y) \qquad eqn.(3)$$

In this gradient extraction, the pixels positions are estimated along with x-coordinate and y-coordinate. In vector calculus, the gradient of a scalar field is a vector field that points in the direction of the greatest increase rate in the scalar , and in the magnitude. The variation in space of any quantity can be represented (e.g. graphically) by a slope in general. The gradient represents the steepness and direction of the slope.

ISSN(Online): 2320-9801
ISSN (Print): 2320-9798

International Journal of Innovative Research in Computer and Communication Engineering

(An ISO 3297: 2007 Certified Organization)

Website: www.ijircce.com

Vol. 5, Issue 3, March 2017

C. *Luminance Extraction*

The image dimensions (width, height and number of channels) are calculated using the image luminance (color variance) which maximizes the visible contrasts over different captured images. The visible contrast of the window between the point and its surrounding points is observed. The image luminance is calculated for each point(x, y) which maximizes the visible contrasts over different captured SDR images. The point (x, y) and its surrounding points form an M × M local window in a scene. The visible contrast $v(x, y)$ is calculated using,

$$v(x,y) = T\left(\Delta \mathrm{I}_{\mathrm{H}}(x,y)\right)\Delta \mathrm{I}_{\mathrm{H}}(x,y) \qquad eqn.(4)$$

Where $T(\gamma) = 1$ which is larger than or equal to a predefined threshold.

D. *Fusion*

The fusion of N images and computation of average weight can be estimated with the help of quality measures which are already computed. To obtain a consistent result, the values are normalized for the N weight maps. The resulting image R can then be obtained by a weighted blending of the input images:

$$\sum_{k=1}^{N} W_{ij,k} I_{ij,k} \qquad eqn.(5)$$

where I_k is the k-th input image in the sequence and 'W' is the weight which varies very quickly, corresponding to the layer that appear. This occurs due to fusion of images which contains different absolute intensities due to their different exposure different exposure times. The sharp weight map transitions can be avoided by smoothing the weight map with a Gaussian filter, but this result in undesirable halos around edges, and spills the information across object boundaries. An edge-aware smoothing operation using the cross-bilateral filter seems a better alternative. However, it is unclear how to define the control image, which gives the information where the smoothing should be stopped. Using the original grey scale image as control image does not work well. Also, it is hard to find good parameters for the cross-bilateral filter (i.e., for controlling the spatial and intensity influence).

IV. Conclusion and Future Work

In this paper presents a new fusion scheme is achieved in the proposed system by considering local variation and gradient reversal suppression. The visible scene contrasts and the scene gradient can be captured adaptively by utilizing the different exposures. A gradient model is proposed to carry out the scene reproduction by preserving both the visible contrasts and the gradient consistency. The proposed system maintains visible contrasts and the gradient consistency effectively. Fusion based on Gradient Exposure technique blends images in a multi-exposure sequence, showed by simple quality measures like saturation and contrast.

References

1. E. H. Adelson, C. H. Anderson, J. R. Bergen, P. J. Burt, and J. Qgden, "Pyramid methods in signal processing," RCA Eng., vol. 29, no. 6, pp. 33–41, Nov./Dec. 1984.
2. H. Yesou, Y. Besnus, and J. Rolet, "Extraction of spectral information from Landsat TM data and merger with SPOT panchromatic imagery—A contribution to the study of geological structures," ISPRS J. Photogramm. Remote Sens., vol. 48, no. 5, pp. 23–36, Oct. 1993.
3. H. Li, S. Manjunath, and S. Mitra, "Multi sensor image fusion using the wavelet transform," Graph. Models Image Process., vol. 57, no. 3, pp. 235–245, May 1995.
4. J. Tang, "A contrast based image fusion technique in the DCT domain," Digit. Signal Process., vol. 14, no. 3, pp. 218–226, May 2004.
5. G. Bergqvist and E. G. Larsson, "The higher-order singular value decomposition: Theory and application," IEEE Signal Process. Mag., vol. 27, no. 3, pp. 151–154, May 2010.
6. T. G. Kolda and B. W. Bader, "Tensor decompositions and applications," SIAM Rev., vol. 51, no. 3, pp. 455–500, Sep. 2009.

S. Kavitha, Assistant Professor of Computer Science	International Journal of Engineering Development and Research		Image Encryption Using Binary Bit Plane and Rotation Method For An Image Security			International 232 1-9939	April 2017

© 2017 IJEDR | Volume 5, Issue 2 | ISSN: 2321-9939

IMAGE ENCRYPTION USING BINARY BIT PLANE AND ROTATION METHOD FOR AN IMAGE SECURITY

[1]R.Aarthi, [2] Mrs. S.Kavitha

[1]M.Phil Scholar, Department of Computer Science, Sakthi College of arts and science for women, oddanchatram, India.

[2]Head of the Department, Department of Computer Science, Sakthi College of arts and science for women, Oddanchatram, India.

Abstract

Image encryption plays a major role in information security. It is mainly used to convert the original image into another form. In this work, we propose a bit plane slicing of digital image to provide the more security. To enhance security of the bitplane decomposition based image encryption methods, this paper introduces a novel image encryption algorithm using a bitplane of a source image as the security key bitplane to encrypt images. It focuses on three techniques such as image scrambling, bit plane slicing and image rotation for efficient image encryption. Arnold scrambling and bit plane slicing process are performed in the source image. From the decomposed source image, particular bitplane is assigned as the security key bit plane to perform the encryption process in the original image. As an example, this paper also proposes a bit-level scrambling algorithm to change bit positions. Simulations and security analysis are provided to demonstrate an excellent encryption performance of the proposed algorithm.

Index Terms – Image Encryption, Bit Plane Slicing, Rotation, Scrambling.

1. INTRODUCTION

Cryptography is an efficient method of transferring information in a secure way. It scrambles the image before transmitting in order to change the structure of an image. Even the attacker cannot able to hack because it is difficult for him to retrieve the original image. It only provides the modified form of an image but it does not hide the image even though it is better secure method. The main intention is to provide better protection of the original image. Bit plane slicing is mainly used for splitting images into binary planes. Each bit is used to represent the intensity of each pixel of an image. Image scrambling is always based on pixel values of an image. The digital image is divided into 8 bit planes because it is useful for analyzing the importance of each bit in an image. Whereas a small change in color affect bit value of an image. The color image is composed of many pixels is decomposed into 8 bit planes. It is used to represent the highest order and lower order bits to specify the contribution of each bit in an image. It achieves better image encryption than the other least significant bit, perceptual masking technique. This process is done on without changing the overall image quality.

Image Encryption is the process of encoding messages in such a way that eavesdroppers or hackers cannot read it, however that authorized parties. With the huge growth of computer networks and the latest advances in digital technologies, a huge amount of digital data is being exchanged over various types of networks. It is often true that a large part of this information is either confidential or private. As a result, different security techniques have been used to provide the required protection. The security of digital images has attracted more attention recently, and many different image encryption methods have been proposed to enhance the security of these images. Image encryption techniques try to convert an image to another one that is hard to understand. On the other hand, image decryption retrieves the original image from the encrypted one. There are various image encryption systems to encrypt and decrypt data, and there is no single encryption algorithm satisfies the different image types. They protect the secret information by

converting the secret information to some unintelligible form using a key. By using a key, we protect the secret information by converting the secret information to some incomprehensible form. We get back information through encrypted information should be converted back to original information. On the Basis of key, the encryption algorithm can be classified into two categories. They are(i) Symmetric key encryption-This algorithm uses same key for both encryption and decryption and (ii) Asymmetric key encryption-This algorithms uses different keys for encryption and decryption. Asymmetric key algorithm has very higher computational costs than Symmetric key encryption algorithms which have comparatively lower cost. Asymmetric key algorithms are most time prohibitive for multimedia data. But the characteristic of multimedia data is totally different from text data. All multimedia data has got a lot of redundancy but text data does not possess any redundancy. The pixel value of a location is highly correlated to values of its neighboring pixels. Like, a sound sample is correlated to its next sample and its previous samples. This correlation proves to be attack points to any standard encryption algorithm. Because they can predict the values of neighboring pixels or next sound sample by finding out pixel value at a location or one sound sample with reasonable accuracy.

Nearly all the available encryption algorithms like .DES, AES, RSA and IDEA are used for text data. Act of them DES, AES, RSA and IDEA can achieve high security, it is not be suitable for images and videos encryption due to the intrinsic characters of images and videos .So we need some other technique for encrypt image and videos. For large data size and high redundancy, encryption special requirements and different encryption algorithms is needed. The image encryption algorithms divided into three major groups: (i) position permutation based algorithm, (ii) value transformation based algorithm (iii) visual transformation based algorithm .Several encryption algorithms are based on chaotic maps. In this project, we propose image encryption using Random Scrambling and XOR operation. Arnold transform that is based on shuffling the image pixels and they encrypting the resulting image using XOR operation. We used 32 bit key that is good for practical purposes.

SCOPE OF THE STUDY

The need for image processing has increased sharply. Encryption and gloves are both dirt-cheap and widely available. Image processing has applications in many fields. Improvement of secured pictorial representation for human interpretation and processing security image information were the two main reasons behind the need for image processing.

OBJECTIVE OF THE STUDY

The main objective of the system is

- To enhance the security of the image.
- To enhance the performance of the image encryption and decryption.

2. LITERATURE SURVEY

Image encryption technique plays a vital role in image processing. Lot of image encryption technique has been developed so far. In this literature review some encryption techniques are discussed. The techniques such as Arnolds algorithm, Bit plane algorithm, Scrambling algorithm by means of block analysis, enhance the security and bit plane generation are discussed.

R.Gopinath et al., Image encryption is used to protect the images and transform into different format. In this paper, lossless encryption for color images using binary key images has been proposed. In proposed method, the key image size is same as the original image. The key image is either a bit plane or an edge map generated from another image. The method is discussed against common attacks such as the plaintext attacks, brute force attack and cipher text attacks. The experimental results shows that the lossless encryption of all type of images.

Rinkipakshwar et al., This paper aims at improving the level of security and secrecy provided by the digital gray scale image encryption. The image encryption and decryption algorithm is designed and implemented to provide confidentiality and security in transmission of the image based data as well as in storage. Since the pixel of the image is highly correlated to their neighboring pixels. Due to this strong correlation any pixel can be practically predicted from a value of its neighbors. So there is a need of a technique that can shuffle the pixels to reduce the correlation between the neighbor pixels. Hence we use scrambling technique that shuffles the pixels of image. This scrambling image is called transformed

image then divided into 2 pixels x 2 pixels blocks and each block is encrypted using XOR operation by four 8 bit keys. The total size of key in our algorithm is 32 bit long which proves to be strong enough. The proposed encryption algorithm in this study has been tested on some Gray scale images and showed good results.

Li W and Yuan Y proposing two attacks to sketch the outline of the original image directly from the scrambled JPEG compressed image. In particular, Li and Yan proposed nonzero count attack to sketch the outline of the original image. However, their method requires the tuning of threshold values.

3. METHODOLOGY

3.1. ARCHITECTURE DIAGRAM

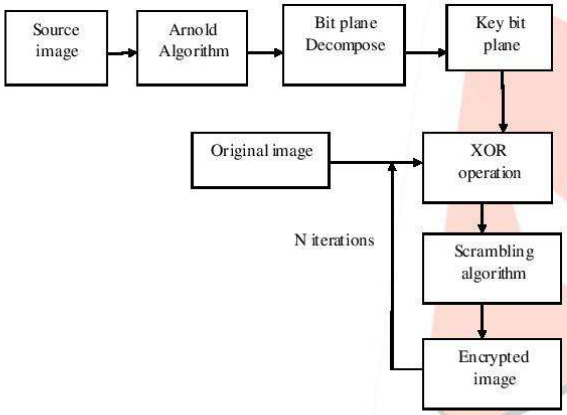

Figure 3.1. Architecture diagram

3.2. FUNCTIONAL COMPONENETS

The modules of the image encryption using Arnolds transform algorithm has briefly described as below:

- Image Scrambling Using Arnold Transformation
- Binary Bitplane Decomposition
- Transformation of Bitplane into Vector
- Scrambling with XOR operation

Image Scrambling using Arnold Algorithm

Arnold scrambling algorithm is base on square digital image and these images are mostly $N \times N$ pixels of the digital image. However, most of the digital images are non-square in the real world, so that this system cannot use Arnold scrambling algorithm widely. To improve the Arnold scrambling algorithm, this system the original Arnold scrambling algorithm, so that this system applies Arnold scrambling algorithm to $M \times N$ non-square pixel digital image, it means the length and width of the image is not equal .

The digital image can be seen as a two-dimensional matrix. When the size of the image is N, then I have $N \times N$ elements, the subscript x, y stand for the position of pixel, x, $y \in \{0, 1, 2..., N\text{-}1\}$. Let x, y corresponds to the x, y of Arnold scrambling, for each pair x, y, after all do Arnold scrambling, become x' and y', which equivalent to the original image of the point from (x, y) move to the $= (x', y')$, so realized the movement of pixels in the image, the image with Arnold scrambling traverse all the points to complete a picture of Arnold scrambling.

The cycle of Arnold scrambling is relate to the size of the image, but not directly proportional. If size is 128 × 128 pixel image of Arnold scrambling cycle is 96, size 240 × 240 pixel image of Arnold scrambling for 60 cycles.

Binary Bit Plane Decomposition

A non-negative decimal number N can be represented by a binary sequence $(b_{n\_1};\ldots; b_1; b_0)$ based on the following equation:

$$N = \sum_{i=0}^{n-1} b_i 2^i = b_0 2^0 + b_1 2^1 + \cdots + b_{n-1} 2^{n-1}$$

Because pixel values in a gray scale image are decimal numbers between 0 and 255,each pixel can be represented by an 8-bit binary sequence. Thus, BBD can decompose a gray scale image into 8 binary bit planes (BBs). The i^{th} bit plane consists of all the i^{th} bits of the binary representation of each pixel within the gray- scale image. Among these bit planes, higher bit planes contain more significantly visual information of the original image while lower bit planes show more details

Transformation of Bit Plane into Vector

In Bit-Plane Slicing image is sliced into eight binary planes. The bits which are presents in the bit plane 0 is the least significant bit and the bits which are present in the bit plane 7 are the most significant bits. All pixel values of the image is converted into binary vector space based on the bit plane slicing.

In terms of 8-bits bytes, plane 0 contains all lowest order bits in the bytes comprising the pixels in the image and plane 7 contains all high order bits.

Separating a digital image into its bit planes is useful for analyzing the relative importance played by each bit of the image, implying, it determines the adequacy of numbers of bits used to quantize each pixel , useful for image compression.

In terms of bit-plane extraction for a 8-bit image, it is seen that binary image for bit plane 7 is obtained by proceeding the input image with a thresholding gray-level transformation function that maps all levels between 0 and 127 to one level (e.g 0)and maps all levels from 129 to 253 to another (eg. 255).

Scrambling With XOR Operation

The algorithm first decomposes the original image (the image to be encrypted) into eight binary bit planes using binary bit plane decomposition. To change bit values, each bitplane is then performed the XOR operation with a security key bitplane, individually. A scrambling algorithm is used to change all bit locations. After n iterations of the XOR and scrambling processes combines all bit- planes to obtain the encrypted image.

The security keys of DecomCrypt consist of the iterations n, source image or its location (the location of an image database or a link of webpage), decomposition method and its parameters, location of the security key bitplane, as well as the scrambling algorithm and its security keys. These security keys are encoded as messages or emails and then transmitted over separated security channels. This ensures that they are safely and correctly delivered to the authorized users for image decryption

3.4. IMAGE SCRAMBLING

Image Scrambling (IS) is a process of scrambling the positions of pixels in an image using permutations. There are several image scrambling techniques like Arnold-Cat map, Standard map, row-column shuffling, SCAN Pattern, Index bit-reversal order and Matrix transformation. In Image Encryption (IE), the value of the pixel is get altered by using some mathematical operations like bitwise xor, bit shuffling, bitwise rotation, matrix addition, matrix multiplication and manipulation in transform domain.

Image scrambling is a process of rearranging the pixels position of an input image using permutations. Correlation between adjacent pixels is more important in an image. Using scrambling process this correlation between adjacent pixels are reduced and hence scrambled image reduces the intelligible property of an image.

4. RESULTS AND DISCUSSION CONCLUSION

Image encryption and decryption using Arnold scrambling and bits scrambling process are written in MATLAB. Simulations have been performed on a Matlab R 2008 platform to verify the validity of the proposed encryption technique.

In the encryption process, first the source image is read from the file. Then perform the Arnold scrambling process for the source image. After completion of Arnold scrambling process, scrambled image's 8 bit planes are extracted individually. From the extracted 8 bit plane, particular key bit plane is selected and passed to the XOR operation and scrambling process with the original image. After completion of this process, original image is selected and read from the image file and histogram is generated for the original image. Generated key from Arnold scrambled image and the original image is passed into the image encryption process. Original image's bit positions are encrypted using key data with XOR and bits scrambling process. Thus the image is encrypted. Encrypted output for the image is obtained. Image decryption is performed in the reverse order of encryption. Thus the original image is obtained.

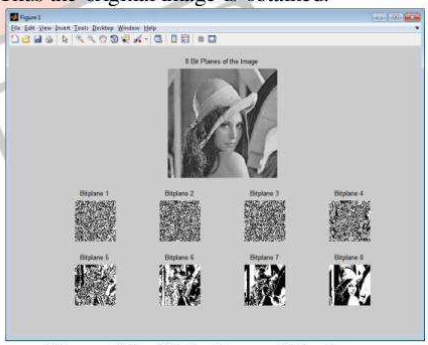

Figure 4.1. 8 bit planes of the image

A bit plane of a digital discrete signal (such as image or sound) is a set of bits corresponding to a given bit position in each of the binary numbers representing the signal.

The above figure 4.1 shows the source image with its bit slicing images.

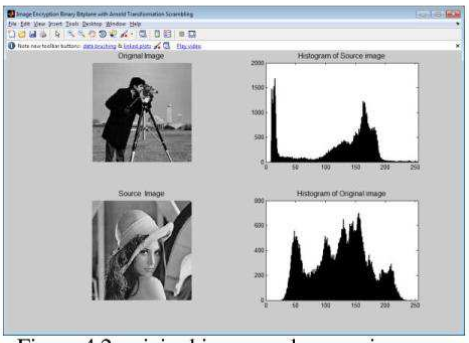

Figure 4.2. original image and source image with histogram

Histogram of the image data calculates the histogram for the intensity image and displays a plot of the histogram. The number of bins in the histogram is determined by the image type. The above figure shows the histogram for the original image and also source image.

Source image is used to perform the Arnold scrambling and select the particular key bit plane. Key bit plane is used to encrypt the original image.

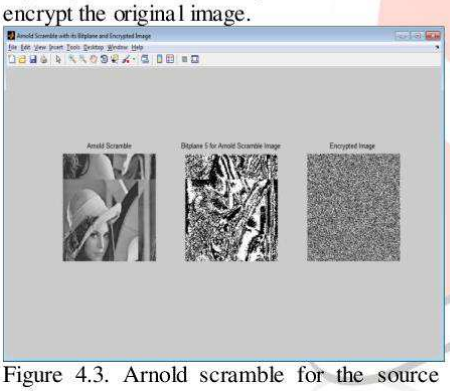

Figure 4.3. Arnold scramble for the source image with selected key bit plane and encrypted original image

The above figure 4.3 shows the Arnold scramble of the given original image and selected key bit plane from the 8 bit planes of the scrambled image. Selected key bit plane is used to perform the encryption process with the selected original image.

In the encryption process, XOR operation is performed in the selected key bit plane and original image's bit data and perform the scramble process. Finally encrypted image is obtained.

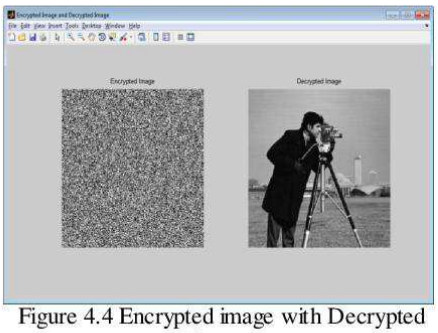

Figure 4.4 Encrypted image with Decrypted image

The above figure 4.4 shows the encrypted image and output of the decryption process. Image decryption is performed in the reverse order of encryption. Thus the original image (decrypted) is obtained.

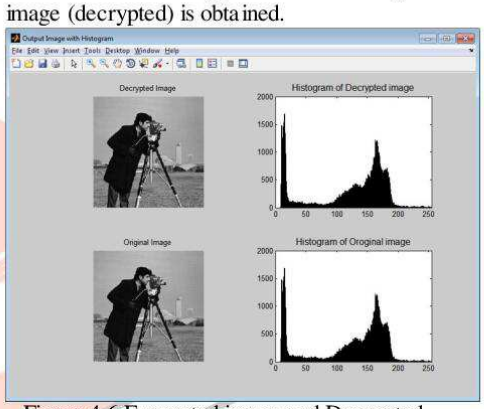

Figure 4.6 Encrypted image and Decrypted image with Histograms

The `psnr` function implements the following equation to calculate the Peak Signal-to-Noise Ratio (PSNR):

$$PSNR = 10\log_{10}(peakval^2/MSE)$$

where *peakval* is either specified by the user or taken from the range of the image data type (e.g. for `uint8` image it is `255`). *MSE* is the mean square error,

i.e. *MSE* between `A` and `ref`.

Peak Signal to Noise Ratio (PSNR) and Mean Square Error (MSE) are used to comparing the squared error between the original image and the reconstructed image. There is an inverse relationship between PSNR and MSE. So a higher PSNR value indicates the higher quality of the image (better). PSNR value of the original and decrypted image is 99.00

REFERENCES

1. R.Gopinath, M.Sowjanya"Image encryption for Color images using bitplane and Edge map Cryptography algorithm

2. Somdip Dey, "SD-AEI: An Advanced Encryption Technique For Images", Proc. Of IEEE 2012 Second International Conference on Digital Information Processing and Communications (ICDIPC2012), Lithuania, pp. 68-73.

3. Shujun Li , Xuan Zheng, —On the Security of an Image Encryption Method—in Proc. IEEE Int. Conference on Image Processing (ICIP'2002 ppII-925 - II-928 vol.2

4. Seyed Hossein Kamali, Reza Shakerian, Maysam Hedayati, Mohsen Rahmani, —A New Modified Version of Advanced Encryption Standard Based Algorithm for Image Encryption‖, in Proc *International Conference on Electronics and Information Engineering (ICEIE 2010), Volume1, pp* V1-141-145.

5. Zhenjun Tang and Xianquan Zhang, Secure Image Encryption without Size Limitation Using Arnold Transform and Random Strategies, Journal of Multimedia, VOL. 6, NO. 2, APRIL 2011, 202-206.

6. Chang-Mok Shin, Dong-Hoan Seo, Kyu-Bo Chol, Ha-Wmn Lee, and SmJmng Kim, " Multilevel Image Encryption by Binary Phase XOR Operations", *IEEE Proceeding in the year 2003*.

7. Qiudong Sun, Wenying Yan, Jiangwei Huang, Wenxin Ma, "Image Encryption Based on Bit-plane Decomposition and Random Scrambling", *Journal of Shanghai Second Polytechnic University , vol. 09 IEEE, 2012.*

8. Hui Liu, Cong Jin," A Color Image Encryption Scheme Based on Arnold Scrambling and Quantum Chaotic" International Journal of Network Security, Vol.19, No.3, PP.347-357, May 2017

S. Yoga, Assistant Professor of Computer Science	International Journal of Engineering Development and Research		Computation of Burnt Forest Region Using Digital Image Processing			International 232 1-9939	April 2017

© 2017 IJEDR | Volume 5, Issue 2 | ISSN: 2321-9939

Computation Of Burnt Forest Region Using Digital Image Processing

[1]N.Nagapriya, [2] Mrs. S.Yoga
[1]M.Phil scholar, [2]Assistant professor,
Department of Computer Science, Sakthi College of arts and science for women, oddanchatram,, India.

Abstract: Predicting the forest fire is an important problem from many points of view. It destroys ecology and decreases the overall life quality. It is important from economical point of view as wood is a valuable resource. Fires not only affect the characteristics of forests but it also affects human lives and livelihood. Due to the lack of collecting the aerial view images of forest fire and also lack of specific techniques for calculation of burnt regions of forests, researchers use different methods. In this paper, we examine the problem of collecting the exact aerial image forest fire detection of different parts of the forest areas. Our approach is based on image pre-processing, segmentation of images are produced using the segmentation methods and compute the burned area. The images are collected from the videos. In the preprocessing phase, forest fire video is converted into frames and stored as images.

Keyword : Theresholding, noise removal, burned region, image scaling

1. INTRODUCTION

Forest fire is one of the most threatening commotions for property, infrastructure and ecosystem. The long vapid and hot summer is responsible for rapid increase in fires with uncontrolled strong wind, results in forest fire and large burnt areas every year. Generally, the wild land fire is initiate through lightening but human negligence is also responsible to burn thousands of square kilo meters. The other important parameter responsible for the burn occur in forest is drying out branches and leaves and become highly flammable. Increment in forest fires not only degrades the modem of forest but also it degrades the human lives and lively hoods. In relation to loss of human lives examples, the forest fires in Victoria, Australia in 2009, which caused 173 fatalities, while fires in Greece in 2007, resulted in 80 dead. Many wilderness urban interface fires have clearly shown how wildfires affect and threaten residential area.

According to precursor, fires acquired in forest will halve the world forest stand before the year 2030. 20% of complete CO2 emission came from forest fires indicates that it is important to deal these phenomenon with great attention. Also the increment in the rate of occurrence of fire is occurred due to the global warming.

Fires affect not only forests and their function and services, but also the other assets that is human lives and livelihoods. The damage can be extend to landscape and results in haze and deposit pollutants as well as the release of greenhouse gases. Presently there is no conventional method to evaluate accurate area of burnt regions of forests and hence researches uses different methods and variables .The main parameter during consideration of computation of burnt regions is speed in performing processes and in damage evaluation. In this report, An aerial digital image which is obtained from forest after the fire occurrence is used to calculate the primary area of burnt regions using digital image processing and to obtain the accurate real area in hectares , coefficient "m" is calculated. This method is dependent on some secondary parameters such as aerial camera and helicopter in order to calculate real area of burnt regions. To obtain accurate and rapid evaluation of burnt regions after the wild land fire suppression is used for the reforestation and restoration in the affected areas and to avoid the post wild fire hazards and degradation of affected areas.

2. LITERATURE SURVEY

Bibek Ranjan Ghosh, Siddhartha Banerjee, Attyuttam Saha, Fire is one of the major problems that are causing great loss to property and ecosystem in today's world. Fires not only affect the characteristics of forests but it also affects human lives and livelihood. Due to the lack of specific techniques for calculation of burnt regions of forests, researchers use different methods. In this research, an automated approach is developed to determine the significant burnt area of forest using different image processing techniques. The proposed method is compared with other existing methods and is found to be capable in more precise measurement of the burnt area. The proposed method produces much more exact results at a single trial and uses no brute force method to determine a proper filter to determine the exact region affected by the wild fire.

Hamidreza, Hamud and Asadollah proposed a method which uses a hit and trial method using median filters. This method is basically a brute force method to search for a proper median filter that serves the purpose of detecting the actual burnt region. After binarizing the image using the thresholding technique, median filters are being applied. Firstly a median filter of 3×3 dimensions have been used followed with filters of 5×5,7×7 dimensions and finally a proper result is obtained using a filter of 9×9 dimensions.

Dr.M.P Sivaram Kumar, Shyamala.R, Priyanka.G, Sneha.R, propose a method for the detection of fire through the usage of photographed data of forest area followed by computer processing of the data. A method for reading information, pre-processing of an image color components, the segmentation and data classification using SVM is proposed. The method is

working very fast and can be used for online calculations and decision making. The efficiency of the proposed procedures is shown: 95 % detection ration and 5 % false detection is shown. The proposed method can be used in the monitoring systems of the area to detect fire.

3. METHODOLOGY

Three situations in the forest fire field is encountered.

- **Pre-Disaster:** In this situation, most researches are about the ways that how to prevent the fire using natural posture or using consolidation and integration image based data which are obtained from different satellites sensors.
- **Meantime-Disaster**: In this situation, researches have been focused on the detection of smoke detection of fire primary has two parameters which are prediction of development of fire and the acceleration in firefighting operation.
- **Post-Disaster**: If firefighting is performed then and then only the calculation of burnt forest region area is possible because the continuation of fire and smoke may disturb the area computing process. Therefore in this situation researches have been focused on burnt area after fire completion.

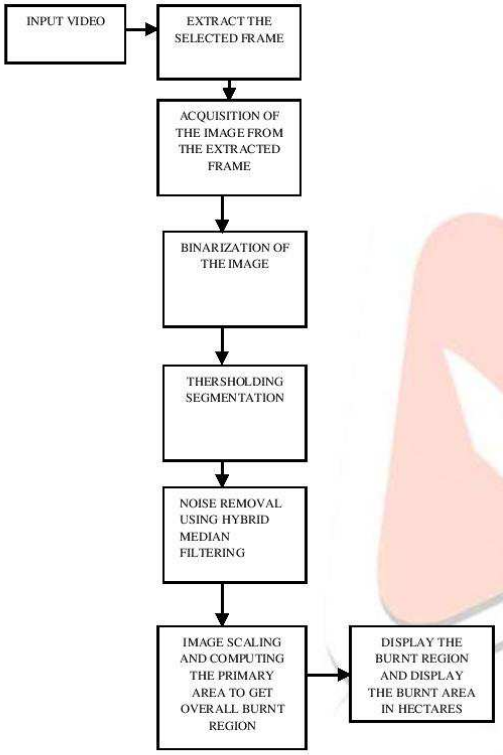

Fig.1. Overall structure

In this work, computation of burned region in the fire forest consists of four phases such as

- Acquisition Of Image from Videos
- Segmentation Of Image
- Cancellation Of Noise
- Image Scaling

Acquisition Of Image

The desired aerial image is obtained from the videos which are taken in Ariel view like using of helicopter and by high resolution camera. From the target point in order to be used in machine vision system, the burnt region will be completely visible in one picture. Extract the exact frame using input videos.

Segmentation Of Image

In segmentation of image, the forest fire region is extracted out of source image using binarization of the image in order to proper draw the burnt region. Thresholding segmentation technique is used for the image segmentation. Gray degree image can converted into black and white image i-e the binary image. The gray degrees of image may varies from 0 to 255 where as black

and white image will be in the form of 0 and 1. In thresholding image segmentation technique, consider primary image in the form of the gray degree like T then determination of pixels with less values or more values than T is occur. If gray level of image is greater than T then convert that pixels into white. If gray level of image is less than T then convert that pixels into black pixels. In the binary image of burnt region , the calculation of burnt area becomes easier.

Cancellation Of Noise

After segmentation of the images, images may have noise which should be detected and remove before further process. To evaluate area with classified accuracy it is necessary that the obtained noise in the image should be strictly reduced or deleted. Two median and average filters can be useful in the process of noise cancellation. But median filter having greater accuracy than the average filters. We use median filter for implementation in this process. Designation of median filter includes necessity of determined dimensions. The pixel which is placed in the centre of matrix of this filter, arrange data surround to it and select median and then replace the original pixel by median pixel.

Image Scaling

Calculation of primary area after binarization and removal of noise. Now the image which is binary image array consists the value 0 and value1 as image has only two colors black and white where black is burnt region and white is a background. It is easy to count the black pixel. Primary area is calculated by simple integration method. After computing the primary area it is necessity to calculate the coefficient 'm' to get overall burnt region. Coefficient can be calculated by applying the imaging scale on the image where, Imaging Scale=focal length of Camera /

Height of flight(h)

The coefficient 'm' is given by,

m=1/Imaging Scale

Hence the real burnt area can be calculated by simple formula

Real area=Primary area*m

By simply calculating the primary area and coefficient "m" we can get real area. Real area is obtained is in Hectare.

4. RESULTS AND DISCUSSION

Forest fires represent a constant threat to ecological systems, infrastructure and human lives. Past has witnessed multiple instances of forest and wild land fires. Fires play a remarkable role in determining landscape structure, pattern and eventually the species composition of ecosystems. The integral part of the ecological role of the forest fires is formed by the controlling factors like the plant community development, soil nutrient availability and biological diversity. Fires are considered as a significant environmental issue because they cause prominent economic and ecological damage despite endangering the human lives.

In the proposed method image captured from the fire forest video as input, process the image and performs forest region detection and computation of burned region.

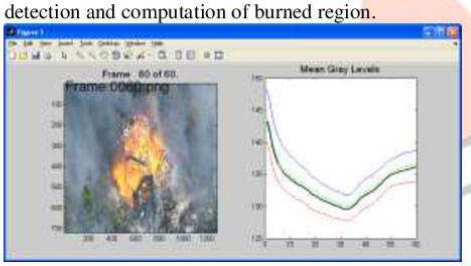

Fig.2. Extraction of frames from video

Selected fire forest video file is loaded and determine the frame count. Initially is extracted from the video with mean value of gray level, red level, green level and blue level. Extracted frames are stored in the folder with frame number as file name. Computation of mean value of Red, green and blue levels and plot the graph is also processed in this phase. it will automatically updates the progress of the frame extraction.

Extracted individual frames from the fire forest video are stored in the separate folder. Frame count is automatically determined by this system based on the fire forest video file properties.

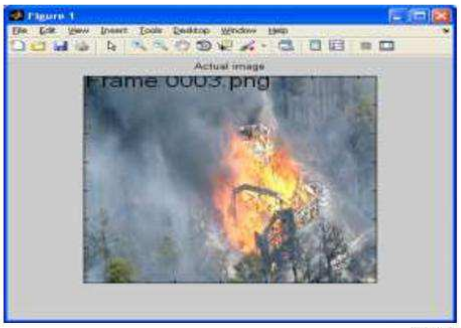

Fig.3. Selected image from frame

The desired aerial image is prepared in order to be used in machine vision system using of a helicopter (or plane) and by an appropriate digital camera from the target point, the burnt region as connected and completed inside one picture, according to above figure.

The desired aerial image is selected from the extracted frame from the fire forest video which one is taken from the helicopter.

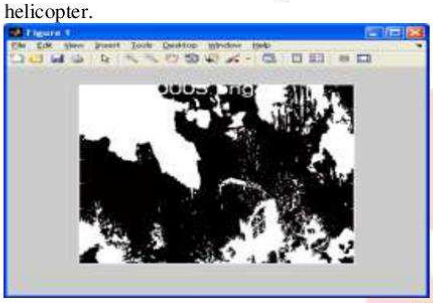

Fig. 4 Binaryzation of the Image

Binarization of the image is one of the effective ways of segmentation in order to draw the burnt regions. The simplest method for this is "Thresholding". An image with gray degrees (between 0 and 255) can be converted into a binary image (black and white or 0 and 1). To do thresholding technique, first consider a gray degree like T in the primary image and then, determining some pixels which have the values less and/or more than T [11]:

Converted into white pixels -> Gray level > T and Converted into black pixels -> Gray level <T

Now, in the calculation of area becomes easier in the binary image of the burnt region in the above figure.

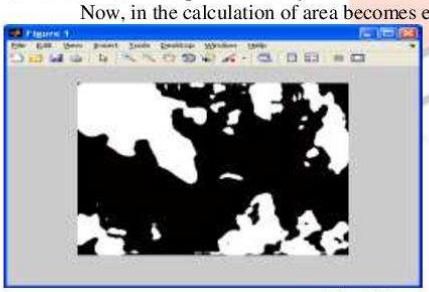

Fig. 5 Segmentation of the Image with noise removal

After image segmentation, it is necessary the obtained noise in the image, i.e. some points which are placed outside of the burnt region, shall also be reduced or deleted. To do this technique, hybrid median filter can be used. It is proved that the hybrid median filter is stronger than median and average filter, hybrid filter is used for implement.

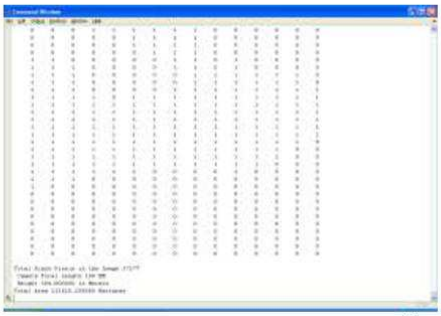

Fig. 6. Burned Region Calculations

The available burnt region in above figures is a binary image array consisting of values of 0s and 1s. In fact, this image has two colors of black (the burnt region) and white (background). It is enough to count the number of black pixels, i.e. the number of 1 available in the image to obtain the primary area by integration method (i.e. the sum of the pixels 1 which represents the approximate value of the area)

Imaging Scale = Camera Focal (f) / Flight height (h) (1)

m = 1 / Imaging Scale (2)

Real Area = Primary area * m (3)

After computing of the primary area of the burnt region, a coefficient, such as "m", should be calculated according to equations (1) and (2). By applying the imaging scale on it, real area is obtained according to equation (3) based on the measurement of forest land surface area.

In the sample image, if we have the values of "f" in millimeter and "h" in meter; therefore, real area obtained in hectare.

Total Black pixels = 37377
Focal length of the camera =100 M
Height of the camera = 304.8 Meters
Total Burned Area= 113260.296 hectares

CONCLUSION

The Computation of real burnt forest region area is dependent on secondary tools which includes an aerial digital camera and special plane or helicopter. Instead of these cause to decrease in the evaluation cost and faster notification of the results when it comes to extensive forest regions damaged by fire. Also secondary option in these technique is rather than using camera photos videos, can be used which will decrease the time and provide accurate scenario and hence the spread of fire with the time accurately is calculated.

The proposed system can be realized in future and can evaluate the performance of the system in real time forest fire monitoring system. Also, instead of using videos calculating the spread of fire with time. Further, the flicker nature of fire can be utilized so as to reduce false alarm rate.

REFERENCES

1. Wang L., Qu J., and Hao X., "Forest Fire Detection using the Normalized Multi-BandDrought Index (NMDI) with Satellite Measurements," Agricultural and ForestMeteorology, vol. 148, no. 11, pp. 1767-1776, 2008.
2. Sifakis N., Iossifidis C., Kontoes C., and Keramitsoglou I., "Wildfire Detection andTracking over Greece using MSG-SEVIRI Satellite Data," Remote Sensing, vol. 3, no. 3, pp. 524-538, 2011.
3. Anggraeni A. and Lin C., "Application of SAM and SVM Techniques to Burned Area Detection for Land Sat TM Images in Forests of South Sumatra," in Proceedings of the 2nd International Conference on Environmental Science and Technology, Singapore, pp. 160-164, 2011
4. Giglio L., Loboda T., Roy D., Quayle B., and Justice C., "An Active-Fire based Burned Are Mapping Algorithm for the MODIS Sensor," Remote Sensing of Environment, pp. 408-420, 2009.
5. Wang S., Miao L., and Peng G., "An Improved Algorithm for Forest Fire Detection using H Data," in Proceedings of the 18th Biennial Conference of International Society for Ecological Modelling, Procedia Environmental Sciences, Beijing, China, pp. 140-150, 2012.
6. CORINE Land cover - Part 1: Methodology, available athttp://reports.eea.eu.int/COR0-part1/enAntónio S. Camara, Francisco Ferreira, Spatial Simulation Modeling, Gasa, 1998
7. Vipin V" Image Processing Based Forest Fire Detection" International Journal of Emerging Technology and Advanced Engineering Website: www.ijetae.com (ISSN 2250-2459,Volume 2, Issue 2, February 2012)
8. David Weinstein, Kass Green, Jeff Campbell, and Mark Finney, Fire Growth Modeling in an Integrated GIS Environment
9. W.Krull, I.Willms, R.R.Zakrzewsk, M.Sadok, J.Shirer, B.Zeliff, "Design and tes video-based cargo fire verification system for commercial aircraft", Fire Saf. J. 41(4), pp. 290–300, 2006.
10. G.Marbach, M.Loepfe, T.Brupbacher, "An image processing technique for fire detection in video images", Fire Saf. J. 41 (4), pp. 285–289, 2006.

11. T.Celik, H.Demirel, H.Ozkaramanli, "Automatic fire detection in video sequences", Proceedings of European Signal Processing Conference, September 2006.
12. JayantSinghala,T.R. Kiranchanda, G. Rajashekara and C.S.Jha" Automated Burned Area Delineation Using IRS AWiFS satellite data" The International Archives of the Photogrammetry, Remote Sensing and Spatial Information Sciences, Volume XL-8, 2014ISPRS Technical Commission VIII Symposium, 09 – 12 December 2014, Hyderabad, India
13. T.Celik, H.Demirel, "Fire and Smoke Detection without Sensors: Image Processing Based Approach", Proceedings of 15th European Signal Processing Conference, Poland, September 3-7, 2007.

N. Nanthini, Assistant Professor of Computer Science	International Journal of Computer Techniques		Image Resolution Enhancement using Biocubic and Spline Interpolation Techniques			International 2394-2231	April 2017

International Journal of Computer Techniques – Volume 4 Issue 2, Mar – Apr 2017

RESEARCH ARTICLE OPEN ACCESS

Image Resolution Enhancement using Bicubic and Spline Interpolation Techniques

T.Nandhini[1], M.Saratha[2]

[1]Assistant Professor in computer science, M.Phil student[2]

Department of computer science, sakthi college of arts and science for women, Dindigul.

----------**********----------

Abstract:

Images are being used in many fields of research. One of the major issues of images is their resolution. In this paper we are studying different image resolution enhancement techniques that use Wavelet Transform (WT). Basis functions of the WT are small waves located in different times. They are obtained using scaling and translation of a scaling function and wavelet function Therefore, the WT is localized in both time and frequency. In this method is used to improve the image resolution for different type of images. In this paper we are comparing different image resolution enhancement techniques those using Wavelet Transform.

In this correspondence, the authors propose an image resolution enhancement technique based on interpolation of the high frequency subband images obtained by discrete wavelet transform (DWT) and the input image. The edges are enhanced by introducing an intermediate stage by using stationary wavelet transform (SWT). DWT is applied in order to decompose an input image into different subbands. Then the high frequency subbands as well as the input image are interpolated. The estimated high frequency subbands are being modified by using high frequency subband obtained through SWT. Then all these subbands are combined to generate a new high resolution image by using inverse DWT (IDWT). The quantitative and visual results are showing the superiority of the proposed technique over the conventional and state-of- art image resolution enhancement techniques.

Keywords— **Image Interpolation, Peak signal-to-noise ratio (PSNR), Discrete Wavelet Transform (DWT), Stationary Wavelet Transform (SWT).**

----------**********----------

I. INTRODUCTION

Image resolution enhancement is a usable preprocess for many satellite image processing applications, such as vehicle recognition, bridge recognition, and building recognition to name a few. Image resolution enhancement techniques can be categorized into two major classes according to the domain they are applied in: 1) image-domain; and 2) transform-domain. The techniques in image-domain use the statistical and geometric data directly extracted from the input image itself [1], [2],while transform-domain techniques use transformations such as decimated discrete wavelet transform to achieve the image resolution enhancement [3]–[6].

The decimated discrete wavelet transform (DWT) has been widely used for performing image resolution enhancement [3]–[5]. A common assumption of DWT-based image resolution enhancement is that the low-resolution (LR) image is the low-passfiltered subband of the wavelet-transformed high-resolution (HR) image. This type of approach requires the estimation of wavelet

coefficients in subbands containing high-pass spatial frequency information in order to estimate the HR image from the LR image.

In order to estimate the high-pass spatial frequency information, many different approaches have been introduced. In [3], [4], only the high-pass coefficients with significant magnitudes are estimated as the evolution of the wavelet coefficients among the scales. The performance is mainly affected from the fact that the signs of estimated coefficients are copied directly from parent coefficients without any attempt being made to estimate the actual signs. This is contradictory to the fact that there is very little correlation between the signs of the parent coefficients and their descendants. As a result, the signs of the coefficients estimated using extreme evolution techniques cannot be relied upon. Hidden Markov tree (HMT) based method in [5] models the unknown wavelet coefficients as belonging to mixed Gaussian distributions which are symmetrical about the zero mean.

HMT models are used to determine the most probable state for the coefficients to be estimated. The performance also suffers mainly from the sign changes between the scales. The decimated DWT is not shift-invariant and, as a result, suppression of wavelet coefficients introduces artifacts into the image which manifests as ringing in the neighbourhood of discontinuities [6]. In order to combat this drawback in DWT-based image resolution enhancement, cycle-spinning methodology was adopted in [6]. The perceptual and objective quality of the resolution enhanced images by their method compare favorably with recent methods [3], [5] in the field.

Dual-tree complex wavelet transform (DT-CWT) is introduced to alleviate the drawbacks caused by the decimated DWT [7]. It is shift invariant and has improved directional resolution when compared with that of the decimated DWT. Such features make it suitable for image resolution enhancement. In this letter, a complex wavelet-domain image resolution enhancement algorithm based on the estimation of wavelet coefficients at high resolution scales is proposed. The initial estimate of the HR image is constructed by applying cycle-spinning methodology [6] in DT-CWT domain. It is then decomposed using the one-level DT-CWT to create a set of high-pass coefficients at the same spatial resolution of the LR image. The high-pass coefficients together with the LR image are used to reconstruct the HR image using inverse DT-CWT.

The letter is organized as follows. Section II gives a brief review of the DT-CWT. Section III describes the proposed DT-CWT domain satellite image resolution enhancement algorithm. Section IV provides some experimental results of the proposed approach and comparisons with the approaches in [1], [2], [4], and [6]. Section V concludes the letter.

Resolution has been frequently referred as an important property of an image. Images are being processed in order to obtain super enhanced resolution. One of the commonly used techniques for image resolution enhancement is Interpolation. Interpolation has been widely used in many image processing applications. Interpolation in image processing is a method to increase the number of pixels in a digital image. Traditionally there are three techniques for image interpolation namely Linear, Nearest Neighbor and cubic. Nearest Neighbor result in significant —Jaggy‖ edge distortion. The Bilinear Interpolation result in smoother edges but somewhat blurred appearance overall. Bicubic Interpolation look's best with smooth edges and much less blurring

than the bilinear result .By applying the 1-D discrete wavelet transform (DWT) along the rows of the image first, and then along the columns to produce 2-D decomposition of image.DWT produce four sub bands low-low(LL),low-high(LH),high-low(HL)and high-high(HH).By using these four sub bands we can regenerate original image.

II. IMAGE ENHANCEMENT TECHNIQUES

Denote a two-dimensional digital image of gray-level intensities by I. The image I is ordinarily represented in software accessible form as an M × N matrix containing indexed elements I(i, j), where 0 ≤i ≤M - 1, 0 ≤j ≤ N - 1. The elements I(i, j) represent samples of the image intensities, usually called pixels (picture elements). For simplicity, we assume that these come from a finite integer-valued range. This is not unreasonable, since a finite wordlength must be used to represent the intensities. Typically, the pixels represent optical intensity, but they may also represent other attributes of sensed radiation, such as radar, electron micrographs, x rays, or thermal imagery.

III. POINT OPERATIONS

Often, images obtained via photography, digital photography, flatbed scanning, or other sensors can be of low quality due to a poor image contrast or, more generally, from a poor usage of the available range of possible gray levels. The images may suffer from overexposure or from underexposure, as in the "mandrill" image in Fig. 1(a). In performing image enhancement, we seek to compute J, an enhanced version of I. The most basic methods of image enhancement involve point operations, where each pixel in the enhanced image is computed as a one-to-one function of the corresponding pixel in the original image: J(i, j) = f[I(i, j)]. The most common point operation is the linear contrast stretching operation, which seeks to maximally utilize the available gray-scale range. If a is the minimum intensity value in image I and b is the maximum, the point operation for linear contrast stretching is defined by

$$J(i,j) = \frac{K-1}{b-a}[I(i,j) - a] \qquad (1)$$

assuming that the pixel intensities are bounded by 0 ≤I(i, j) ≤K - 1, where K is the number of available pixel intensities. The result image J then has maximum gray level K - 1 and minimum gray level 0, with the other gray levels being distributed in-between according to Eq. (1). Figure 1(b)shows the result of linear contrast stretching on Fig. 1(a).

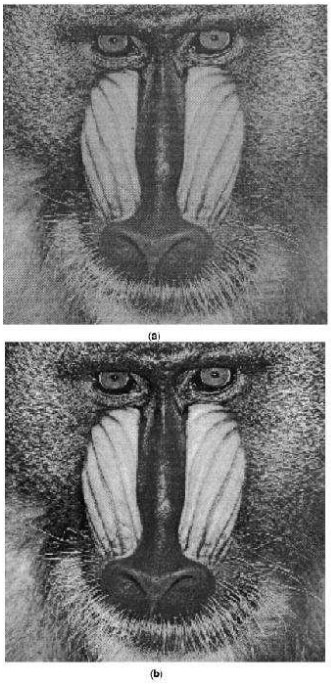

Figure 1. (a) Original "Mandrill" image (low contrast). (b) "Mandrill" enhanced by

linear contrast stretching. (c) "Mandrill"

Several point operations utilize the image histogram, which is a graph of the frequency of occurrence of each gray level in I. The histogram value $H_I(k)$ equals n only if the image I contains exactly n pixels with gray level k. Qualitatively, an image that has a flat or well-distributed histogram may often strike an excellent balance between contrast and preservation of detail. Histogram flattening, also called histogram equalization in Gonzales and Woods (1), may be used to transform an image I into an image J with approximately flat histogram. This transformation can be achieved by assigning

$$J(i,j) = (K-1)P(i,j) \tag{2}$$

where P(i, j) is a sample cumulative probability formed by using the histogram of I:

$$P(i,j) = \frac{1}{MN}\sum_{k=0}^{I(i,j)} H_1(k) \tag{3}$$

The image in Fig. 1(c) is a histogram-flattened version of Fig. 1(a).

A third point operation, frame averaging, is useful when it is possible to obtain multiple images G_i, i = 1, . . ., n, of the same scene, each a version of the ideal image I to which deleterious noise has been unintentionally added:

$$\mathbf{G}_i = \mathbf{I} + \mathbf{N}_i \tag{4}$$

where each noise "image" N_i is an M × N matrix of discrete random variables with zero mean and variance σ^2. The noise may arise as electrical noise, noise in a communications channel, thermal noise, or noise in the sensed radiation. If the noise images are not mutually correlated, then averaging the n frames together will form an effective estimate $\hat{I}$ of the uncorrupted image I, which will have a variance of only σ^2/n:

$$\hat{I}(i,j) = \frac{1}{n}\sum_{i=1}^{n} G_i(i,j) \tag{5}$$

This technique is only useful, of course, when multiple frames are available of the same scene, when the information content between frames remains unchanged (disallowing, for example, motion between frames), and when the noise content does change between frames. Examples arise quite often, however. For example, frame averaging is often used to enhance synthetic aperture radar images, confocal microscope images, and electron micrographs.

IV. WAVELET SHRINKAGE

Recently, wavelet shrinkage has been recognized as a powerful tool for signal estimation and noise reduction or simply de-noising (16). The wavelet transform utilizes scaled and translated versions of a fixed function, which is called a "wavelet," and is localized in both the spatial and frequency domains (17). Such a joint spatial-frequency representation can be naturally adapted to both the global and local features in images. The wavelet shrinkage estimate is computed via thresholding wavelet transform coefficients:

where DWT and IDWT stand for discrete wavelet transform and inverse discrete wavelet transform, respectively (17), and f[ ] is a transform-domain point operator defined by either the hard-thresholding rule or the soft-thresholding rule where the value of the threshold t is usually determined by the variance of the noise and the size of the image. The key idea of wavelet shrinkage derives from the approximation property of wavelet bases. The DWT compresses the image I into a small number of DWT

coefficients of large magnitude, and it packs most of the image energy into these coefficients. On the other hand, the DWT coefficients of the noise N have small magnitudes; that is, the noise energy is spread over a large number of coefficients. Therefore, among the DWT coefficients of G, those having large magnitudes correspond to I and those having small magnitudes correspond to N. Apparently, thresholding the DWT coefficients with an appropriate threshold removes a large amount of noise and maintains most image energy. Though the wavelet shrinkage techniques were originally proposed for the attenuation of image-independent white Gaussian noise, they work as well for the suppression of other types of distortion such as the blocking artifacts in JPEG-compressed images (18,19). In this case, the problem of enhancing a compressed image may be viewed as a de-noising problem where we regard the compression error as additive noise. We applied the wavelet shrinkage to enhancing the noisy image shown in Fig. 2(b) and show the de-noised image in Fig. 2(f), from which one can clearly see that a large amount of noise has been removed, and most of the sharp image features were preserved without blurring or ringing effects. This example indicates that wavelet shrinkage can significantly outperform the linear filtering approaches.

Figure 2 illustrates an example of the enhancement of JPEG-compressed images (20). Figure 2(a) shows a part of the original image. Fig. 2(b) shows the same part in the JPEG-compressed image with a compression ratio 32:1, where blocking artifacts are quite severe due to the loss of information in the process of compression. Figure 2(b) reveals the corresponding part in the enhanced version of Fig. 2(b), to which we have applied wavelet shrinkage. One can find that the blocking artifacts are greatly suppressed and the image quality is dramatically improved.

V. LITERATURE SURVAY

PAPER-1 S. SINDHUMOL; A. KUMAR; K. BALAKRISHNAN: A NEW ENHANCEMENT APPROACH FOR ENHANCING IMAGE OF DIGITAL CAMERAS BY CHANGING THE CONTRAST

There are four well-known traditional interpolation techniques namely nearest neighbor, linear, and Lanczos. In [4] using bilinear, bicubic method the PSNR values for Lena's image are 26.34 and 26.86. W. Knox. Carey, Daniel. B. Chuang, and S. S. Hemami in [5] presented the regularity-preserving interpolation technique for image resolution enhancement synthesizes a new wavelet subband based on the known wavelet transform coefficients decay. Which gives PSNR (db) value for Lena's Image as 31.7 [5]. Xin. Li and Michael. T. Orchard in [6] presented a hybrid approach produced by combining bilinear interpolation and covariance-based adaptive interpolation called New Edge-Directed Interpolation Which gives PSNR(db) value for Lena's Image as 28.81 [4]. Alptekin. Temizel and Theo. Vlachos in [7] presented technique named "Wavelet domain image resolution enhancement using cycle-spinning and edge modelling ", which improves PSNR (db) values for Lena's image up to 29.27 [4]. Hasan. Demirel and Gholamreza. Anbarjafari in [8] presented an approach DT- CWT based image resolution enhancement which gives PSNR (db) value for Lena's Image as 33.74 [4]. Gholamreza. Anbarjafari and Hasan. Demirel in [9] presented a method named "Image super resolution based on interpolation of wavelet domain high frequency subbands and the spatial domain input image", whichgives PSNR(db) value for Lena's image up to 34.79 [4]. Hasan. Demirel and Gholamreza.

Anbarjafari in [4] presented new method named "Image Resolution Enhancement by Using Discrete and Stationary Wavelet Decomposition", which give PSNR(db) value for Lena's image as 34.82 [4].

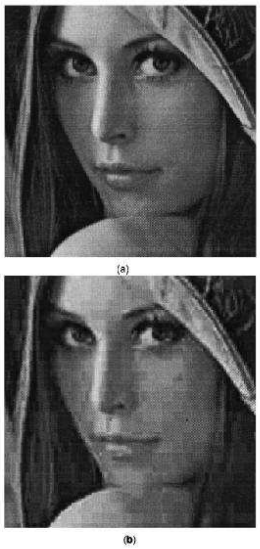

Figure 2. (a) Original "Lena" image. (b) "Lena" JPEG-compressed at 32:1. (c) Wavelet shrinkage applied to Fig. 2b

Regularity-Preserving Image Interpolation

Traditional interpolation methods work in the time domain. As stated in, the regularity-preserving interpolation technique synthesizes a new wavelet sub band based on the known wavelet transform coefficients decay. The lowpass output of a wavelet analysis stage can be Considered as the image to be interpolated. The original image can given as input to a single wavelet synthesis stage along with the corresponding high frequency sub bands to produce an image interpolated by a factor of two in both directions. The creation of unknown high-frequency sub bands is necessary in the regularity-preserving interpolation strategy.

VI. CONCLUSION AND FUTUREWORK

A method for image resolution enhancement from a single low-resolution image using the dual-tree complex wavelet is presented. The initial rough estimate of the high-resolution image is decomposed to estimate the complex-valued high-pass wavelet coefficients for the input low-resolution image. Estimated complex wavelet coefficients are used together with the input low-resolution image to reconstruct the resultant high-resolution image by employing inverse dual-tree complex wavelet transform. Extensive tests and comparisons with the state-of-the-art methods show the superiority of the method presented in this letter. The proposed resolution enhancement method retains both intensity and geometric features of the low-resolution image. Although the method for image enhancement based on Spline is sufficient but in future efficient methods can be develop for image enhancement which can give more accurate result.

VII. REFERENCES

[1] Muhammad Zafar Iqbal, Abdul Ghafoor, and Adil Masood Siddiqui, "Satellite Image Resolution Enhancement Using Dual-Tree Complex Wavelet Transform and Nonlocal Means," IEEE Trans.Geosciences and Remote Sensing Letter,2012.

[2] Rafel C. Gonzalez and Richard E. woods and Steven L. Eddins," Digital Image Processing Using MATLAB (Second Edition)."

[3] Shutao Li, Leyuan Fang and Haitao Yin, " Multitemporal Image Change Detection Using a Detail Enhancing Approach With Nonsubsampled Contourlet Transform,"

IEEE Geosciences and Remote Sensing Letter, VOL. 9, NO. 5, pp836-840, SEPTEMBER 2012.

[4] Hasan. Demirel and Gholamreza. Anbarjafari, "Image Resolution Enhancement by Using Discrete and Stationary Wavelet Decomposition," IEEE Trans. IMAGE PROCESSING, VOL. 20, NO. 5, MAY 2011.

[5] W. Knox. Carey, Daniel. B. Chuang, and S. S. Hemami, "Regularity Preserving image interpolation," IEEE Trans. Image Process., vol. 8,no. 9, pp. 1295 - 1297, Sep. 1999.

[6] Xin. Li and Michael. T. Orchard, "New edge-directedinterpolation," IEEE Trans. Image Process., vol. 10, no. 10, pp. 1521-1527, Oct. 2001.

[7] Alptekin. Temizel and Theo. Vlachos, "Wavelet domain image resolution enhancement using cycle spinning," Electron. Lett. vol. 41, no. 3, pp. 119-121, Feb. 3, 2005.

[8] Hasan. Demirel and Gholamreza. Anbarjafari, "Satellite image resolution enhancement using complex wavelet transform," IEEE Geosci. Remote Sens. Lett, vol. 7, no. 1, pp. 123-126, Jan. 2010.

[9] Gholamreza. Anbarjafari and Hasan. Demirel, " Imagesuper resolution based on interpolation of wavelet domain high frequency subbands and the spatial domain input image," ETRI J., vol. 32, no. 3, pp. 390-394, Jun. 2010.

[10] Hasan. Demirel and Gholamreza. Anbarjafari, "Discrete Wavelet Transform-Based Satellite Image Resolution Enhancement," IEEE Trans. Geosciences and Remote Sensing Letter, VOL. 49, NO. 6, JUNE 2011.